



The University of
Nottingham

Institute of Engineering, Surveying
and Space Geodesy

**HEAVE COMPENSATION USING
TIME-DIFFERENCED CARRIER OBSERVATIONS
FROM LOW COST GPS RECEIVERS**

**By
Stephen J. Blake BEng**

**GEORGE GREEN LIBRARY OF
SCIENCE AND ENGINEERING**

Thesis submitted to the University of Nottingham for
the degree of Doctor of Philosophy
June 2007

BEST COPY AVAILABLE.

VARIABLE PRINT QUALITY

ABSTRACT

Vertical reference for hydrographic survey can be provided in two ways: through the use of an expensive and very accurate GPS-aided INS system, or through the classical method of compensating for heave motion measured on board the vessel and tide data taken from a nearby tide gauge. Whilst the GPS-aided INS approach offers significant advantages in terms of accuracy their high cost has prohibited their widespread use within the hydrographic survey industry and the classical method is still prevalent.

Heave motion of a survey vessel has traditionally been measured using inertial technologies, which can be expensive and have problems with usability and instability, resulting in higher survey costs and a significant hydrographer input burden. Heave can also be measured through the use GPS receivers by the differencing of measured carrier phase pseudo-range from adjacent epochs and the recent introduction by U-Blox of the Antaris AEK-4T, an off the shelf low cost GPS receiver capable of measuring and recording the carrier phase pseudo-range observable, has allowed the exploration of a novel method of measuring and compensating for vessel heave using off the shelf low cost GPS receivers.

The work presented in this thesis details a method of compensating for vessel heave motion in bathymetry data that has been developed specifically for use with the U-Blox Antaris receiver. The technique is based on the production of highly accurate velocity estimates using the carrier phase observable. Carrier phase measurements are differenced across adjacent epochs to give relative delta range estimates between receiver and satellite along the direct line of sight, which are then processed to calculate an accurate estimate of receiver delta position across the epoch, a measurement analogous to receiver velocity. This technique has been termed Temporal Double Differencing (TDD).

Integrated vertical velocity estimates produce the relative vertical displacement of the vessel over time. Because of bias errors in the velocity estimates from TDD, this vertical displacement is subject to drift. The drift is removed by passing the data through a high-pass filter designed to stop the drift frequencies yet pass the required frequencies of vertical vessel motion.

An obvious advantage of this technique over conventional technologies is cost. Instruments currently on the market are centred on inertial sensors and generally have prices ranging from £12,000 to £25,000. Low cost GPS receivers are priced at around £200 and so this technique can have sizeable cost implications for the hydrographic survey industry. In addition the nature of the TDD algorithm results in a heave sensing technology that is not subject to turn induced heave which can affect inertial based sensors, and also imposes no requirement on the user to account for parameters such as vessel heave characteristics and current heave state. A further advantage over interferometric GPS heave compensation techniques is that the TDD algorithm is stand-alone and requires no reference receiver.

Two trials have been undertaken to test the ability of the low cost U-Blox receiver to record accurate phase pseudo-range observables and subsequently produce a heave estimate: a Spirent GPS hardware simulator trial, and a sea trial. The simulator trial has been the first to quantify the errors associated with the measurement of carrier phase pseudo-range observables using low cost commercially available receivers. The trial used three separate receivers: a Novatel OEM4, a Leica 530 and a low cost U-Blox Antaris. Three scenarios were programmed into the simulator to rigorously test the effects of receiver quality and receiver dynamics on the resulting velocity estimates using the TDD algorithm. The sea trial involved fitting various sensors to the vessel including a Honeywell HG1700 IMU, an Applanix POS-RS GPS-aided INS system and the same three GPS receivers as used in the simulator trial. The POS-RS system and the inertial based heave sensor were used to provide a reference against which the novel low cost heave output could be compared. The comprehensive nature of the sea trial makes it the first work to compare the results from the TDD heave algorithm using varying grades of receiver, and against truth data from both an inertial based heave system and a GPS-aided INS.

The results of the simulator trial have shown that under static conditions the TDD velocity estimation using the U-Blox Antaris is of comparable quality to that produced using both the Novatel OEM4 and the Leica 530. Under dynamic conditions the performance of the U-Blox Antaris is greatly degraded when undergoing large accelerations, an artefact of the inferior componentry used in the signal tracking loops.

The sea trial has demonstrated the ability of the TDD heave algorithm developed for use with commercially available low cost GPS receivers to measure vessel heave to a similar standard as inertial based technologies at a fraction of the cost and with greatly reduced instability and usability issues that are traditionally associated with inertial based heave sensors.

Acknowledgements

This PhD project has been undertaken at the Institute of Engineering Surveying and Space Geodesy, University of Nottingham in conjunction with Sonardyne International Limited. Funding for the project has been supplied by both the EPSRC, and Sonardyne International Limited through an Industrial CASE award.

I would like to extend my thanks to all those who have aided me as I conducted the research for the project with particular thanks to my academic supervisors: Prof. Terry Moore, Dr. Chris Hide, Dr. David Park and Dr. Chris Hill. I would also like to thank Sonardyne International Ltd. and my industrial supervisors there: Jonathan Martin and Chris Pearce.

Contents

1	Introduction	1
1.1	Background	1
1.2	Research Aims and Objectives	3
1.3	Research Methodology	4
1.4	Thesis Overview	5
2	Inertial Navigation Systems	8
2.1	Introduction	8
2.2	The Principles of Inertial Navigation	9
2.2.1	Reference Frames	9
2.2.2	Frame Rotations	11
2.2.2.1	Euler Angles	11
2.2.2.2	Quaternions	15
2.2.3	The Strapdown Inertial Navigation Concept	17
2.3	System Initialization and Alignment	18
2.3.1	Initialization	18
2.3.2	Alignment	19
2.3.2.1	Coarse Alignment	19
2.3.2.2	Fine Alignment	21
2.4	System Mechanisation in the Navigation Frame	22
2.5	Attitude and Heading Reference Systems	25
2.5.1	AHRS Alignment and Operation	25
2.6	Grades of IMU	27

3	The Global Positioning System	30
3.1	Introduction	30
3.2	GPS Overview	31
3.2.1	The Basic Concept	31
3.2.2	GPS Hardware	31
3.2.2.1	The Space Segment	32
3.2.2.2	The Control Segment	33
3.2.2.3	The User Segment	33
3.3	GPS Observables	34
3.3.1	The Code Pseudo-range Observable	34
3.3.2	The Carrier Phase Pseudo-range Observable	37
3.3.3	The Pseudo-range Rate Observable	37
3.3.4	Quality of Recorded Observables	38
3.3.4.1	Signal Tracking with Feedback Control Loops	38
3.3.4.2	Feedback Control Loop Performance	39
3.4	GPS Error Sources	41
3.4.1	Satellite Errors	41
3.4.1.1	Satellite Clock Offset	42
3.4.1.2	Ephemeris Error	42
3.4.2	Measurement Errors	43
3.4.2.1	Receiver Clock Offset	43
3.4.2.2	Multipath Error	44
3.4.2.3	Receiver Noise and Tracking Loop Errors	44
3.4.3	Propagation Errors	44
3.4.3.1	Ionospheric Effects	44
3.4.3.2	Tropospheric Delay	46
3.5	Obtaining User Position from GPS Observables	47
3.5.1	Stand-alone GPS	47
3.5.2	Differential Positioning	51
3.5.3	Interferometric Positioning	53
3.5.3.1	Single Difference	53

3.5.3.2	Double Difference	54
3.5.4	Spatial Decorrelation	54
3.6	Obtaining User Velocity from a Stand-alone GPS Receiver	55
3.6.1	Velocity from the Pseudo-range Rate Observable	55
3.6.2	Velocity from Temporally Differenced Carrier Phase Observables	57
4	Vertical Reference for Hydrographic Survey	58
4.1	Introduction	58
4.2	Chart Datum	59
4.3	Classical Hydrographic Methods	59
4.3.1	Tidal Compensation	60
4.3.2	Heave Compensation	62
4.3.2.1	Analogue Heave Reduction	62
4.3.2.2	Digital Heave Compensation	63
4.3.3	Errors and Problems Associated with Classical Hydrographic Methods	65
4.3.3.1	Tide Specific Errors	65
4.3.3.2	Heave Specific Errors	66
4.3.3.3	General Classical Methodology Errors	67
4.4	Single Water Level Correction	68
4.4.1	GPS-aided INS	68
4.4.2	Interferometric GPS	69
4.4.3	Factors Prohibitive to the Widespread Use of Single Water Level Correction Techniques	70
4.4.3.1	GPS-aided INS Specific Factors	70
4.4.3.2	Interferometric GPS Specific Factors	70
4.4.3.3	General Single Water Level Correction Methodology Factors	71
4.5	The International Hydrographic Organization Survey Standards	71
5	Development of an INS Based Heave Algorithm	74
5.1	Introduction	74

5.2	INS Mechanisation	75
5.2.1	Initialization and Alignment	75
5.2.2	The INS Mechanisation Computation Loop	76
5.2.2.1	Earth and Transport Rate	76
5.2.2.2	Gravity Compensation	77
5.2.2.3	Formation of the Navigation Frame Mechanisation Equation	77
5.2.2.4	Velocity and Position Updates	78
5.2.2.5	Attitude Computation	78
5.2.2.6	Subsequent Loop Iterations	79
5.2.3	Fourth Order Runge-Kutta Numerical Integration	79
5.3	INS Vertical Channel Damping	80
5.3.1	The Baro-inertial Altimeter	81
5.3.1.1	A Heave Filter Based on the Baro-inertial Altimeter	81
5.3.1.2	Frequency and Transient Analysis of the Baro-inertial Altimeter Based Heave Filter	83
5.3.1.3	Redesign of the Heave Filter to Incorporate a Damping Coefficient	85
5.3.1.4	Transient Analysis of the Redesigned Heave Filter	86
5.3.2	Heave Filter Tuning	86
5.4	Use of Inertial Based Heave Algorithms in Hydrographic Survey	88
5.4.1	Summary of Inertial Heave Algorithm	88
5.4.2	Turn Induced Heave and Filter Transient Behaviour	88
5.4.3	Heave Filter Tuning	90
5.4.4	Cost Implications of Inertial Heave Systems	90
6	Development of a GPS Velocity Based Heave Algorithm	91
6.1	Introduction	91
6.2	Velocity From Time-Differenced Carrier Phase Pseudo-range	92
6.2.1	The Temporal Double Difference Observation Equation	92
6.2.2	The TDD Processing Algorithm	93

6.2.3	Specific Models and Techniques Used in the TDD Velocity Algorithm	96
6.2.3.1	Satellite Ephemeris Calculation	96
6.2.3.2	Stand-alone GPS Position	97
6.2.3.3	Tropospheric Correction	97
6.2.3.4	Ionospheric Correction	99
6.2.3.5	Correction for Satellite Loss	101
6.2.3.6	Cycle Slip Handling	102
6.2.3.7	Carrier-to-Noise Density Weighting Scheme	103
6.3	The TDD Heave Algorithm	104
7	The Spirent GSS7700 GPS/SBAS Simulator Trials	107
7.1	Introduction	107
7.2	The Spirent GSS7700 GPS/SBAS Simulator	108
7.2.1	Simulator Hardware	108
7.2.2	Simulator Software	109
7.2.3	Simulator Setup and Error Models	109
7.3	Trial Methodology	110
7.3.1	The Simulated Scenarios	111
7.3.1.1	Static	111
7.3.1.2	Marine	112
7.3.1.3	High Dynamics	112
7.3.2	The Trials	114
7.3.2.1	Trial 1: Receiver Test	116
7.3.2.2	Trial 2: Tropospheric Delay Compensation Test	117
7.3.2.3	Trial 3: Ionospheric Delay Compensation Test	117
7.3.2.4	Trial 4: Full Simulation Test	117
7.3.2.5	Trial 5: Real Static Data	117
7.4	Trial Results	118
7.4.1	Trial 1	118
7.4.1.1	Static Scenario	118

7.4.1.2	Marine Scenario	121
7.4.1.3	High Dynamic Scenario	127
7.4.2	Trial 2	128
7.4.3	Trial 3	130
7.4.4	Trial 4	132
7.4.5	Trial 5	135
7.5	Spirent Simulator Trial Summary	136
8	The Plymouth Sea Trial	140
8.1	Introduction	140
8.2	Trial Methodology	141
8.2.1	Trial Overview	141
8.2.2	The Applanix POSRS System	142
8.2.3	The Marco and the Sensor Configuration	142
8.2.4	Trial Trajectory	144
8.2.5	Vessel Reference Point and Lever Arm Separations	148
8.3	Trial Results	150
8.3.1	POSRS SBET Data	150
8.3.1.1	SBET Data Quality	150
8.3.1.2	SBET Heave	153
8.3.2	IMU Derived Heave	155
8.3.3	TDD Heave	158
8.3.3.1	Leica SR 530 Receiver	159
8.3.3.2	NovAtel OEM4 Receiver	162
8.3.3.3	U-Blox Antaris AEK-4T Receiver	162
8.3.4	The Effect of GPS Data Rate on the Sea Trial Results	168
8.3.4.1	Frequency Range of SBET Heave and 1 Hz TDD Heave Error	168
8.3.4.2	NovAtel OEM4 4 Hz TDD Heave	170
8.4	Plymouth Sea Trial Summary	172
8.4.1	IMU Derived Heave	173

8.4.2	TDD Heave	174
9	Summary, Conclusions and Future Recommendations	176
9.1	Thesis Summary	176
9.2	Conclusions	178
9.2.1	The Spirent Simulator Trials	178
9.2.2	The Sea Trial	180
9.3	Recommendations for Future Work	181

List of Figures

2.1	The inertial frame	12
2.2	The earth fixed frame	12
2.3	The navigation frame	13
2.4	The body frame	13
2.5	Schematic representation of a possible layout of gyros and accelerometers on an IMU platform	17
2.6	Strapdown INS mechanisation in the navigation frame (Titterton and Weston, 2004)	23
3.1	Comparison of received satellite signal and receiver generated signal	34
3.2	Block schematic representation of a delay lock loop	39
3.3	Spatial decorrelation of DGPS corrections	55
4.1	Discrete tidal zones surrounding Popof Island, Alaska	61
4.2	Sketch detailing the parameters necessary for tidal compensation	62
4.3	Bode plot of the frequency ranges represented in the classical method of providing vertical hydrographic survey reference	67
4.4	Block schematic diagram of a POS/MV 320	68
5.1	Block schematic diagram of a third order feedback damping loop	83
5.2	Frequency and phase response of baro-inertial altimeter with varying time constant	84
5.3	Impulse response of baro-inertial altimeter with varying time constant	85
5.4	Impulse response of redesigned heave filter with varying time constant	87

5.5	Impulse response of redesigned heave filter with varying damping coefficient	87
5.6	Block schematic diagram of the inertial heave algorithm	89
6.1	High pass filter design criteria required by Matlab filter design and analysis tool	105
6.2	Frequency and phase response of high pass heave filter	106
6.3	Block schematic diagram of the TDD heave algorithm	106
7.1	Spirent GNSS Simulator	110
7.2	Plan view of simulated marine scenario trajectory	113
7.3	Height profile of simulated marine scenario	113
7.4	Velocity profile of simulated marine scenario	114
7.5	Plan view of simulated high dynamics scenario	115
7.6	Height profile of simulated high dynamics scenario	115
7.7	Velocity profile of simulated high dynamics scenario	116
7.8	Leica SR 530 dual frequency receiver TDD velocity from simulated static	119
7.9	Novatel OEM4 dual frequency receiver TDD velocity from simulated static data	120
7.10	U-Blox Antaris single frequency receiver TDD velocity from simulated static data	120
7.11	Leica SR 530 integrated TDD position drift error from the marine scenario	122
7.12	Leica SR 530 TDD heave error from the marine scenario	123
7.13	Novatel OEM4 TDD heave error from the marine scenario	123
7.14	U-Blox Antaris TDD heave error from the marine scenario	124
7.15	Magnitude of simulated vessel acceleration during the marine trial . .	126
7.16	Frequency analysis of error in U-Blox Antaris TDD velocity during marine trial	127
7.17	Leica SR 530 dual frequency receiver induced velocity error from simulated high dynamics data	128
7.18	Novatel OEM4 dual frequency receiver induced error from simulated high dynamics data	129

7.19	U-Blox Antaris single frequency receiver induced error from simulated high dynamics data	129
7.20	Leica SR 530 TDD velocities from simulated static data with tropospheric error modeled and no correction applied	131
7.21	Leica SR 530 TDD velocities from simulated static data with tropospheric error modeled and STANAG correction applied	131
7.22	TDD processed simulated static data with ionosphere modeled and no correction applied	133
7.23	TDD processed simulated static data with ionosphere modeled and Klobuchar correction applied	133
7.24	TDD processed simulated static data with ionosphere modeled and dual frequency correction applied	134
7.25	TDD processed static GPS collected using Leica SR 530 dual frequency receiver	136
7.26	TDD processed static GPS data collected using OEM4 dual frequency receiver	137
7.27	TDD processed static GPS data collected using U-Blox Antaris single frequency receiver	137
8.1	The Applanix POSRS	143
8.2	The Marco	144
8.3	IMU configuration below deck on the Marco	145
8.4	Placement of Novatel Pinwheel antenna for OEM4 receiver and POSRS system	145
8.5	The placement of the Leica 504 and U-Blox ANN-MS-0-005 antennas	146
8.6	Diagram of the boom with the Leica 504 and U-Blox ANN-MS-0-005 antennas fitted	146
8.7	Sea trial plan trajectory	147
8.8	Sea trial height profile	147
8.9	The number of GPS satellites available during the sea trial	152

8.10	The POSGPS quality factor of the processed GPS solution for the sea trial	152
8.11	SBET heave over the complete trial	154
8.12	SBET heave data for the two survey lines within the breakwater (section 3 of figure 8.11)	154
8.13	SBET heave data for the two survey lines outside the breakwater (section 5 of figure 8.11)	155
8.14	Comparison of SBET heave and IMU derived heave during initialization turns	156
8.15	Comparison of SBET heave and IMU derived heave during survey lines within the breakwater	157
8.16	Comparison of SBET heave and IMU derived heave during survey lines outside of the breakwater	157
8.17	Satellite availability for Leica SR 530 receiver during sea trial	160
8.18	Leica SR 530 TDD heave error during initialization turns	160
8.19	Leica SR 530 TDD heave error during survey lines within the breakwater	161
8.20	TDD Leica SR 530 heave error during survey lines outside the breakwater	161
8.21	NovAtel OEM4 TDD heave error during initialization turns	163
8.22	NovAtel OEM4 TDD heave error during survey lines within the breakwater	163
8.23	NovAtel OEM4 TDD heave error during survey lines outside the breakwater	164
8.24	Satellite availability for U-Blox Antaris during sea trial	165
8.25	U-Blox Antaris TDD heave error during initialization turns	166
8.26	U-Blox Antaris TDD heave error during survey lines within the breakwater	166
8.27	U-Blox Antaris TDD heave error during survey lines conducted outside the breakwater	167
8.28	Magnitude of acceleration experienced during the plymouth sea trial .	168
8.29	Frequency analysis of SBET heave across the entire trial	169

8.30	Frequency analysis of SBET heave during line 1 (a) and line 2 (b) conducted within the breakwater	170
8.31	NovAtel OEM4 4 Hz TDD heave error during initialization turns . . .	171
8.32	NovAtel OEM4 TDD 4 Hz heave error during survey lines conducted within the breakwater	172
8.33	NovAtel OEM4 TDD 4 Hz heave error during survey lines conducted beyond the breakwater	173

List of Tables

2.1	IMU grades: performance and cost data	29
3.1	Location of the elements of the control segment (Farrell and Barth, 1999)	32
4.1	Summary of minimum standards for hydrographic surveys (IHO, 1998)	72
5.1	Table showing the generalised effect of the damping coefficient and the time constant on heave measurement	86
7.1	Table of sea states used in simulated marine scenario	112
7.2	Results of static test of TDD velocity algorithm using error free simulated data	121
7.3	Receiver induced heave errors for each section of the simulated marine scenario	125
7.4	Mean accelerations simulated during the marine trial	125
7.5	Leica SR 530 TDD velocity error for static data with tropospheric delay modeled	130
7.6	Standard deviation and mean error using Klobuchar and dual frequency ionospheric correction	132
7.7	Standard deviation and mean error of TDD processed simulated static data with tropospheric and ionospheric correction	135
7.8	Standard deviation and mean error of TDD processed simulated marine data with tropospheric and ionospheric correction	135
7.9	Standard deviation and mean error of TDD processed static GPS data	136
8.1	Times for each action conducted during the sea trial	148

8.2	IMU derived heave errors	158
8.3	Leica SR 530 TDD heave errors	162
8.4	NovAtel OEM4 TDD heave errors	164
8.5	U-Blox Antaris TDD heave errors	165
8.6	NovAtel OEM4 1 Hz TDD heave error during lines conducted within the breakwater	169
8.7	NovAtel OEM4 4 Hz TDD heave errors	170
8.8	NovAtel OEM4 4 Hz TDD heave errors when compared to SBET data processed using 1 Hz Leica SR 530 GPS data	172

Acronyms

AHRS	Attitude and heading Reference System
CORS	Continually Operating Reference Station
DCM	Direction Cosine Matrix
DGPS	Differential Global Positioning System
DLL	Delay Lock Loop
ECEF	Earth Centered Earth Fixed coordinate system
IESSG	Institute of Engineering Surveying and Space Geodesy
IHO	International Hydrographic Organisation
INS	Inertial Navigation System
IMU	Inertial Motion Unit
GAMS	GPS Azimuth Subsystem
GPS	Global Positioning System
L ₁	GPS L1 signal
L ₂	GPS L2 signal
MCS	Master Control Station
MEMS	Micro Electro-mechanical Systems
MLLW	Mean Lowest Low Water
PLL	Phase Lock Loop
POSMV	(Applanix) Position and Orientation System Marine Vehicles
POSRS	(Applanix) Position and Orientation System Reference System
RINEX	Receiver Independent Exchange Format
SBET	Smoothed Best Estimate of Trajectory
SNR	Signal to Noise Ratio
STANAG	Standard Nato Agreement
TEC	Total Electron Count
TDD	Temporal Double Difference
USDOD	US Department of Defense
WGS84	World Geodetic System of 1984

Chapter 1

Introduction

1.1 Background

Around 90 % of the world's trade is transported around the globe by the international shipping industry. The UK's ports alone saw 367.2 million tonnes of imports and exports in 2003, a figure which is growing year on year (Port of London Authority, 2004). This tonnage of cargo equates to a large volume of marine traffic using Britain's waterways each year, and produced £6,650 million of revenue for the UK economy in 2004 (Chamber of Shipping, 2004). On a global scale, world seaborne trade tonnage has more than doubled over the last thirty years to reach 5,070 million tonnes in 1998 and is set to increase further with Reefer (2007) predicting a 50 % increase between 2006 and 2010.

Whenever merchant vessels come into port to unload and load their cargo, the navigator or pilot relies on nautical charts and tide information to plot a course and decide upon when it is safe to enter port for loading and unloading. Charts referred to by ship's pilots are created from data collected during hydrographic surveys which record bathymetry data to produce a relief of the sea or river bed (henceforth referred to as the seabed).

Bathymetry data collected during a hydrographic survey must be reduced to a local datum before it can be used in nautical charts. The providence of vertical reference for a survey allows this reduction to take place. Therefore any improvements in the providence of a survey's vertical reference translate directly into improvements in the

providence of the nautical charts to the shipping industry.

According to the Marine Accidents and Investigations Branch (2004) there were a total of 1,492 accidents involving British shipping, or ships in British waters in 2004. Whilst it is accepted that this figure is not solely due to accidents that could have been avoided through better charts, their improvement can have a dramatic effect on marine safety (Imahori et al., 2003). Moreover, more accurate nautical charts which can afford the captain of cargo vessels more confidence in the depths they display can improve the limits for under keel clearance. This can have a direct impact on how quickly a vessel can enter, and how late it may leave port, potentially reducing the time to load and unload the vessel's cargo resulting in monetary saving for the freight company.

In addition to safety improvements and monetary savings for shipping companies mentioned above, benefits from improved providence of vertical control of hydrographic survey will also be felt by port authorities, dredging companies and the hydrographic survey industry as a whole. Improvements need not just be in terms of accuracy but may also be seen in the areas of cost and usability. If the cost and usability of equipment providing vertical control are improved this will give immediate benefits to any company wishing to conduct a survey, and also to the surveyors themselves.

This thesis and the research contained within it concentrates on the fixing of the vertical position of the survey vessel with respect to a given datum. Specifically, the work conducted during the project has focused on the providence of heave compensation for hydrographic survey vessels. Heave of the sea is defined by the Oxford English Dictionary as "the force exerted by the swell of the sea in quickening, retarding, or altering a vessel's course". This definition is altered slightly when applied to the hydrographic survey industry to mean the vertical displacement of the vessel due to the same effects. As is explained in this thesis, measurement and compensation of this vessel motion for hydrographic survey vessels has direct implications for the accuracy of surveys of certain orders. The method of recording heave has cost and usability implications that are of significant interest to the hydrographic survey industry.

The surveying of the world's sea and river beds is of great economic and scientific

importance to all nations. Data collected during hydrographic surveys produce nautical charts of the world's ports. Improvements in providing vertical survey control whether they relate to cost, accuracy or usability will have benefits that may be felt, not just in the hydrographic survey industry, but by the world economy as a whole.

1.2 Research Aims and Objectives

Heave motion of a hydrographic survey vessel is currently measured throughout the hydrographic survey industry using sensors based on inertial measurement units. This method of heave measurement has some disadvantages such as high user input, high cost and instability due to the feedback algorithms they employ.

The recent release of a low cost GPS receiver that allows the user to measure and record raw carrier phase pseudo-range observables has paved the way for research into the use of these receivers for heave measurement. This PhD project has produced a novel method of heave measurement for use with just this kind of off the shelf low cost GPS receiver, namely the U-Blox Antaris AEK-4T. The algorithm is based on stand-alone GPS carrier phase pseudo-range measurements, differenced to produce a velocity output, which is then integrated to create relative position. In addition an algorithm to measure heave motion based on inertial sensor outputs has also been developed, which provided a reference for testing of the GPS based algorithm. Heave measurement technologies based the stand-alone GPS algorithm developed as part of the thesis provide benefits over current inertial based technologies in three key areas:

- Cost
- Stability
- Usability

The research contained within this thesis has been focused around the thorough testing of the stand-alone GPS based heave algorithm and its constituent parts both in a simulated environment and against current technologies in a marine environment. An aim was to produce, for the first time, a comprehensive test of the GPS velocity

algorithm based on differenced carrier phase pseudo-range measurements with low cost receivers in a simulated environment. This was to be achieved through the comparison of GPS velocity based on simulated data collected using both dual frequency and low cost single frequency receivers, quantifying the errors associated with both.

It has also been an aim of the project to ascertain the performance of the GPS heave algorithm in a marine environment. It was intended to conduct sea trials that would provide the first full and comprehensive test of the heave algorithm as used with the U-Blox off the shelf low cost receiver through a comparison of its heave output to a range of other heave sensing technologies. These were to include the the TDD GPS heave output from data collected using higher grade dual frequency receivers, the output using inertial based sensors and the output from the highly accurate Applanix POSRS reference system held by the IESSG and discussed in §8.2.2.

An important aspect of the work undertaken was that it should provide the basis of a technology that can have immediate industrial application. It has been a focus of the project from the very outset and has been achieved through the maintenance of a close working relationship with Sonardyne, the industrial partner in the project. It is anticipated that the algorithms developed over the course of the project and the testing conducted on them as part of the PhD will be used in future product developments.

A new heave measurement system based on the U-Blox off the shelf low cost GPS receiver and showing advances in the three areas highlighted above has been achieved. Their performance has been tested in both simulated and marine environments and, as will be seen through the course of this thesis, the research undertaken during the project shows that raw observables logged using low cost GPS receivers can be used to produce a heave estimate that can approach current inertial based systems in terms of accuracy and surpass them in terms of cost, stability and usability.

1.3 Research Methodology

The research methodology detailed in this thesis is as follows:

- Research the field of providing heave compensation for hydrographic survey

vessels to assess the current state of the art.

- Develop Matlab code to recreate current heave compensation technologies based on inertial sensors.
- Identify alternative approaches to providing heave compensation exploiting low-cost GPS receivers and develop algorithms to implement these approaches.
- Conduct a simulator trial using a Spirent Hardware Simulator to assess the performance of the algorithm when used with both dual frequency receivers and single frequency low cost receivers enabling errors associated with receiver dynamics and receiver grade to be quantified.
- Conduct a sea trial of the developed GPS heave algorithm again using both dual frequency and single frequency low cost receivers, the results compared to the developed inertial based algorithm and a highly accurate reference system.

An important aspect of the research conducted during this project has been the development of the two contrasting heave algorithms and the subsequent comprehensive test of the GPS based algorithm when using the U-Blox low cost GPS receiver. The simulator trial allowed the errors associated with receiver dynamics and grade to be quantified and the subsequent sea trial allowed the GPS heave algorithm, processed using data collected from varying grades of receiver, to be compared to the inertial based algorithm and a highly accurate reference.

1.4 Thesis Overview

There follows a brief description of each of the subsequent chapters presented in this thesis.

Chapter 2 explains the principles and techniques involved in inertial navigation systems and the estimation of user velocity and position using these technologies. The strapdown INS is discussed as opposed to gimbaled systems and a full explanation of the strapdown mechanisation process, along with the derivation of the equations

required, is given. Chapter 2 is included to give the necessary background for the understanding of inertial based heave systems.

Chapter 3 gives similar information for the GPS system with a full explanation of how user velocity and position are estimated. Special attention is given to the estimation of user velocity using the GPS and also the likely error sources encountered when doing this, particularly with reference to the signal tracking loops within the receiver. This chapter is required information when understanding the development of the low cost GPS heave algorithm developed during the project.

The last of the background chapters is chapter 4, which explains the processes currently employed within the hydrographic industry to provide vertical reference. The complete process of vertical reference in a classical sense is discussed, including tidal and heave compensation, before attention is given to new and emerging technologies. A discussion of the problems, drawbacks and errors associated with the various techniques is also given.

Chapter 5 details the development of an inertial based heave algorithm that was to be used as an alternative method of measuring vessel heave for comparison with the new GPS velocity based heave algorithm developed for the project. It explains the process of strapdown INS mechanisation coded into Matlab and also gives a thorough analysis of the feedback damping loop applied to the vertical channel of the mechanisation to produce a heave output.

The algorithm for the new method for heave estimation based on GPS velocities developed for this project is given in chapter 6. It details the technique of temporally double differencing carrier phase pseudo-range observations in order to estimate user velocity. The observation equations are derived and a thorough explanation of the algorithm is given with all of the ancillary techniques and algorithms also explained. The final section of this chapter shows how estimated GPS velocities are used to produce a heave output through the implementation of a high pass filter on integrated vertical velocity.

Two trials were conducted on the techniques developed in the thesis and these are discussed and results presented in chapters 7 and 8. Chapter 7 covers a series of trials undertaken using a Spirent hardware simulator that provided the first comprehensive

test of the GPS velocity estimation algorithm of chapter 6 when used with the U-Blox Antaris low cost GPS receiver. The use of the simulator allowed all receiver specific errors to be quantified with comparison to higher grade dual frequency receivers. This trial is the first to use such a simulator to quantify the errors associated with the use of low cost receivers to collect data for a velocity algorithm based on temporally differenced carrier phase pseudo-range observations.

Chapter 8 built on the work in the simulator trial with a comparison of the new GPS based heave algorithm with traditional inertial based heave technologies, developed during the project, and a highly accurate GPS-aided INS reference system. This trial was conducted in Plymouth during August 2006 and assessed the performance of the GPS based algorithm in a marine environment. Tests were undertaken on the accuracy and stability of the GPS based heave output under varying sea conditions and vessel dynamics.

The thesis ends with chapter 9 which contains a summary of the work undertaken and conclusions that can be drawn from it. There is also a section on recommendations for future work.

Chapter 2

Inertial Navigation Systems

2.1 Introduction

Inertial Navigation Systems (INS) have been used extensively for the navigation and positioning of aircraft, ships, missiles and spacecraft for decades (Titterton and Weston, 2004; Jekeli, 2001; Farrell and Barth, 1999). Since inertial technologies were demonstrated in early rocket systems, such as the German V1 and V2 rocket programs of World War II, there have been significant advancements in the technology that have led to greater positioning accuracies and reductions in unit size. This has helped facilitate the emergence of new markets for INS technology such as the supply of reference data for the survey industry. INS technology is now routinely used in hydrographic survey, photogrammetry and land survey and is often coupled with GPS to produce high accuracy position and orientation information.

The use of inertial technology within the hydrographic survey industry has, until recently, been limited predominantly to providing attitude and heading reference and heave compensation. Systems such as those manufactured by VT TSS Ltd, Kongsberg Seatex AS and CDL still provide survey reference for many of the hydrographic survey vessels in operation. Newer and significantly more expensive systems such as the Applanix POSMV employ a GPS-aided INS, which often utilize real time kinematic GPS to provide a three dimensional position and velocity solution which is accurate to a few centimetres provided there are sufficient GPS measurements.

This chapter is included here to give a solid background in the technology and

techniques employed in inertial navigation. A major part of the work in this thesis used inertial based sensors to recreate the heave output that would be seen from any of the commercial units mentioned above. This was done with the aim of using the inertial based heave output to compare to the new heave algorithm developed for use with off the shelf low cost GPS receivers that have the ability to measure and record the raw carrier phase pseudo-range observable. The chapter aims to convey the essential elements of an INS with particular reference to a strapdown system as opposed to a gimbaled gyro-stabilized platform. It will also describe how position and orientation data can be obtained using an INS. A section is also included which shows the current relevant technologies used and their approximate cost, an issue which the development of the GPS based heave algorithm was designed to overcome through the use of low cost GPS receivers.

2.2 The Principles of Inertial Navigation

Certain principles and techniques must be explained before a complete understanding of INS technology is gained. These are laid out in the following sections.

2.2.1 Reference Frames

In order to describe the operation of an INS it is first necessary to define a number of coordinate reference frames. These frames are predominantly cartesian in nature and allow the data recorded by the various sensors of the INS to be transferred into meaningful navigation data. Some coordinate reference frames commonly used when dealing with INS data are given below.

- **Inertial Frame**

The inertial frame is considered to be fixed and non rotating with respect to the stars. It is convenient to describe the inertial frame as having its origin at the centre of the earth and axes X , Y and Z ; the Z axis being coincident with the earth's spin axis. The inertial frame is depicted in figure 2.1.

- **Earth Frame**

The earth frame, as with the inertial frame, has its origin at the centre of the earth and a Z axis coincident with the spin axis of the earth. The earth frame rotates about the Z axis at a rate known as the earth rate ω_{ie} as can be seen in figure 2.2. The rate of this rotation can be calculated as (Farrell and Barth, 1999)

$$\omega_{ie} \approx \frac{1 + 365.25 \text{cycles}}{(365.25)(24)h} \cdot \frac{2\pi \text{rad/cycle}}{3600s/h} \approx 7.292115 \times 10^5 \text{rad/s}$$

with values used relating to the daily earth rotation and the annual revolution about the sun. This value can only be considered approximate due to its reliance on the approximation of the earth's geoid to an ellipsoid.

It should be noted here that positions represented in the earth frame can be expressed either as cartesian coordinates or as latitude, longitude and height relative to an ellipsoid, most commonly the WGS 84 ellipsoid.

- **Navigation Frame**

The navigation frame is a local reference frame and one which is often used in navigation as it describes the familiar axes of North, East and Down. The location of the origin of the navigation frame can be any point on the earth's surface but is often taken to be the current position of the navigation system. This is shown in figure 2.3 which depicts the navigation frame with axes pointing north, east and down at the current latitude and longitude of the navigation system. The navigation frame is then generated by the formation of a tangential plane at this point on the earth's ellipsoid. The X axis is aligned with North, the Y axis with East and the Z axis completes the right-handed system and is aligned with Down. The navigation frame is subject to a rotation with respect to the earth frame referred to as transport rate (ω_{en}). This is caused as the origin moves across the earth's surface with the navigation system.

- **Body Frame** The body frame is an orthogonal axis set with each axis aligned with the roll pitch and yaw axis of the vehicle, the origin being at the vehicle centre of gravity as represented in figure 2.4. Ideally, the three gyros and

accelerometers that form the INS are aligned on each axis of this reference frame. In practice there will be some misalignment between the IMU sensors and the body frame. This should be minimised through careful installation as any misalignment will cause errors in the navigation solution.

2.2.2 Frame Rotations

In order to present the data collected using an INS in ways that may be more useful to the user it is necessary to rotate it from the body frame into a more suitable reference frame. This can be achieved through the implementation of Euler angles or quaternions as explained below.

2.2.2.1 Euler Angles

A common method for rotating data from one reference frame to another is through the use of Euler angles. A transformation using this method may be carried out as three successive rotations about three separate axes (Jekeli, 2001; Titterton and Weston, 2004). For example

- Rotate through angle ψ about reference z -axis
- Rotate through angle θ about reference y -axis
- Rotate through angle ϕ about reference x -axis

where ψ , θ and ϕ are referred to as the Euler angles.

The three rotations described above may be expressed as three direction cosine matrices:

$$\text{Rotation } \psi \text{ about reference } z\text{-axis, } C_1 = \begin{bmatrix} \cos\psi & \sin\psi & 0 \\ -\sin\psi & \cos\psi & 0 \\ 0 & 0 & 1 \end{bmatrix} \quad (2.1)$$

$$\text{Rotation } \theta \text{ about reference } y\text{-axis, } C_2 = \begin{bmatrix} \cos\theta & 0 & -\sin\theta \\ 0 & 1 & 0 \\ \sin\theta & 0 & \cos\theta \end{bmatrix} \quad (2.2)$$

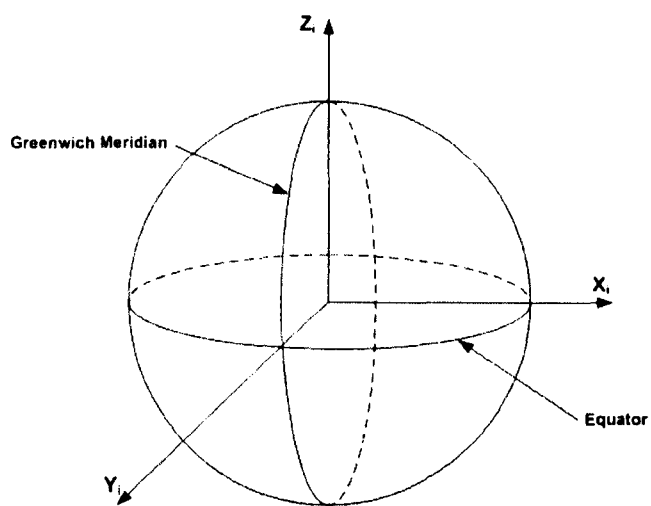


Figure 2.1: The inertial frame

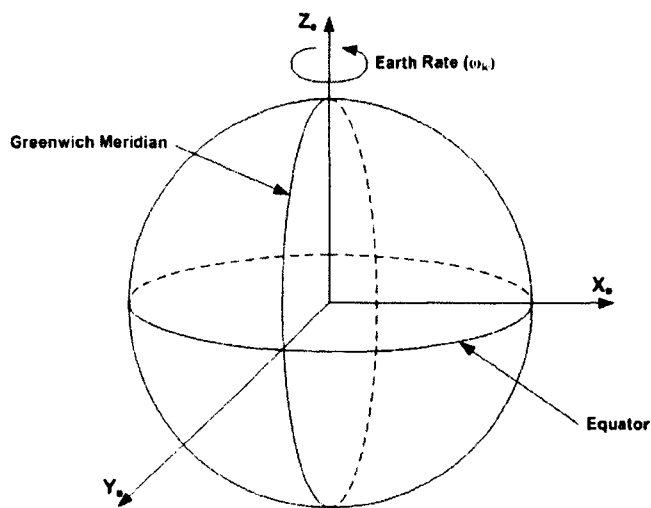


Figure 2.2: The earth fixed frame

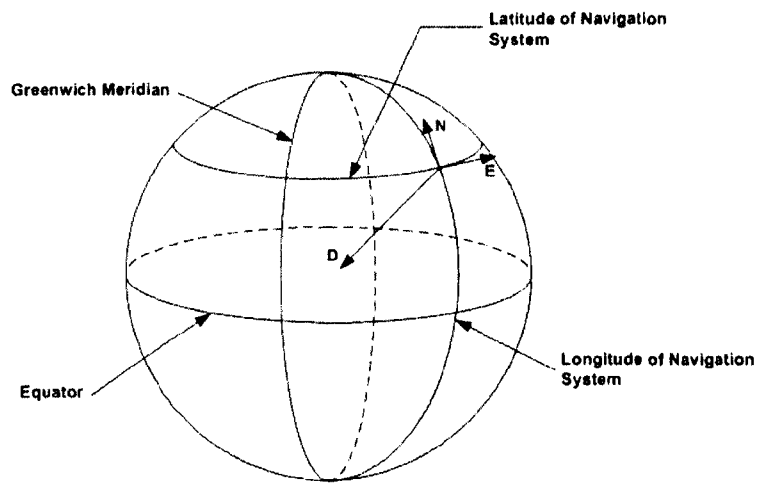


Figure 2.3: The navigation frame

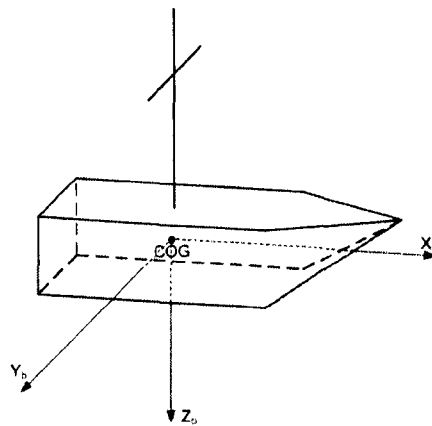


Figure 2.4: The body frame

$$\text{Rotation } \phi \text{ about reference } x\text{-axis, } C_3 = \begin{bmatrix} 1 & 0 & 0 \\ 0 & \cos\phi & \sin\phi \\ 0 & -\sin\phi & \cos\phi \end{bmatrix} \quad (2.3)$$

The complete direction cosine matrix can then be formulated through the product of equations 2.1, 2.2 and 2.3.

$$C = C_1 C_2 C_3 \quad (2.4)$$

In the case of the transformation from body frame to navigation frame, a transformation often used in the mechanisation of IMU data, ψ , θ and ϕ are defined as yaw, pitch and roll respectively. C_n^b can then be written as

$$C_n^b = \begin{bmatrix} \cos\theta \cos\psi & -\cos\phi \sin\psi + \sin\phi \sin\theta \cos\psi & \sin\phi \sin\psi + \cos\phi \sin\theta \cos\psi \\ \cos\theta \sin\psi & \cos\phi \cos\psi + \sin\phi \sin\theta \sin\psi & -\sin\phi \cos\psi + \cos\phi \sin\theta \sin\psi \\ -\sin\theta & \sin\phi \cos\theta & \cos\phi \cos\theta \end{bmatrix} \quad (2.5)$$

A similar direction cosine matrix can be produced that will transform data from the navigation frame into the earth frame (Hide, 2003; Farrell and Barth, 1999). This is often required as GPS data is expressed in the earth frame. For this transformation only two rotations are required: one about the earth's z -axis to bring the y -axis in line with the navigation frame east axis ; and one about the new y -axis to align the z -axis with the navigation frame down axis. This results in the direction cosine matrix C_e^n :

$$C_e^n = \begin{bmatrix} -\sin\lambda \cos\phi & -\sin\phi & \cos\lambda \cos\phi \\ -\sin\lambda \sin\phi & \cos\phi & -\cos\lambda \sin\phi \\ \cos\phi & 0 & -\sin\phi \end{bmatrix} \quad (2.6)$$

Both C_n^b and C_e^n are orthogonal. consequently the transpose of these matrices will transform from navigation frame to body frame (C_b^n) and the earth frame to the navigation frame (C_n^e) respectively.

$$C_b^n = (C_n^b)^T \quad (2.7)$$

$$C_n^e = (C_e^n)^T \quad (2.8)$$

2.2.2.2 Quaternions

An alternative approach to frame rotation is the use of quaternions (Titterton and Weston, 2004; Hide, 2003; Jekeli, 2001). Quaternions are a four parameter representation derived from Euler angles and utilize the fact that any sequence of rotations can be represented as a single rotation about a single axis (Grubin, 1970). They take the form

$$q = \begin{bmatrix} a \\ b \\ c \\ d \end{bmatrix} = \begin{bmatrix} x \sin(\zeta/2) \\ y \sin(\zeta/2) \\ z \sin(\zeta/2) \\ \cos(\zeta/2) \end{bmatrix} \quad (2.9)$$

where x , y and z are the components of a unit vector and ζ is a positive rotation such that a transformation from one coordinate frame to another results from a rotation of ζ radians about the vector $[x \ y \ z]^T$. The quaternion q can also be represented as a four component complex number:

$$q = a\mathbf{i} + b\mathbf{j} + c\mathbf{k} + d \quad (2.10)$$

This is an extension of the more common two component complex number, which contains one real and one imaginary part. In the case of the quaternion d is the real part and a , b and c are orthogonal imaginary parts. The complex conjugate of q is

$$q^* = -a\mathbf{i} - b\mathbf{j} - c\mathbf{k} + d \quad (2.11)$$

The product of two quaternions can be calculated using the usual rules for the multiplication of complex numbers. The product of $q = a\mathbf{i} + b\mathbf{j} + c\mathbf{k} + d$ and $p = e\mathbf{i} + f\mathbf{j} + g\mathbf{k} + h$ is:

$$\begin{aligned} q \cdot p &= -ae - bf - cg + dh + (ah + ed + bg - fc)\mathbf{i} \end{aligned}$$

$$+(bh + fd + ce - ag)\mathbf{j} + (ch + gd + af - be)\mathbf{k} \quad (2.12)$$

$$= \begin{bmatrix} d & -c & b & a \\ c & d & -a & b \\ -b & a & d & c \\ -a & -b & -c & d \end{bmatrix} \begin{bmatrix} e \\ f \\ g \\ h \end{bmatrix} \quad (2.13)$$

Vector quantities expressed in a particular frame, say the body frame, can be transformed into a reference frame, say the navigation frame, using quaternions. Beginning with a vector expressed in the body frame:

$$r^b = x\mathbf{i} + y\mathbf{j} + z\mathbf{k} \quad (2.14)$$

A quaternion $r^{b'}$ is then created such that the complex elements of $r^{b'}$ are equal to the components of r^b , and the real element is set to zero.

$$r^{b'} = x\mathbf{i} + y\mathbf{j} + z\mathbf{k} + 0 \quad (2.15)$$

The quaternion $r^{b'}$ can then be defined in the navigation frame as $r^{n'}$ by:

$$r^{n'} = qr^{b'}q^* \quad (2.16)$$

$$= (a\mathbf{i} + b\mathbf{j} + c\mathbf{k} + d)(x\mathbf{i} + y\mathbf{j} + z\mathbf{k} + 0)(-a\mathbf{i} - b\mathbf{j} - c\mathbf{k} + d) \quad (2.17)$$

Using equation 2.13 this can be written as:

$$r^{n'} = C' r^{b'} \quad (2.18)$$

where

$$C' = \begin{bmatrix} (d^2 + a^2 - b^2 - c^2) & 2(ab - dc) & 2(ac + db) & 0 \\ 2(ab + dc) & (d^2 + a^2 - b^2 - c^2) & 2(bc - da) & 0 \\ 2(ac - db) & 2(bc + da) & (d^2 + a^2 - b^2 - c^2) & 0 \\ 0 & 0 & 0 & 1 \end{bmatrix} \quad (2.19)$$

This can also be written as:

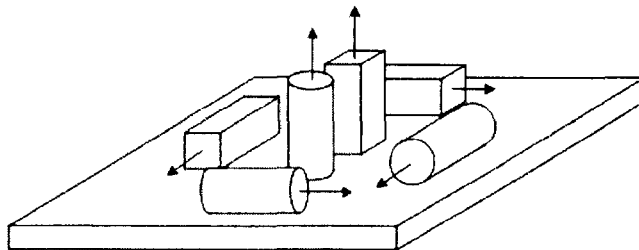


Figure 2.5: Schematic representation of a possible layout of gyros and accelerometers on an IMU platform

$$r^n = Cr^b \quad (2.20)$$

where

$$C = \begin{bmatrix} (d^2 + a^2 - b^2 - c^2) & 2(ab - dc) & 2(ac + db) \\ 2(ab + dc) & (d^2 + a^2 - b^2 - c^2) & 2(bc - da) \\ 2(ac - db) & 2(bc + da) & (d^2 + a^2 - b^2 - c^2) \end{bmatrix} \quad (2.21)$$

The matrix C , above, can be seen to relate directly to that seen in equation 2.5.

Quaternions are often the preferred approach to vector transformation in INS mechanisation as the linear nature of the quaternion differential equations, lack of trigonometric functions and requirement for only four parameters allow for efficient implementation.

2.2.3 The Strapdown Inertial Navigation Concept

Inertial navigation is a form of dead reckoning. Dead reckoning methods of navigation have been employed for centuries, primarily to calculate the position of ships at sea, and involve the plotting of a new position based on: a last known position; vehicle velocity; vehicle course; and the time that that velocity and course are held for.

An INS is made up of two main components: an inertial measurement unit (IMU) and a navigation computer. The IMU consists of three accelerometers and three gyros orthogonally mounted on a platform as depicted schematically in figure 2.5.

The IMU is fitted in the vehicle such that the axis of the sensors on the platform are aligned with those of the body frame. Accelerations and rotations of the vehicle in the body frame are then sensed by the sensors mounted in the IMU.

The gyros output angular rate measured in rads/s, and the accelerometers output accelerations measured in m/s^2 . These measurements can be used, along with an initial position, velocity and attitude, to determine current vehicle velocity, position and attitude. This process takes place in the navigation computer and is explained in more detail in the following section. Broadly speaking it involves the integration of the gyro output to provide angular displacement, and the double integration of the accelerometer output to provide velocity and spacial displacement. These values can then be added to the initial values for attitude, velocity and position provided to the navigation computer.

2.3 System Initialization and Alignment

Initialization and alignment of an INS are required in order that navigation information can be provided by the navigation computer. The differential equations that are employed in the navigation computer calculate angular and spacial displacements from the gyro and accelerometer outputs respectively; without initial quantities upon which to sum these displacements, the information from the navigation computer would not provide absolute position, but relative position. Generally, initialization of an INS is considered to be the providence of position and velocity data, and alignment the process of calculating initial attitude. The process of initialization and alignment of an INS is discussed in many texts such as Titterton and Weston (2004); Hide (2003); Jekeli (2001); Rogers (2000); Farrell and Barth (1999).

2.3.1 Initialization

Initialization of an INS involves providing the system with initial position and velocity data. This can be achieved in many ways but must always result from an external measurement taken by a separate navigation system. In the case where an INS is to be coupled with a GPS receiver, the GPS can be used to gain the required information.

Alternatively these initial quantities may be manually input by the user, for instance if the vehicle is stationary and in a known position.

2.3.2 Alignment

The purpose of alignment is to ascertain the initial attitude (roll, pitch and heading) of the INS. The most difficult of these parameters to calculate is the heading. There are two methods of aligning an INS: self alignment and aided alignment. In the case where it is possible to hold the INS in a fixed and known position alignment can be achieved by the system without external input. Where this is not possible or impractical an aided, or dynamic, alignment can be executed. The self alignment is split into two phases: coarse alignment and fine alignment. As their names suggest they each provide different degrees of accuracy which can be exploited dependent on user requirements.

2.3.2.1 Coarse Alignment

A stationary INS can align itself with respect to the navigation frame either through the use of external sensors to provide an approximation of attitude, or by using the outputs from the INS sensors and known facts about the Earth.

If the INS is stationary with respect to the Earth the accelerometers on the IMU platform will experience no accelerations except those due to gravity. Thus, the platform can be said to be level when the X and Y accelerometers are measuring a zero acceleration. In the case of a strapdown INS the component of the gravity vector that is sensed by the X and Y accelerometers can be used to provide an initial roll and pitch of the system using:

$$\phi = \text{atan2}(-f_y, -f_z) \quad (2.22)$$

$$\theta = \text{atan2}(f_x, \sqrt{f_x^2 + f_y^2}) \quad (2.23)$$

where f_x , f_y and f_z are the three accelerometer outputs aligned with the body frame as shown in 2.4. The accuracy of this form of levelling is dependent on: vehicle

stability; the accuracy of the accelerometers; and the magnitude of any misalignment between the platform and the body frame and each accelerometer mounted on the platform.

In addition, the alignment of a stationary INS with respect to heading can be achieved through measurements from the platform gyros using a process referred to as gyro compassing. In essence this process utilizes the fact that the Earth rotation will be sensed by the platform gyros and that the East component of the Earth rate is zero. If the platform is aligned in azimuth the X-axis gyro is aligned to North and the Y-axis gyro is aligned to East. This results in a zero angular rate sensed by the Y-axis gyro. Therefore, a stationary platform can be said to be aligned with North when the Y-axis gyro senses zero angular rate.

In the case of a strapdown INS attitude information is stored as either a direction cosine matrix or a quaternion. This data can be calculated using the method outlined below (Rogers, 2000).

Assume that the following are available as outputs from the INS

$$g^b = C_n^b g^n \quad (2.24)$$

$$\omega_{ie}^b = C_n^b \omega_{ie}^n \quad (2.25)$$

Then the following can be formed

$$[g^b, \omega_{ie}^b, g^b \times \omega_{ie}^b] = C_n^b [g^n, \omega_{ie}^n, g^n \times \omega_{ie}^n] \quad (2.26)$$

Which, transposed, yields:

$$[g^b, \omega_{ie}^b, g^b \times \omega_{ie}^b]^T = C_b^n [g^n, \omega_{ie}^n, g^n \times \omega_{ie}^n]^T \quad (2.27)$$

Therefore

$$C_b^n = [g^n, \omega_{ie}^n, g^n \times \omega_{ie}^n]^{-T} [g^b, \omega_{ie}^b, g^b \times \omega_{ie}^b]^T \quad (2.28)$$

C_b^n can then be solved for using the following gravity and Earth rotation vectors for the navigation frame

$$g^n = \begin{bmatrix} 0 \\ 0 \\ g \end{bmatrix} \quad (2.29)$$

where g is the local gravity vector in the navigation frame, which can be calculated based on global gravity models (Farrell and Barth, 1999; Jekeli, 2001; Titterton and Weston, 2004).

$$\omega_{ie}^n = \begin{bmatrix} \omega_{ie} \cos L \\ 0 \\ -\omega_{ie} \sin L \end{bmatrix} \quad (2.30)$$

where L is the system latitude. The cross product of these two vectors is now given by

$$g^n \times \omega_{ie}^n = \begin{bmatrix} 0 \\ g\omega_{ie} \cos L \\ 0 \end{bmatrix} \quad (2.31)$$

The inverse transpose matrix in equation 2.28 can then be written as

$$[g^n, \omega_{ie}^n, g^n \times \omega_{ie}^n]^{-T} = \begin{bmatrix} \frac{\tan L}{g} & \frac{1}{\omega_{ie} \cos L} & 0 \\ 0 & 0 & \frac{1}{g\omega_{ie} \cos L} \\ \frac{1}{g} & 0 & 0 \end{bmatrix} \quad (2.32)$$

This matrix can now be substituted into equation 2.28 to compute the direction cosine matrix C_b^n .

This method of alignment relies on the INS having gyros of sufficient quality that they are able to sense Earth rate and also on the INS being stationary during the alignment process. Inertial based systems that are used in the hydrographic survey industry cannot be stationary during alignment due to wave motion. In this case external sensors are used to aid the alignment of the inertial system, a process explained in §2.5.

2.3.2.2 Fine Alignment

Fine alignment is the process of refining the estimation of system attitude calculated during coarse alignment. Coarse alignment is achievable in a few seconds and leaves only small angle differences between indicated and true attitude. These differences are primarily caused by systematic errors in the outputs of the gyros and accelerometers that cannot be calibrated during manufacture. Once again using a static system, the sensor errors can be defined as

$$\delta f^n = f^n - \hat{f}^n \quad (2.33)$$

$$\delta \omega^n = \omega^n - \hat{\omega}^n \quad (2.34)$$

where f^n and ω^n are the known accelerations and rotation rates experienced by the stationary system at the current position, and \hat{f}^n and $\hat{\omega}^n$ are the measured quantities from the platform sensors.

A Kalman filter (Maybeck, 1979; Gelb, 1982) can then be driven by these errors allowing the calculation of a refined estimation of system attitude. This process is explained in detail in Jekeli (2001).

This process of fine alignment is for use in stationary INS systems where f^n and ω^n can be calculated. In the case of INS sensors used in the marine environment stationary alignment is not possible

2.4 System Mechanisation in the Navigation Frame

It is possible to express INS derived position and velocity in any of the reference frames mentioned in §2.2.1. For the purposes of navigation, however, INS data is best expressed in the navigation frame. In navigation frame mechanisation velocity (v^n) is expressed in navigation coordinates with component parts v_N , v_E and v_D and position is expressed as latitude (λ), longitude (ϕ), and height (h).

When INS systems are in use as part of a heave motion sensor the mechanisation of the accelerometer and gyro outputs provides position estimation in three channels as detailed above. The height channel is used to produce an estimation of vessel heave through the implementation of a damping loop within the meachanisation process of

that channel. This process is explained in detail in chapter 5 where the development of the INS heave algorithm used in this thesis is discussed. This section details how standard mechanisation is undertaken within an INS as a prelude to the vertical channel damping given in chapter 5.

The process of navigation frame mechanisation is shown in figure 2.6 where notation for angular rates uses two subscripted letters and one superscripted letter. Of the two subscripted letters the first denotes the reference frame, the second denotes the frame of which the rotation is being measured. The superscripted letter denotes the frame in which the angular rotation is expressed. Example: ω_{ib}^b denotes the angular rate of the body frame with respect to the inertial frame expressed in the body frame. The outputs from the platform gyros (ω_{ib}^b) can be seen on the far left of the diagram and are used to calculate the angular rate of the body frame with respect to the navigation frame using

$$\omega_{nb}^b = \omega_{ib}^b - C_b^n [\omega_{ie}^n + \omega_{en}^n] \quad (2.35)$$

ω_{ie}^n represents the earth rate expressed in the navigation frame and ω_{en}^n represents the transport rate.

$$\omega_{ie}^n = \begin{bmatrix} \omega_{ie} \cos \lambda & 0 & -\omega_{ie} \sin \lambda \end{bmatrix}^T \quad (2.36)$$

$$\omega_{en}^n = \begin{bmatrix} \frac{v_E}{R_\lambda + h} & \frac{-v_N}{R_\phi + h} & \frac{v_E \tan \lambda}{R_\lambda + h} \end{bmatrix}^T \quad (2.37)$$

where R_λ is the meridian radius of curvature at a given latitude and R_ϕ is the transverse radius of curvature.

C_b^n is now calculated using one of the methods described in §2.2.2. When using Euler angles, C_b^n propagates through the equation:

$$\dot{C}_b^n = C_b^n \Omega_{nb}^b \quad (2.38)$$

where Ω_{nb}^b is the skew symmetric form of ω_{nb}^b ,

$$\Omega_{nb}^b = \begin{bmatrix} 0 & -\omega_z & \omega_y \\ \omega_z & 0 & -\omega_x \\ -\omega_y & \omega_x & 0 \end{bmatrix} \quad (2.39)$$

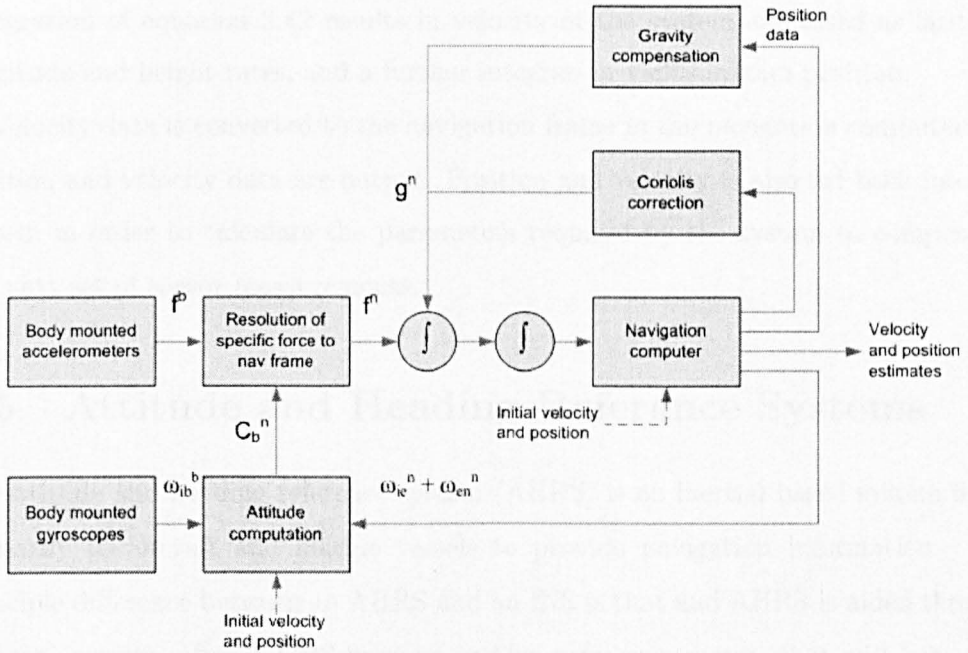


Figure 2.6: Strapdown INS mechanisation in the navigation frame (Titterton and Weston, 2004)

If, as is more often the case, quaternions are to be used for attitude representation,

\dot{q} can be calculated using:

$$\dot{q} = 0.5q \cdot p_{nb}^b \quad (2.40)$$

where

$$p_{nb}^b = \begin{bmatrix} \omega_{nb}^b \\ 0 \end{bmatrix} \quad (2.41)$$

and the updated quaternion parameters can be used to calculate the updated C_b^n .

C_b^n is then used to rotate the platform accelerometer outputs from the body frame to the navigation frame. The force expressed in the navigation frame can then be compensated for the local gravity vector (g^n), calculation of which is given in Jekeli (2001), and Coriolis acceleration.

$$\dot{v}^n = f^n - (2\omega_{ie}^n + \omega_{en}^n) \times v^n + g^n \quad (2.42)$$

Integration of equation 2.42 results in velocity of the system expressed as latitude, longitude and height rates, and a further integration yields system position.

Velocity data is converted to the navigation frame in the navigation computer and position and velocity data are output. Position and velocity is also fed back into the system in order to calculate the parameters required by the system to compensate the next set of sensor measurements.

2.5 Attitude and Heading Reference Systems

An attitude and heading reference system (AHRS) is an inertial based system fitted primarily to aircraft and marine vessels to provide navigation information. The principle difference between an AHRS and an INS is that an AHRS is aided through external sensors, often a GPS receiver and/or a magnetometer, that will help with system initialization and alignment and also controls sensor alignment during operation.

AHRS units often output heave along with information concerning the attitude of the vessel. Indeed, it is these systems that form the primary method of heave estimation in the hydrographic survey industry.

2.5.1 AHRS Alignment and Operation

As has been previously stated, the alignment of an INS is based on the sensing of the local gravity acceleration and a process of gyro compassing that senses Earth rate and can align the INS to true North from the proportion of the Earth rate that is measured by each of the X-axis and Y-axis gyros. This alignment process requires a stationary IMU platform so that the sensing of the local gravity acceleration and Earth rate are not confused with accelerations and turn rates due to platform motion.

In the case of an AHRS fitted to a vessel the platform can never be truly stationary whilst the vessel is not in dry dock. For this reason the system is velocity aided, usually by GPS, to compensate for platform motion and allow alignment of the system. The following derivation of the velocity aiding equations are taken from Luscombe (2003).

Accelerations in the body frame due to platform motion are compensated for

through a differentiated velocity provided by the aiding sensor. From the equation presented in 2.42 the acceleration in the body frame due to motion can be calculated by

$$f_{motion}^n = \dot{v}^n + (2\omega_{ie}^n + \omega_{en}^n) \times v^n \quad (2.43)$$

where \dot{v}^n is provided by differentiating the aiding sensor velocity, which cannot sense accelerations in the inertial frame. Compensation of the body frame accelerations sensed by the accelerometers (f^n) for the accelerations due to platform motion (f_{motion}^n) allows the sensing of the local gravity acceleration in isolation.

Heading alignment is achieved through the calculation of platform rotations due to platform velocity across the curved surface of the Earth. Given a platform velocity in the navigation frame with a North velocity component (v_N) and an East velocity component (v_E), the rates of change of latitude and longitude are given by

$$\dot{\lambda} = \frac{v_N}{R_\lambda} \quad (2.44)$$

$$\dot{\phi} = \frac{v_E}{R \cos \lambda} \quad (2.45)$$

where $\dot{\lambda}$ and $\dot{\phi}$ are the rate of change of latitude and longitude respectively, R_λ is the meridional radius and R is the radius of the Earth at the equator. It is possible to show that the angular rate of the platform due to the change in latitude and longitude is

$$\omega_{motion} = [\dot{\phi} \cos \lambda \quad -\dot{\lambda} \quad -\dot{\phi} \sin \lambda]^T \quad (2.46)$$

Therefore

$$\omega_{motion} = \left[\frac{v_E}{R} \quad \frac{-v_N}{R_\lambda} \quad \frac{-v_E \tan \lambda}{R} \right]^T \quad (2.47)$$

This yields angular rotation in the body frame of the y-axis due to platform motion:

$$\omega_y = -\frac{v_N}{R_\lambda} \quad (2.48)$$

Rotation about the x-axis due to Earth rate is given by

$$\omega_x = \Omega \cos \lambda \quad (2.49)$$

where Ω is the Earth rate. Resulting in a heading error, $\Delta\phi$ of

$$\Delta\phi = \frac{\omega_y}{\omega_x} \quad (2.50)$$

$$= \frac{v_N}{R_\lambda \Omega \cos \lambda} \quad (2.51)$$

During operation of the AHRS unit velocity aiding is maintained in order that the platform can remain level through the sensing of the local gravity acceleration, an important point for the purposes of heave measurement using an AHRS unit as it is this that causes turn induced heave in an inertial heave sensor. Lateral accelerations caused by vessel turns bring about a distortion in the measurement of the local gravity acceleration, resulting in some of the lateral acceleration being sensed in the vertical channel of the AHRS. This large input to the heave algorithm results in a ‘ringing’ of the heave output due to heave filter transient characteristics, which are discussed in §5.3.1.2.

2.6 Grades of IMU

IMU technologies can be classified into three main grades.

- Low cost
- Tactical grade
- Navigation grade

Low cost IMUs are constructed using Micro-electromechanical Systems (MEMS) technology. This technology creates sensors that produce outputs based on vibration and which contain no moving parts. This means that they are more rugged and can be mass produced in integrated circuits, resulting in very cheap sensors and, hence, cheap IMUs. This grade of IMU are rarely used in the marine survey industry due to their relatively low performance; low cost IMUs could not be used to provide a heave output

for instance. Recent research however, notably Hide (2003), has attempted to extract better performance from these sensors by aiding them with GPS measurements.

Tactical grade IMUs get their name from their main application area. They are predominantly designed for the military market and are often fitted to tactical missiles for their short term navigation requirements. Tactical grade IMUs are of a size that means they can also be utilized for civilian applications and this has been the case over recent years. They cannot, however, provide long term navigation data and their cost still prohibits widespread civilian exploitation. It is this grade of IMU that is used most extensively in marine survey. They are contained within many of the GPS aided INS systems currently on the market, for example the Applanix POSMV system uses a Litton LN200 IMU. They are also capable of providing an adequate heave output and are often used in Attitude and Heading Reference Systems.

Navigation grade IMUs represent the best inertial technology currently available. They are often large in size and expensive to purchase. This means that their primary application area is in the navigation of military and civilian aircraft where financial requirements are less restrictive. A Honeywell CIMU navigation grade IMU is held by the IESSG and forms part of the Applanix POSRS system purchased to provide the best possible truth trajectory in research trials. This system has been utilized as part of this project to provide a truth trajectory for the sea trials undertaken in Plymouth and is explained in §8.2.2.

Examples of each grade can be seen in table 2.1 with their performance and cost data. The data in this table is taken from the manufacturers accuracy data published in the data sheets for each IMU.

The cost of the tactical grade IMU gives a rough idea of the cost of heave measurement systems. This is the grade of inertial technology they employ and their cost ranges from £12,000 to £25,000. It is with this range of costs that any heave measurement system produced as an outcome of this project must compete.

Grade of IMU	Low Cost	Tactical	Navigation
Example	Systron MMQ50	Honeywell HG1700	Honeywell CIMU
Dimensions (mm)	48x48x65	94dia, 74ht	168x192x134
Cost	≈£3,500	≈£14,000	≈£60,000
Gyro	MEMS	Fibre Optic	Ring Laser
Bias (°/hr)	50-200	1-10	0.0035
Scale Factor Error	≤ 5000ppm	150ppm	5ppm
Noise	$20.88^\circ/\text{hr}/\sqrt{Hz}$	$0.125\text{-}0.5^\circ/\sqrt{hr}$	$0.0025^\circ/\sqrt{hr}$
Accelerometer	Silicon	Silicon	Silicon
Bias (mg)	≤ 3	1-2	0.05
Scale Factor Error	≤ 5000ppm	300ppm	100ppm
Noise (mg/ \sqrt{Hz})	0.5	-	-

Table 2.1: IMU grades: performance and cost data

Chapter 3

The Global Positioning System

3.1 Introduction

The Global Positioning System (GPS) is capable of providing a user with instantaneous position and velocity estimates anywhere on or near the Earth. The position and velocity are calculated based on a process of trilateration using ranges derived from signals which are continuously transmitted from a constellation of satellites.

A sound knowledge of GPS was developed over the course of the work in this thesis, particularly in the processing of raw GPS observables to produce position and velocity. The approach to heave measurement designed as part of the work in this thesis relies on the processing of temporally differenced carrier phase pseudo-range data to produce an accurate velocity estimate that can be integrated to produce relative position. This method of heave measurement has provided significant advantages over the traditional approach, which is based on inertial technologies.

This chapter aims to cover all the elements of the system essential to fully understanding the research presented in this thesis. Particular emphasis is placed on the derivation of equations used to position using the GPS observables and the error sources associated with this type of processing. For a more detailed description of the GPS the reader is directed to prominent texts on the subject such as Parkinson and Spilker (1996a,b); Kaplan (1996); Farrell and Barth (1999); Hoffmann-Wellenhoff et al. (2001); Misra and Enge (2004).

3.2 GPS Overview

3.2.1 The Basic Concept

The GPS project was initiated in 1973 when the US Department of Defense instructed the Joint Programs Office to undertake the task of establishing a space based navigation system. From this undertaking was born the present system: Navigation System with Timing and Ranging Global Positioning System, now universally abbreviated to GPS. The very first launch of a GPS satellite took place on 22 February 1978. This was a navigation development Block I satellite of which there were eventually eleven in operation. The first of the Block II satellites that formed the full system was declared operational on 10 August 1989. Initial operational capability was announced at the end of 1993, and full operational capability at the end of 1994 (Parkinson and Spilker, 1996a).

The GPS was designed to provide instantaneous navigation information to users in all weather conditions, twenty-four hours a day, anywhere on or near the Earth. In the most basic manifestation of the system this is achieved through the use of ranges calculated from the transit time of signals transmitted from the orbiting GPS satellites to the user receiver. These ranges are termed pseudo-ranges because they are not corrected for satellite and receiver clock errors. The position of the satellites is known because they follow predetermined orbital paths and hence, with enough pseudo-ranges, user position can be calculated through trilateration.

Trilateration is possible using three ranges but, as already mentioned, the pseudo-ranges are not corrected for any difference between satellite and receiver clocks. This difference in time must be solved for when calculating position and has the effect of introducing a fourth unknown into the GPS range equations. It is therefore necessary to have ranges from four GPS satellites before a position can be obtained.

3.2.2 GPS Hardware

The GPS that is currently in operation consists of three separate segments:

- The space segment

Master control station	Falcon Air Force Base, Colorado Springs, CO
Master control station (backup)	Gaithersburg, MD
Monitor station	Schrifer Air Force Base, Colorado Springs, CO
Remote monitor station	Cape Canaveral, FL
Remote monitor station	Hawaii
Remote monitor station	Diego Garcia
Remote monitor station	Kwajalein
Remote monitor station	Ascension Island
Ground antenna	Cape Canaveral, FL
Ground antenna	Ascension Island
Ground antenna	Diego Garcia
Ground antenna	Kwajalein

Table 3.1: Location of the elements of the control segment (Farrell and Barth, 1999)

- The control segment
- The user segment

Each of these is explained in the following subsections.

3.2.2.1 The Space Segment

The space segment consists of the GPS satellites orbiting the Earth. There are 24 operational satellites orbiting in six planes (four satellites per plane) each at an angle of 55° to the equator. The six planes have approximately equal spacing around the equator resulting in a nominal separation of 60° between each (Farrell and Barth, 1999). The satellites have a near circular orbit at an approximate altitude of 20,200 km. This constellation of satellites is designed to ensure that it is possible to view, and hence range to, at least four satellites from any position on or near the Earth's surface.

The satellites themselves provide a platform for the equipment necessary to allow a receiver to compute pseudo-range between itself and the satellite. This equipment primarily consists of an atomic clock to allow accurate time keeping and a transceiver

to receive data from the control segment, and transmit signals to the user segment. The signals transmitted to the user segment are received on two separate carrier waves: L1 and L2. These are modulated with timing codes known as C/A and P and it is these timing codes which are explicitly used to calculate pseudo-ranges. Superimposed on the timing codes is the navigation message. This message contains ephemeris data for the satellite from which it is transmitted, and satellite clock error polynomials which describe the behaviour of the satellite clock with respect to GPS system time.

3.2.2.2 The Control Segment

The control segment comprises a Master Control Station (MCS), six monitor stations and four ground antennas. The location of the various elements of the control segment is represented in table 3.1. The purpose of the control segment is to monitor the health and status of the space segment. To do this the monitor stations monitor the signals transmitted by the satellites and relay them to the MCS. The MCS then calculates the satellite orbit parameters and clock corrections. This data is passed to the ground antennas for upload to the satellites. The satellites then transmit this data in the navigation message to the user segment, along with ranging signals.

3.2.2.3 The User Segment

The user segment of the GPS is made up of all the antennas and receivers currently used to receive and decode the GPS signals from the space segment. These signals can then be used within the receiver processor to calculate user position and velocity. This process is described in detail in §3.5. Because a GPS receiver is a simplex device, the GPS space segment is able to serve an infinite number of user segment receivers.

A further point to add at this stage is that there exist a plethora of different GPS receivers in what is now a very mature consumer market. These can be generally categorized into two distinct groups, however: low cost and geodetic. Low cost receivers are cheap, small, readily available and have recently begun to offer access to the raw GPS observables; this fuels their increasing use in more precise applications. Geodetic grade receivers have traditionally provided the highest quality observables

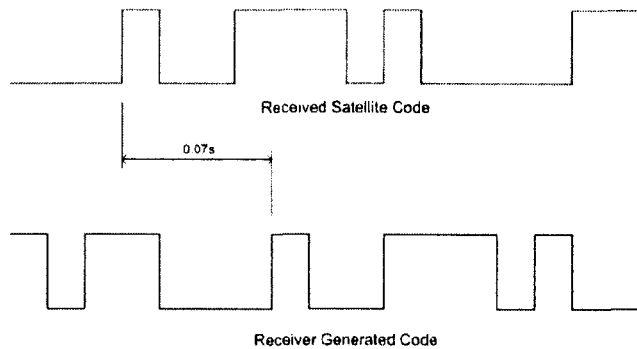


Figure 3.1: Comparison of received satellite signal and receiver generated signal

to the survey industry and are priced accordingly. They offer access to all the raw GPS observables, often at various data rates, which can go as high as 100Hz. As a quick comparison low cost receivers cost approximately £200, and geodetic receivers can be in the order of £10,000.

3.3 GPS Observables

The GPS satellites are continuously transmitting an RF signal that can be utilised by a user receiver to determine position and velocity estimates. The receiver uses the signal from each satellite to calculate the range between it and the satellite along a direct line of sight at discrete time intervals. These ranges are the GPS observables and are based on measured time or phase differences between the code received from the satellite, and one generated within the receiver.

3.3.1 The Code Pseudo-range Observable

In practical terms the pseudo-range measurement is calculated within the receiver by comparing the receiver generated code with that received from the transmitting satellite. The principle is that receiver code is generated at the same time as transmission of the satellite code and by comparing the two and calculating the time offset between them, as represented in figure 3.1, it is possible to determine the transit time of the signal from satellite to receiver. This transit time can then be scaled by the velocity of light in vacuo to give the line of sight range between receiver and satellite.

This process is complicated by the fact that different time frames are in use within the GPS. Satellites are each installed with a precise atomic clock which operates in a satellite time frame (t). The time of transmission of all signals transmitted from the satellites is given with reference to this time frame. Receivers also contain their own quartz clock although this is significantly less accurate than the atomic clocks fitted to the satellites. The reception times of each signal are recorded with reference to the receiver clocks in the receiver time frame (τ). Both these time frames are related to the GPS system time (T) by:

$$T = t + \delta t \quad (3.1)$$

$$T = \tau + \delta \tau \quad (3.2)$$

where δt denotes the satellite clock offset and $\delta \tau$ denotes the receiver clock offset.

There follows a derivation of the pseudo-range observation equation which follows the notation and convention of Bingley (1998). For the purposes of this derivation a superscript will denote a satellite related term and a subscript will denote a receiver related term. It is necessary to define two terms related to the ranging from receiver to satellite: namely pseudo-range and geometric range.

- Pseudo-range (PR) can be defined as the difference between the time of signal reception in the receiver time frame (τ_r) and the time of signal transmission in the satellite time frame (t^s) scaled by the speed of light in vacuo (c).
- Geometric range (ρ) is defined as the difference between the time of signal reception in the GPS time frame (T_r) and the time of signal transmission in the GPS time frame (T^s) scaled by the speed of light in vacuo.

These definitions lead to the equations:

$$PR_r^s = c(\tau_r - t^s) \quad (3.3)$$

$$\rho_r^s = c(T_r - T^s) \quad (3.4)$$

substituting equations 3.1 and 3.2 into equation 3.4 yields:

$$\rho_r^s = c((\tau_r + \delta\tau_r) - (t^s + \delta t^s)) \quad (3.5)$$

rearranging gives:

$$\rho_r^s = c(\tau_r - t^s) - c(\delta\tau_r - \delta t^s) \quad (3.6)$$

now substituting equation 3.3 into equation 3.6 and rearranging results in the basic pseudo-range equation.

$$PR_r^s = \rho_r^s - c[\delta\tau_r - \delta t^s] \quad (3.7)$$

This basic pseudo-range equation needs a more rigorous definition of the time frames involved before it can be considered complete. Each of the terms in equation 3.7 can be associated with its time frame thus:

- PR_r^s is the pseudo-range measured at the receiver in the receiver time frame, ie $PR_r^s(\tau_r)$.
- ρ_r^s is the geometric range calculated using the GPS time of reception at the receiver and the GPS time of transmission from the satellite, ie $\rho_r^s(T^s, T_r)$.
- $\delta\tau_r$ is the receiver clock offset in the receiver time frame, ie $\delta\tau_r(\tau_r)$.
- δt^s is the satellite clock offset measured in the satellite time frame, ie $\delta t^s(t^s)$.

If these more explicitly defined terms are substituted into equation 3.7 then a more rigorous pseudo-range equation results. More terms can be added to this equation to account for common error sources. It is sufficient here to generalise these into three terms: ionospheric delay (I), tropospheric delay (T) and miscellaneous errors (ϵ). These errors and the methods of compensation for them are discussed in detail in §3.4.

$$PR_r^s(\tau_r) = \rho_r^s(T^s, T_r) - c[\delta\tau_r(\tau_r) - \delta t^s(t^s)] + I + T + \epsilon \quad (3.8)$$

3.3.2 The Carrier Phase Pseudo-range Observable

The code signal is modulated onto a carrier signal within the satellite using binary bi-phase modulation. It is this modulated carrier signal that is transmitted from the transceiver mounted on the satellite. By measuring the phase of the carrier signal an observable that can be considered much more precise than that of the code pseudo-range is produced. The carrier phase pseudo-range measurement is the difference between the phase of the carrier signal generated within the receiver, and that which is received from the satellite. This pseudo-range consists of a fractional carrier phase element ($\phi_r^s(\tau_r)$) and an integer number of cycles termed the integer ambiguity (N_r^s). The integer ambiguity is so called because the number of integer cycles is ambiguous and cannot be determined from the carrier phase pseudo-range measurement.

This new pseudo-range measurement can be substituted into the basic pseudo-range equation shown in equation 3.7 yielding:

$$\phi_r^s(\tau_r) = \frac{f}{c} \rho_r^s(T^s, T_r) - f[\delta\tau_r(\tau_r) - \delta t^s(t^s)] + N_r^s \quad (3.9)$$

Equation 3.9 shows the basic carrier phase pseudo-range equation. In reality the receiver will actually make an arbitrary guess at the value of the integer ambiguity when it first locks on to each satellite. Thus N_r^s represents the correction required to that arbitrary guess in order that it represents the true integer ambiguity. Adding in the error terms introduced in equation 3.8 yields the full carrier phase pseudo-range equation:

$$\phi_r^s(\tau_r) = \frac{f}{c} \rho_r^s(T^s, T_r) - f[\delta\tau_r(\tau_r) - \delta t^s(t^s)] + N_r^s + I + T + \epsilon \quad (3.10)$$

3.3.3 The Pseudo-range Rate Observable

The Doppler shift is a measure of the frequency shift of the carrier signal and is measured routinely within the GPS receiver as an output from the carrier tracking loop (Parkinson and Spilker, 1996a). The Doppler shift of the signal from the nominal L_1 or L_2 frequency is caused by a number of factors including motion of the satellite, motion of the user receiver and errors due to the drift of satellite and receiver clocks.

Ignoring the error terms and time frames and scaling any frequency shift by the transmitted frequency over the speed of light in vacuo yields the Doppler equation.

$$D_r^s = - \left(\frac{v^s - v_r}{c} \cdot e_r^s \right) L \quad (3.11)$$

where e_r^s is the line of sight unit vector and L is the nominal transmitted frequency.

The measured Doppler shift can then be expressed as a pseudo-range rate by incorporating the receiver clock drift term:

$$PR_r^s = (v^s - v_r) \cdot \frac{r^s - r_r}{|r^s - r_r|} + \delta\dot{\tau}_r + \epsilon \quad (3.12)$$

3.3.4 Quality of Recorded Observables

Consideration of a generalized receiver architecture concerning the measurement of the various observables of the GPS can give some indication of their accuracy and reliability. Generally the measurement of the code pseudo-range observable utilizes a delay lock loop (DLL) and measurement of carrier phase based observables utilizes a phase lock loop (PLL) although carrier phase tracking can also be undertaken using a frequency lock loop. There follows a broad description of the measurement of the GPS observables using feedback control loops as it relates to the work presented in this thesis. For a more thorough analysis read van Dierendonck (1996) or Misra and Enge (2004) although much of the details of receiver architecture are proprietary and specific to particular manufacturers.

3.3.4.1 Signal Tracking with Feedback Control Loops

After signal acquisition GPS receivers utilise a DLL to track the code signal from each satellite and a PLL to track the carrier signal. Both DLLs and PLLs are feedback control loops that use an error signal which is fed back in order to control a process. In the case of a DLL the error signal is the time difference between the code signal received from a satellite and the replica code generated within the receiver. Figure 3.2 shows a simplified block schematic representation of a delay lock loop. In figure 3.2

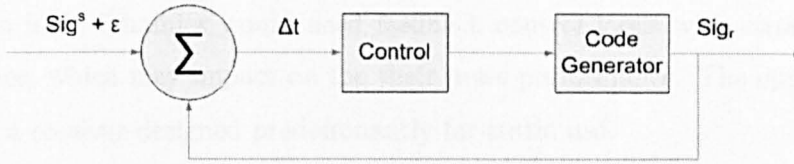


Figure 3.2: Block schematic representation of a delay lock loop

the DLL is used as a loop filter producing a clean signal output from a noisy signal input, but the operation of this loop filter adequately demonstrates the principle of a DLL. The noisy received code signal from the satellite ($\text{Sig}^s + \epsilon$) is compared to the code generated within the receiver (Sig_r) to produce a signal proportional to the time difference between the two (Δt) which is a measure of signal transit time and hence pseudo-range. Based on this difference signal the control element of the loop issues commands to the code generator or, more precisely, the code generator clock to slew the generated code to match the received code.

The operation of a PLL is broadly the same as that of a DLL except that the error signal in this instance is the difference in phase between the received carrier signal and the replica carrier generated within the receiver, and that the process to be controlled is the numerically controlled oscillator within the PLL that governs the phase of the replica carrier. Here, the error signal gives a measure of carrier phase, although this measurement is ambiguous in range terms because only the fractional part of a cycle is recorded and the integer number of complete cycles is unknown.

3.3.4.2 Feedback Control Loop Performance

Analysis of feedback control loop performance falls into two categories: noise performance and dynamic performance (Kaplan, 1996; Misra and Enge, 2004). These two performance characteristics are in direct conflict within a feedback control loop in that better noise performance will lead to a more sluggish dynamic performance and vice-versa. This results in a trade off between the two which can be tuned to receiver requirements.

The tuning of this trade off will have a direct impact on the quality and integrity of the recorded GPS observables within a given receiver. For example, a receiver designed

to undergo high dynamics would need feedback control loops with strong dynamic performance, which may impact on their noise performance. The opposite could be true of a receiver designed predominantly for static use.

Errors in the measurement of the GPS observables that occur due to the receiver itself can be broadly split into two sections: system noise and tracking loop noise.

System noise is made up of the noise introduced by the antenna, the cables and the electronic componentry within the receiver. Formulae exist with which to accurately quantify this noise for a given receiver (Langley, 1997) but this is a difficult task in reality as the parameters required for the calculations are not easy to ascertain. As a generalisation for the purposes of this thesis the system noise created by a low cost receiver such as the U-Blox Antaris can be said to be greater than that created by better grade receivers such as the Novatel OEM4 or Leica SR 530. System noise has a great effect on the measurement of the code phase pseudo-range observable, but little effect on the accuracy of the measurement of the carrier phase pseudo-range observable although it does affect the dynamic range of the carrier tracking loops (Kunysz, 1998).

Tracking loop noise is dependent on two factors: tracking loop bandwidth and signal-to-noise ratio of the GPS signal. This is demonstrated by the approximation of the formulae for the calculation of the noise contributed by the delay lock loop and phase lock loop taken from Langley (1997).

$$\sigma_{DLL} = \sqrt{\frac{\alpha B_L}{c/n_0}} \lambda_c \quad (3.13)$$

$$\sigma_{PLL} = \sqrt{\frac{B_L}{c/n_0}} \lambda_c \quad (3.14)$$

It is clear that the error in both these loops is very similar. The σ_{DLL} and σ_{PLL} are measured in metres, B_L is the loop noise bandwidth in Hz, c/n_0 is the carrier-to-noise density (signal-to-noise ratio) of the signal expressed as a ratio ($=10^{\frac{C/N_0}{10}}$), λ_c is the carrier wave length and α is the delay lock loop discriminator factor. As a guide to carrier loop noise values σ_{PLL} is 0.6 mm when C/N_0 is 45 dB-Hz and carrier tracking loop bandwidth is 15 Hz (values not unexpected in typical GPS receivers).

In summary it can be said that system noise can have a direct impact on the

quality of the code phase pseudo-range observation but not on the quality of the carrier phase pseudo-range observation, although it can affect the dynamic range of the carrier tracking loop. Noise introduced by the carrier tracking loop is small and will not impact heavily on the quality of the carrier phase pseudo-range observable, but the quality of the componentry used in the loop, such as the numerically controlled oscillator, can have a significant influence on the carrier tracking loop output (van Dierendonck, 1996).

In the case of the low cost receiver the carrier phase observation would be expected to be of a slightly degraded quality compared to that recorded using a higher grade receiver, perhaps with an increased noise level due to lower grade components. The effect of increased system noise on the dynamic range of the carrier tracking loop will result in a carrier phase pseudo-range observable with a greater number of cycle slips due to signal loss and could result in greater noise levels due to the need to increase tracking loop bandwidth.

3.4 GPS Error Sources

GPS measurements recorded by the receiver are corrupted by a number of various error sources. In most cases techniques are available that can help to mitigate these errors and so improve the integrity and accuracy of the recorded observables. In this section the main error sources are discussed along with any mitigation techniques available.

As part of the GPS heave algorithm developed during this thesis and presented in chapter 6 both stand-alone user position and velocity are estimated. Stand-alone position requires that code pseudo-ranges are corrected for absolute errors whereas the velocity estimation uses temporally differenced carrier phase pseudo-ranges and so the rate of change of each error source is required. As part of the discussion of each error source in this section there is also an assessment of the rate of change of that error source and the likely impact of it upon user velocity estimation.

3.4.1 Satellite Errors

Errors emanating from the satellites fall into two main categories, namely satellite clock offset and ephemeris error. These both add bias terms into the measurement of the GPS observables when used to correct the code pseudo-range observable and, in the case of satellite clock error, can also have a significant effect on velocity estimation if unmitigated.

3.4.1.1 Satellite Clock Offset

The timing on board the satellites of the GPS is provided by highly accurate atomic clocks. These clocks are very stable but there will inevitably be some deviation from GPS time which can be as large as 1 ms (Parkinson and Spilker, 1996a). The deviation of each satellite's clock from GPS time is monitored by the control segment, which then calculates up to three polynomial terms relating to clock bias, clock drift and clock drift rate. These data are then uploaded to the satellites for broadcast in the navigation message. They can then be used by the stand-alone positioning user to correct for the satellite clock offset. The two polynomial terms relating to satellite clock drift and clock drift rate explicitly describe the rate of change of the satellite clock error with time.

The polynomials are only an estimation of how the satellite clock offset will propagate into the future and so some of this error will remain for the stand-alone user. In reality though the residual error will be small enough to be considered negligible, particularly when considering the rate of change of that residual error. Differential or interferometric positioning users will be able to completely remove this error as it is common mode for all receivers.

3.4.1.2 Ephemeris Error

The control segment of the GPS also computes the predicted orbit path of each of the satellites. The various elements that describe this orbit path are uploaded to the satellites and, as with the clock polynomials, are transmitted in the navigation message to form the broadcast ephemeris. The position of each satellite can be

calculated as a function of time based on the broadcast ephemeris although some residual error will remain due to divergence of the predicted orbit from the actual orbit over time. This residual error is in the order of 4.2m (1σ) (USDOD, 1991).

Generally, real time users calculate satellite position as a function of time based on the broadcast ephemeris although precise ephemerides are offered by organizations such as the International GPS Service. The more accurate of these are available only with a number of hours latency. As mentioned in §3.5.2, when differential or interferometric techniques are employed the ephemeris error is largely removed for short baselines.

When considering the GPS heave algorithm developed for this project satellite velocity, achieved through the use of a central difference algorithm on satellite positions at adjacent epochs, is required. This parameter is computed in real time based on the satellite positions calculated using the broadcast ephemeris data in the navigation message. The velocities derived in this way are accurate to ± 1 mm/s when compared to the International GPS Service SP3 precise ephemeris velocities (Zhang et al., 2006).

3.4.2 Measurement Errors

Receivers introduce errors and noise as part of the process of measuring the GPS observables. This can be caused by the algorithms used within the firmware of the receiver, or can be a function of the quality of componentry used: the low cost receivers having a greater amount of error. Within the scope of this work receiver error is particularly important as low cost receivers are used and this can impact directly on the quality of the measured observables.

3.4.2.1 Receiver Clock Offset

The timing of operations within a GPS receiver is governed by a quartz clock, which is significantly less stable than the atomic clocks used on board the satellites. The quartz clock in the receiver introduces a large bias to the measurement of the GPS observables by the receiver. The stand-alone positioning user has to take a measurement to a fourth satellite in order to solve for receiver clock error. However, interferometric

positioning users that have calculated the double differenced phase observable have completely removed the effects of receiver clock.

The rate of change of the receiver clock offset will depend largely on the quality of the receiver used to collect the raw observables. When processing GPS observables to estimate user position the receiver clock can also be resolved as part of the least squares calculation as has been done in the past or it can be differenced away through the production of the temporal double difference observable developed for this project. This technique is detailed in chapter 6.

3.4.2.2 Multipath Error

Multipath is the term given to an error source that is caused by the signal from the GPS satellite taking one or more indirect routes to the receiver. Signals, as well as taking the direct route to the receiver, can also bounce off objects or buildings that may be nearby to the receiver antenna, resulting in a pseudo-range measurement that appears greater than it should. There are techniques available to mitigate the effects of multipath based on propagation geometry or sidereal analysis but these are not generally used for navigation purposes and have not been employed on this project.

3.4.2.3 Receiver Noise and Tracking Loop Errors

Measurement errors are also introduced by the receiver tracking loops. These can take the form of noise or a bias. The noise produced by the receiver is predominantly thermal noise and is proportional to the quality of the components used. Bias terms can be introduced by dynamic stress in the tracking loops with the effects often varying dependent on the algorithms employed in receiver firmware. These bias terms have particular relevance to the algorithms developed during this project and are analysed in greater detail in §3.3.4

3.4.3 Propagation Errors

As the GPS signals travel through the earth's atmosphere they are subject to refraction, which causes a delay in the transit time of the signal. Two regions of the

atmosphere have an effect on the propagation of the radio frequency waves: the ionosphere and the troposphere. These effects and their mitigation techniques are discussed below.

3.4.3.1 Ionospheric Effects

The ionosphere occupies a region between 70 km and 1000 km above the earth's surface. It is a dispersive medium, which means that the propagation velocity of radio signals through the medium varies with frequency. The phase pseudo-range observable and the code pseudo-range observable experience different effects as they pass through the ionosphere, caused by the different indices of refraction for each. Generally it can be said that the phase observable will experience an advance, and the code observable a delay (Misra and Enge, 2004).

The magnitude of the ionospheric effect on the GPS signal is proportional to the total electron count (TEC) along the signal path. The TEC is a function of time of day, user location, satellite elevation angle, season, ionizing flux, magnetic activity, sunspot cycle and scintillation (Kaplan, 1996). There exist models that attempt to compensate for the effects of the ionosphere, the most commonly used being the Klobuchar model (Klobuchar, 1996), which is a function of time and latitude. The co-efficients required in the Klobuchar model are transmitted as part of the navigation message and appear in the header of the RINEX navigation file. Stand-alone GPS users can make use of these co-efficients to mitigate range errors caused by the ionosphere but residual errors will remain due to the inadequacies of the model. The Klobuchar model accounts for approximately 50% of the effects of the ionosphere at mid latitudes (Farrell and Barth, 1999).

Dual frequency GPS users can take advantage of the dispersive nature of the ionosphere to almost completely remove its effects from their observations. Taking pseudo-range measurements on both the L1 and L2 frequencies transmitted by the GPS allows the following equation to be employed to estimate the ionospheric correction to the pseudo-range measured on L1.

$$I_{L1} = \left(\frac{L_2^2}{L_2^2 - L_1^2} \right) (\rho_{L1} - \rho_{L2}) \quad (3.15)$$

Where L_1 and L_2 are the frequencies of those signals, and ρ_{L1} and ρ_{L2} are the pseudo-range measurements recorded on each frequency.

As previously mentioned the ionospheric delay will change as a result of many factors, the most significant being the elevation angle. As a result models such as Klobuchar have an elevation dependent mapping function that will alter the computed delay. The rate of change of the ionospheric delay on the GPS signals will differ between satellites but empirical data collected during this project suggest velocity errors in the order of $\pm 1-2$ mm/s.

In this thesis the Klobuchar model has been used when observations have been recorded using a low cost single frequency receiver, and dual frequency removal of the ionosphere has been used where possible.

3.4.3.2 Tropospheric Delay

The troposphere is the region of the earth's atmosphere between the surface of the earth and an altitude of 17 km. The troposphere is a non-dispersive medium so the delay experienced by signals on both L_1 and L_2 is the same, and the delay to code pseudo-ranges is the same as that to phase pseudo-ranges. The troposphere consists of a wet component and a dry component. Around 90% of the tropospheric delay is caused by the dry component and can be well modelled (Hoffmann-Wellenhoff et al., 2001). Under ideal circumstances atmospheric readings such as temperature, pressure and humidity would be recorded and input into any model but in practice these are often difficult to obtain and a standard atmosphere model is used instead. The delay due to the wet component is primarily caused by water vapour and the nature of the temporal and spatial variations makes this difficult to model.

Tropospheric errors when computing user velocity are similar in nature to those seen from the ionosphere in so much as they change with elevation. The rate of change of the error will be predominantly decided by the mapping function of the model used and satellite elevation. Data collected during the course of this project suggests that velocity errors up to ± 5 mm/s may be seen if the troposphere is unmitigated.

The non-dispersive nature of the troposphere forces the use of a model for the stand-alone GPS user to compensate for tropospheric delay. Most simple models are accurate to about 1 m or better (Parkinson and Spilker, 1996a). The model employed in this thesis is STANAG (1990). Where differential or interferometric techniques are employed most of the tropospheric delay can be removed from pseudo-range observations.

3.5 Obtaining User Position from GPS Observables

The GPS observables discussed in §3.3 can be utilised in a number of algorithms to provide the user with instantaneous position and velocity of varying degrees of accuracy. The simplest of these algorithms is to use the pseudo-range equation to derive three dimensional position using a single GPS receiver. Other techniques employ two receivers in order that some of the significant error sources associated with the GPS can be reduced, and so that use can be made of the more accurate carrier phase observable. For the purposes of the thesis the following industry accepted definitions will apply.

- Stand-alone GPS: The use of a single receiver to provide instantaneous user position.
- Differential GPS: The use of two receivers, one in a fixed known position used to provide code pseudo-range corrections to the second roving receiver.
- Interferometric GPS: Positioning using two receivers, one in a fixed known position which provides its carrier phase observations to the second roving receiver. The roving receiver then uses differencing techniques to calculate a new, more accurate, observable.

The following subsections present a more detailed description of these techniques.

3.5.1 Stand-alone GPS

Stand-alone positioning uses the code pseudo-ranges recorded with one gps receiver to calculate user position. The pseudo-range rate observable from a single receiver can also be used to calculate user velocity. This type of GPS processing can produce user position with an accuracy of approximately ten metres and, as such, is usually considered too inaccurate to be used for marine survey, particularly for vertical reference.

Three dimensional instantaneous user position is derived from the pseudo-range observation equation given in equation 3.8. Neglecting the noise term, there are five unknowns in this equation: geometric range, receiver clock offset, satellite clock offset, ionospheric delay and tropospheric delay. Atmospheric delays are modelled during processing and the satellite clock offset is compensated for using navigation message transmitted from the satellite. There follows a derivation of the linearized geometric range and a demonstration of its use to solve for user position taken from Hoffmann-Wellenhoff et al. (2001).

User earth frame position is implicit within the geometric range:

$$\rho_r^s(T^s, T_r) = \sqrt{(X^s - X_r)^2 + (Y^s - Y_r)^2 + (Z^s - Z_r)^2} \quad (3.16)$$

where X^s , Y^s and Z^s are the earth frame co-ordinates of the satellite and X_r , Y_r and Z_r are the earth frame co-ordinates of the receiver. The satellite positions are calculated from the ephemeris data leaving four unknowns to be solved, and requiring pseudo-range measurements from at least four satellites.

Once all the terms that can be modelled or compensated for have been removed the pseudo-range observation equation becomes

$$PR_r^s = \rho_r^s + c\delta\tau_r \quad (3.17)$$

This equation is non-linear and so must be linearized about an initial position estimate. This enables the system of equations that the pseudo-range measurements produce to be solved using a least squares process. Linearization begins by defining an estimated geometric range from the initial position estimate:

$$\rho_{r0}^s = \sqrt{(X^s - X_{r0})^2 + (Y^s - Y_{r0})^2 + (Z^s - Z_{r0})^2} \quad (3.18)$$

$$\equiv f(X_{r0}, Y_{r0}, Z_{r0}) \quad (3.19)$$

Where X_{r0} , Y_{r0} and Z_{r0} are the earth frame co-ordinates of the initial position estimate. Equation 3.16 can also be written as $f(X_r, Y_r, Z_r)$.

The unknown user position values can be written as

$$X_r = X_{r0} + \Delta X_r \quad (3.20)$$

$$Y_r = Y_{r0} + \Delta Y_r \quad (3.21)$$

$$Z_r = Z_{r0} + \Delta Z_r \quad (3.22)$$

This introduces the new unknowns of ΔX_r , ΔY_r and ΔZ_r , which are the required corrections to the initial position estimate. These new representations of user position allow the replacement of $f(X_r, Y_r, Z_r)$ with the equivalent function $f(X_{r0} + \Delta X_r, Y_{r0} + \Delta Y_r, Z_{r0} + \Delta Z_r)$. Using a first order, and hence linear, Taylor series expansion with respect to the initial position estimate yields

$$f(X_r, Y_r, Z_r) \equiv f(X_{r0} + \Delta X_r, Y_{r0} + \Delta Y_r, Z_{r0} + \Delta Z_r) \quad (3.23)$$

$$\begin{aligned} &= f(X_{r0}, Y_{r0}, Z_{r0}) + \frac{\partial f(X_{r0}, Y_{r0}, Z_{r0})}{\partial X_{r0}} \Delta X_r \\ &\quad + \frac{\partial f(X_{r0}, Y_{r0}, Z_{r0})}{\partial Y_{r0}} \Delta Y_r + \frac{\partial f(X_{r0}, Y_{r0}, Z_{r0})}{\partial Z_{r0}} \Delta Z_r \end{aligned} \quad (3.24)$$

The partial derivatives of equation 3.24 can be calculated as

$$\frac{\partial f(X_{r0}, Y_{r0}, Z_{r0})}{\partial X_{r0}} = -\frac{X^s - X_{r0}}{\rho_{r0}^s} \quad (3.25)$$

$$\frac{\partial f(X_{r0}, Y_{r0}, Z_{r0})}{\partial Y_{r0}} = -\frac{Y^s - Y_{r0}}{\rho_{r0}^s} \quad (3.26)$$

$$\frac{\partial f(X_{r0}, Y_{r0}, Z_{r0})}{\partial Z_{r0}} = -\frac{Z^s - Z_{r0}}{\rho_{r0}^s} \quad (3.27)$$

which, along with equation 3.19, can be substituted into equation 3.24 to yield the geometric range equation linearized with respect to ΔX_r , ΔY_r and ΔZ_r :

$$\rho_r^s = \rho_{r0}^s - \frac{X^s - X_{r0}}{\rho_{r0}^s} \Delta X_r - \frac{Y^s - Y_{r0}}{\rho_{r0}^s} \Delta Y_r - \frac{Z^s - Z_{r0}}{\rho_{r0}^s} \Delta Z_r \quad (3.28)$$

The linearized geometric range can then be substituted into the pseudo-range equation derived in §3.3, which can subsequently be used to create a system of equations solvable using a least squares. An example of this is given below that neglects atmospheric terms which can be modelled or mitigated as explained in §3.4, and assumes the satellite clock bias is known from the navigation message.

$$PR_r^s = \rho_{r0}^s - \frac{X^s - X_{r0}}{\rho_{r0}^s} \Delta X_r - \frac{Y^s - Y_{r0}}{\rho_{r0}^s} \Delta Y_r - \frac{Z^s - Z_{r0}}{\rho_{r0}^s} \Delta Z_r - c[\delta t^s - \delta \tau_r] \quad (3.29)$$

Collecting the known terms on the left side of the equation yields

$$PR_r^s - \rho_{r0}^s - \delta t^s = -\frac{X^s - X_{r0}}{\rho_{r0}^s} \Delta X_r - \frac{Y^s - Y_{r0}}{\rho_{r0}^s} \Delta Y_r - \frac{Z^s - Z_{r0}}{\rho_{r0}^s} \Delta Z_r + c\delta \tau_r \quad (3.30)$$

This equation clearly has four unknown terms: ΔX_r , ΔY_r , ΔZ_r and $\delta \tau_r$, requiring four equations, or pseudo-range measurements from separate satellites, in order to solve for all of them. In order to simplify these sets of equations the following shorthand representations will be used.

$$\begin{aligned} l^s &= PR_r^s - \rho_{r0}^s + \delta t^s \\ a_{X_r}^s &= -\frac{X^s - X_{r0}}{\rho_{r0}^s} \\ a_{Y_r}^s &= -\frac{Y^s - Y_{r0}}{\rho_{r0}^s} \\ a_{Z_r}^s &= -\frac{Z^s - Z_{r0}}{\rho_{r0}^s} \end{aligned}$$

These allow the much simplified expression of the series of equations required to solve for instantaneous user position; the satellites are numbered s1 to s4:

$$\begin{aligned}
 l^{s1} &= a_{X_r}^{s1} \Delta X_r + a_{Y_r}^{s1} \Delta Y_r + a_{Z_r}^{s1} \Delta Z_r + c\delta\tau \\
 l^{s2} &= a_{X_r}^{s2} \Delta X_r + a_{Y_r}^{s2} \Delta Y_r + a_{Z_r}^{s2} \Delta Z_r + c\delta\tau \\
 l^{s3} &= a_{X_r}^{s3} \Delta X_r + a_{Y_r}^{s3} \Delta Y_r + a_{Z_r}^{s3} \Delta Z_r + c\delta\tau \\
 l^{s4} &= a_{X_r}^{s4} \Delta X_r + a_{Y_r}^{s4} \Delta Y_r + a_{Z_r}^{s4} \Delta Z_r + c\delta\tau
 \end{aligned} \tag{3.31}$$

The set of equations in 3.31 can be presented in matrix form by

$$\underline{l} = \underline{A} \underline{x} \tag{3.32}$$

where

$$\underline{l} = \begin{bmatrix} l^{s1} \\ l^{s2} \\ l^{s3} \\ l^{s4} \end{bmatrix} \tag{3.33}$$

$$\underline{A} = \begin{bmatrix} a_{X_r}^{s1} & a_{Y_r}^{s1} & a_{Z_r}^{s1} & c \\ a_{X_r}^{s2} & a_{Y_r}^{s2} & a_{Z_r}^{s2} & c \\ a_{X_r}^{s3} & a_{Y_r}^{s3} & a_{Z_r}^{s3} & c \\ a_{X_r}^{s4} & a_{Y_r}^{s4} & a_{Z_r}^{s4} & c \end{bmatrix} \tag{3.34}$$

$$\underline{x} = \begin{bmatrix} \Delta X_r \\ \Delta Y_r \\ \Delta Z_r \\ \delta\tau \end{bmatrix} \tag{3.35}$$

Solving for \underline{x} allows the estimation of the required corrections to the initial position estimate, and also the receiver clock offset.

3.5.2 Differential Positioning

Differential GPS (DGPS) positioning is a technique that allows for the mitigation of many of the errors associated with stand-alone GPS. The technique utilizes two GPS receivers, with one reference receiver commonly placed over a fixed and known point. The basic principle is that the known position of the reference receiver can be used to calculate a correction to each measured pseudo-range that accounts for the errors introduced by both the control and space segments of the GPS. The pseudo-range corrections can then be transmitted in real time to other receivers in the vicinity of the reference receiver and used to compensate for the same errors in their own pseudo-range measurements.

The mitigation of errors associated with stand-alone GPS can improve the position accuracy obtainable to less than five metres. DGPS is routinely used in hydrographic survey to provide plan position of the survey vessel, It is, however, still considered too inaccurate to provide any vertical reference and the setup for the majority of hydrographic survey vessels is to use DGPS to calculate horizontal position and then use an inertial based heave motion sensor to give vertical reference.

A generalization of the basic pseudo-range equation for a receiver, A, highlights the range biases caused by each of the GPS segments:

$$PR_A^s = \rho_A^s + \Delta\rho_A^s + \Delta\rho^s + \Delta\rho_A \quad (3.36)$$

The $\Delta\rho_A^s$ term represents the errors caused by the control segment and receiver position such as ephemeris error and atmospheric effects, $\Delta\rho^s$ are those errors which are due solely to the satellite such as satellite clock offset and $\Delta\rho_A$ are receiver dependent errors such as receiver clock offset and multipath. From equation 3.36 it is possible to derive a pseudo-range correction term:

$$PRC^s = \rho_A^s - PR_A^s \quad (3.37)$$

This can be calculated for the reference receiver because the receiver position is known, allowing the calculation of ρ_A^s . Now the pseudo-range measurement to the same satellite but from a second receiver, B, can be corrected for the majority of the errors:

$$PR_B^s = \rho_B^s + \Delta\rho_B^s + \Delta\rho^s + \Delta\rho_B \quad (3.38)$$

$$PR_{BCorr}^s = PR_B^s + PRC^s \quad (3.39)$$

$$PR_{BCorr}^s = \rho_B^s + [\Delta\rho_B^s - \Delta\rho_A^s] + [\Delta\rho^s - \Delta\rho^s] + [\Delta\rho_B - \Delta\rho_A] \quad (3.40)$$

The satellite dependent terms cancel completely and, provided the distance between the roving receiver and the reference receiver is not too great, so do the orbit and atmospheric errors. Removing the satellite related terms and neglecting the satellite to receiver errors yields

$$PR_{BCorr}^s = \rho_B^s + \Delta\rho_{BA} \quad (3.41)$$

where, if multipath is neglected, the term $\Delta\rho_{BA}$ is the difference between the receiver clock bias of the two receivers. A system of corrected pseudo-range equations can then be formed and solved for in exactly the same way as shown in §3.5.1.

3.5.3 Interferometric Positioning

Interferometric positioning, as with differential positioning, uses two receivers, one commonly set up over a fixed known point. However, instead of calculating a correction term, carrier phase observations from different receivers and satellites are differenced to produce an observable with many of the errors mitigated or removed. This can be done in real time via a suitable transmission media, or as a post processing technique.

3.5.3.1 Single Difference

Single differencing is the process of differencing two carrier phase observations either from the same satellite to different receivers (differencing across receivers) or from different satellites to the same receiver (differencing across satellites). The single difference observable is often considered to be that resulting from differencing across receivers but in either case results in the cancellation of common mode errors. The sin-

gle difference observation equation results from the differencing of the phase pseudo-range equation 3.10 to satellite, E, from two receivers, A and B.

$$\phi_{AB}^E = \phi_B^E - \phi_A^E \quad (3.42)$$

$$= \frac{f}{c} \rho_{AB}^E - f\delta\tau_{AB} + N_{AB}^E + I_{AB}^E + T_{AB}^E \quad (3.43)$$

The satellite clock offset terms have cancelled out and for moderate distances from the reference receiver the ephemeris errors and atmospheric effects are greatly reduced. Single difference observation equations to satellites N, O and V can also be produced. These can then be processed using on-the-fly ambiguity resolution techniques, or used as the basis for the formation of the double difference observation equation.

3.5.3.2 Double Difference

The double difference observation equation is now formed by differencing the single difference equations derived in the previous section. The second difference is a difference across satellites and so removes the common mode error, in this case the receiver clock offset. An example of a double difference equation using two receivers, A and B, and two satellites, E and N is given below.

$$\phi_{AB}^{EN} = \phi_{AB}^N - \phi_{AB}^E \quad (3.44)$$

$$= \frac{f}{c} \rho_{AB}^{EN} + N_{AB}^{EN} + I_{AB}^{EN} + T_{AB}^{EN} \quad (3.45)$$

If two more of these double difference observation equations are formed then they can be processed using OTF ambiguity resolution techniques to provide highly accurate positioning.

3.5.4 Spatial Decorrelation

The spatial decorrelation of the ephemeris and atmospheric errors mentioned in the §3.5.2 and 3.5.3 is shown clearly in figure 3.3. It can be seen that the further away the roving receiver is from the reference receiver the greater the change in the line

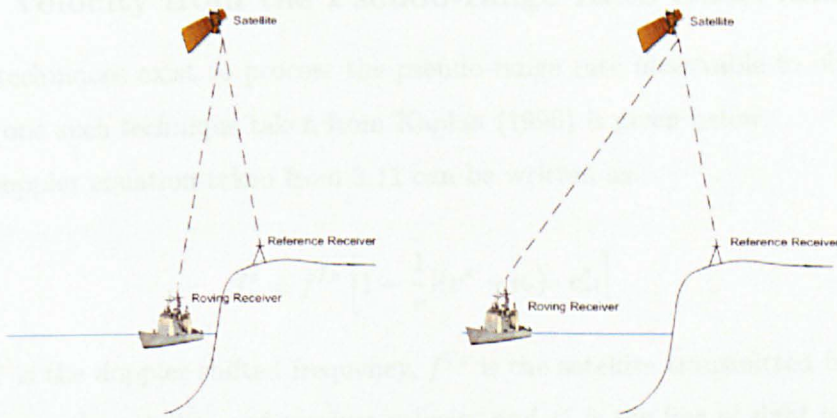


Figure 3.3: Spatial decorrelation of DGPS corrections

of sight vector to the satellite. This change in the line of sight vector results in the signal passing through a different amount of atmosphere and also a different section of atmosphere. In addition the correction to the range errors associated with the broadcast ephemeris also only apply along the line of sight vector between satellite and reference receiver. As the roving receiver moves further away from the reference receiver the greater the change in the line of sight vector and the less relevant the correction for both atmospheric and ephemeris errors.

3.6 Obtaining User Velocity from a Stand-alone GPS Receiver

The GPS provides the user with the ability to calculate three dimensional velocity as well as position. This can be done in a number of ways, the simplest of which is to form an approximate derivative of user position. However, the work contained within this thesis is primarily concerned with stand-alone GPS; under these conditions user position is too inaccurate to be able to determine user velocity in this way. This section concentrates on the two most accurate methods of calculating user position from a stand-alone GPS receiver.

3.6.1 Velocity from the Pseudo-range Rate Observable

Various techniques exist to process the pseudo-range rate observable to obtain user velocity, one such technique taken from Kaplan (1996) is given below.

The doppler equation taken from 3.11 can be written as

$$f_r^s = f^{Ts} \left[1 - \frac{1}{c} [(v^s - v_r) \cdot e_r^s] \right] \quad (3.46)$$

where f_r^s is the doppler shifted frequency, f^{Ts} is the satellite transmitted frequency, v^s and v_r are the satellite and receiver velocity and e_r^s is the line of sight unit vector between satellite and receiver. The transmitted frequency from the satellite is based on the atomic clock installed on it. The true transmitted frequency will, therefore, differ from the nominal frequency by an amount proportional to the satellite clock drift given by the polynomials in the navigation message. Therefore

$$f^{Ts} = f_0 + \Delta f^{Ts} \quad (3.47)$$

where f_0 is the nominal transmitted frequency (either L1 or L2) and Δf^{Ts} is the correction to the nominal frequency based on the satellite clock error polynomials. The measured received frequency (f_{rRx}^s) is also in error by an amount proportional to receiver clock drift ($\delta\tau$) and can be related to the doppler shifted frequency through the relationship

$$f_r^s = f_{rRx}^s (1 + \delta\tau) \quad (3.48)$$

where $\delta\tau$ is positive for a receiver clock running faster than GPS system time. Equation 3.48 can now be substituted into equation 3.46 to yield

$$f_r^s (1 + \delta\tau) = f^{Ts} \left[1 - \frac{1}{c} [(v^s - v_r) \cdot e_r^s] \right] \quad (3.49)$$

which, after moving all known terms to the left, becomes

$$\frac{c(f_r^s - f^{Ts})}{f^{Ts}} + v^s \cdot e_r^s = v_r \cdot e_r^s - \frac{cf_r^s \dot{\delta\tau}}{f^{Ts}} \quad (3.50)$$

The term $\frac{f_r^s}{f^{Ts}}$ on the right hand side of the equation is very close to 1 and this approximation will result in little error. Collecting the left hand side terms together and expanding the dot product on the right hand side yields

$$d_r^s = v_{rX}e_{rX}^s + v_{rY}e_{rY}^s + v_{rZ}e_{rZ}^s - c\delta\tau \quad (3.51)$$

If at least four such equations are formed using measurements from separate satellites then similarities are obvious between this and the set of equations 3.31. Indeed this system of equations can be solved for in exactly the same way to yield an estimate of user position and receiver clock drift.

3.6.2 Velocity from Temporally Differenced Carrier Phase Observables

Another method of extracting user velocity from a stand-alone GPS receiver is obtained through differencing two temporally adjacent carrier phase pseudo-range observations (Itani et al., 2000; Serrano et al., 2004a,b; van Graas and Soloviev, 2004). From this temporal differencing a doppler observable is derived based on the carrier phase pseudo-range observable. This new carrier based doppler observable is averaged over a much longer time than the pseudo-range rate observable, which provides almost instantaneous doppler, and so contains significantly less noise (Serrano et al., 2004a).

This form of velocity estimation from a stand-alone GPS receiver forms the mainstay of the research presented in this thesis. As such a detailed explanation of the approach is given in Chapter 6 along with a derivation of all the equations required.

Chapter 4

Vertical Reference for Hydrographic Survey

4.1 Introduction

Hydrographic survey is the process of recording depth, or bathymetry, data with the intention of producing a chart that shows the relief of the sea bed being surveyed. The bathymetry data is usually recorded from a vessel that is on or below the surface of the sea and most commonly involves echo sounder technology.

Survey vessels on the sea surface undergo vertical displacement due to wave and tidal effects, resulting in a echo sounder platform that is never truly stationary. Vertical reference must be provided for the echo sounder transponder firstly so that the bathymetry data can be reduced to a meaningful datum, and also so that motion of the vessel due to waves and tides can be compensated for and removed from the bathymetry data. Failure to do so would result in vessel motion appearing as noise on the plotted relief of the sea bed as changes to vessel height actually manifest as changes in recorded depth by the echo sounder.

This chapter looks in detail at the current practices in providing vertical reference to hydrographic surveys and explains their significance to the hydrographic survey industry. There is a strong focus on heave measurement and in depth analysis of the current classical methods of heave measurement used within the industry. The

errors and problems with classical heave measurement highlighted in this chapter are exactly those which the GPS based heave measurement method developed as part of this project have overcome.

4.2 Chart Datum

The purpose of hydrographic surveying is to measure the depth of a body of water with the intention of depicting the relief of the seabed, in a manner similar to the topographic mapping of land areas (Ingham, 1992). For this data to be of use to mariners in the form of charts, the depth to the seabed must be given relative to a common datum. This datum is often referred to as chart datum and, in the current hydrographic industry, is usually selected to be coincident with the lowest astronomical tide or mean lowest low water (MLLW) (Milne, 1980).

Nautical charts express the relief of the seabed by showing depths relative to chart datum, as explained by the Admiralty (1987). It is for this reason that chart datum has traditionally been chosen to be coincident with MLLW as it will always display the depth of the water when at its most shallow, which has obvious implications for safety. The main problem with the use of MLLW as the chart datum is that this level is locally affected and consequently not consistent along a given stretch of coastline. Because tides are locally specific they change from area to area, which can produce vastly different tidal regimes over relatively short distances, and even across the face of a single chart.

A true definition of chart datum is the height reference surface used in hydrography (Martin and Broadbent, 2004), and is currently accepted to be MLLW. Moves are underway, however to standardize chart datum to an ellipsoidal reference, and the time is approaching when charted depths may be given to a geodetic, rather than local, datum.

4.3 Classical Hydrographic Methods

The classical method for the providence of vertical reference to survey vessels takes the view that vertical vessel motion can be split into the two discrete categories of tidal motion and heave motion. Tidal motion refers to the low frequency and long period motion of the vessel due to tidal effects, and heave motion is the relatively higher frequency shorter period motion experienced by the vessel as a result of waves.

Whilst some more modern and more expensive systems, discussed in §4.4, consider the motion of the vessel across the entire frequency range, the classical methods are still widely practiced within the industry. They are often favoured due to their ease of use and relatively low cost when compared to techniques that use a single water level correction. This section looks at methods of providing compensation for tidal and heave motion of a survey vessel.

4.3.1 Tidal Compensation

Tidal effects on the vertical position are seen as low-frequency vertical displacements of the vessel. They are caused primarily by astronomical effects, but can also be influenced by meteorological and oceanographic factors. This vertical displacement of the survey vessel must be accounted for in any reduction of bathymetric data as it actually represents an increase or decrease in recorded depth; uncompensated this would translate into changes in the height of the seabed.

Compensation for tide in hydrographic surveying is complicated by the fact that surveys are seldom conducted in close proximity to tide gauges. Often the survey area can be several nautical miles from the gauge itself and, in areas of complex tidal systems, this can cause significant errors when the calculation of the tide at the survey site is attempted.

The predominant method for the transference of tidal data to the survey site is through discrete tidal zoning, a system that defines areas of similar tidal characteristics using polygons, or discrete zones (Imahori et al., 2003). An example of these zones is seen in figure 4.1, which shows the discrete zone makeup around Popof Island off the Alaskan coast. This data is a good example of how an area of ocean surrounding

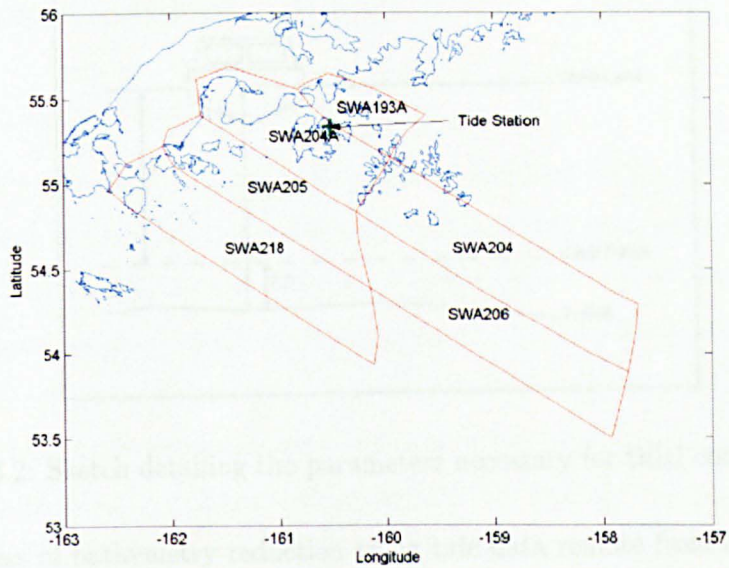


Figure 4.1: Discrete tidal zones surrounding Popof Island, Alaska

a tide gauge is split into discrete zones. Along with the data describing the shape and position of the discrete zones comes a time and range offset for each. These offsets must be applied to the tide data collected at the gauge to produce the tidal effects experienced in a given zone.

Other techniques exist that allow for the transference of tide reduction data to a survey site. Chang and Sun (2004) used GPS measurements taken at tide gauge sites to reduce the errors associated with transferring data away from the tide gauge. Also GPS-tracked buoys may be temporarily installed at survey sites, which can then be used to provide tidal reduction data from the site at which the survey is to be conducted (Ashkenazi et al., 1996; Chang and Sun, 2004; Bisnath et al., 2004). A further method is to use interferometric GPS techniques, sometimes in a GPS-aided INS system, to provide tidal motion of the vessel itself (Sanders, 2003; Zhoa et al., 2004). This involves the installation of the GPS equipment on board the vessel, long period vertical displacement can then be used to correct for the motion of the vessel directly.

Once suitable tide data has been established at the survey site, the process of compensating for tidal motion is relatively simple. Figure 4.2 shows the parameters

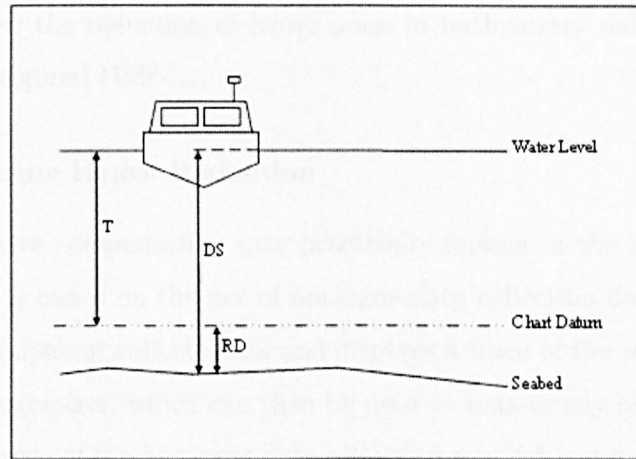


Figure 4.2: Sketch detailing the parameters necessary for tidal compensation

in the process of bathymetry reduction using tide data remote from the survey site. The result of the tidal compensation is the reduced depth, which can be easily achieved from

$$RD = DS - T \quad (4.1)$$

where RD is Reduced Depth, DS is Depth Sounding and T is Tide level.

4.3.2 Heave Compensation

Equation 4.1 and figure 4.2 offer a simplified model of how bathymetry can be reduced to chart datum, assuming that the survey vessel is stationary on a perfectly flat sea surface. This is never the case and real sea conditions contain short period perturbations from the mean sea level caused by such things as weather, the wake of other vessels and currents (Alkan, 2003). These perturbations from mean sea level are termed heave and are perceived by the hydrographer as changes in measured depth, or noise on the depth soundings and, as such, must be compensated for to improve the accuracy of the bathymetry.

Heave is a very localized phenomenon, even more so than tide, and so must be recorded and compensated for on board the survey vessel. There are two main

methodologies for the reduction of heave noise in bathymetry data as discussed by Kielland and Hagglund (1995).

4.3.2.1 Analogue Heave Reduction

A method of heave compensation now practically unseen in the industry, analogue heave reduction is based on the use of analogue data collection during hydrographic surveys. This equipment collects data and displays a trace of the seafloor representation to the hydrographer, which can then be used to remove any obvious heave noise visually. The nature of the analogue data collection precludes any attempt to correct for heave measurement automatically. There are major shortcomings associated with this method of heave reduction, particularly if the seafloor is rough, making the separation of heave and seafloor artefacts more difficult.

4.3.2.2 Digital Heave Compensation

This technique is used in most modern surveys and also forms the backbone of the majority of research in the field of heave compensation. If survey data is collected digitally, it becomes possible to measure the vessel heave motion and correct each sounding as it is recorded.

Within the hydrographic survey industry this is typically done using inertial technology to measure the vertical acceleration of the vessel, which can be double integrated to produce vertical displacement. The vertical displacement of the vessel can be used to correct each sounding in real time as it is logged from the echo sounder. Systems measuring heave in this way are provided by many manufacturers and this process of heave measurement is discussed in detail in Chapter 5.

Methods of heave compensation that utilise GPS technology are also available. Much of the research into the use of GPS for vertical reference for hydrographic survey, however, has been concentrated on its use for single water level corrections and is discussed in §4.4. There was an early attempt by Kielland and Hagglund (1995) to use DGPS to measure heave motion of a vessel. This resulted in heave measurement of the order of ± 1 decimetre which underperforms inertial based heave sensors, which routinely achieve errors at the ± 5 centimetre level (VTTSS Ltd, 2005;

Kongsberg, 2005). In addition there is the obvious drawback of the need to have multiple receivers for any differential GPS approach. The technique was, however, shown to have significant cost advantages over inertial based heave sensors.

Approaches to providing GPS based heave using GPS velocities are also known. There are two papers in particular, the work in which has been built upon by the work in this thesis. In their paper Itani et al. (2000) developed a wave sensor based on low cost GPS receivers that monitors wave heights to aid in the collection of meteorological records, building of breakwaters and tsunami warnings. The work detailed in the paper is based upon measurements taken with a Furuno GN-77 low cost GPS receiver. Velocity estimates were calculated using the temporally differenced carrier phase technique outlined in §3.6 and explained in detail in Chapter 6. The vertical velocity calculated was then integrated to produce relative vertical position, any drift in this relative position caused by bias errors in the calculated velocity was filtered out with a simple high pass filter. Heave outputs were compared to wave heights calculated using interferometric GPS, and were found to agree to within a ± 8 centimetres, a level of performance just below that of inertial based heave sensors. The work undertaken by Itani et al. (2000) shows the ability of low-cost GPS receivers to measure heave with a slightly degraded accuracy when compared to inertial based sensors.

The work of Itani et al. (2000) was endorsed by Reinking and Harting (2002) who used a Leica SR 530 geodetic grade receiver to calculate GPS velocities and, subsequently, heave in a similar way. Comparison in that instance was with both interferometric GPS and the heave output from a TSS DMS-25 inertial based heave sensor. The heave output created using temporally differenced carrier phase pseudo-range observations from the Leica geodetic receivers was found to be of equivalent accuracy to that which can be produced by an inertial based system although in that work the inertial outputs were post processed forwards and backwards through a high pass filter.

Both these papers demonstrated the ability of an algorithm based on GPS velocities to measure heave but only Itani et al. (2000) looked at the use of low cost receivers for heave measurement. The receiver used in that instance was a Furuno G-77 and

carrier phase observations were not available from this unit to the general consumer. Indeed the U-Blox Antaris receiver used during the work carried out for this project is one of the first low cost receivers to offer raw carrier phase observations making this project the first to look at heave measurement using off the shelf low cost GPS receivers. Itani et al. (2000) compared a low cost GPS heave output to post processed float solution GPS heave but does not assess the performance of low cost receivers against geodetic grade receivers, nor does it compare the results of the algorithm to either an inertial based sensor or an accurate reference such as the Applanix POS-RS system held by the IESSG.

It is worth noting that none of the GPS based heave measurement techniques have been accepted into the hydrographic survey industry to date. The industry is still dominated by inertial based heave and attitude sensors, primarily because vessel attitude is often required for steering of the echo sounder beam and this is currently not available using a GPS only system.

4.3.3 Errors and Problems Associated with Classical Hydrographic Methods

The use of classical methods for vertical reference of hydrographic surveys has associated with it some shortcomings that limit the accuracy obtainable. This subsection will discuss some of those shortcomings.

4.3.3.1 Tide Specific Errors

The methods of tidal reduction involving transference of tide data away from the tide gauge site to the survey site will obviously introduce some error into the tide data. Any model chosen to do this will have within it inherent inaccuracies due to unmodelled parameters. This is largely a result of tidal motion being essentially an unknown quantity away from coastlines and significant ports. In addition to this there are further inaccuracies associated with any discretization of an analogue motion. The attempt to group together areas of similar tidal behaviour into discrete zones can lead to such quantization errors in the discrete tidal zoning system. The nature of the

algorithm can suggest step changes in sea level at the junction between two zones, a scenario which is empirically unsound.

Methods that incorporate GPS techniques also have usability and accuracy problems associated with them. Installation of GPS-tracked buoys at the survey site is required for not less than 29 days before the survey is conducted in order that the tide data conforms to the International Hydrographic Office Standards for Hydrographic Survey (IHO, 1998). The same document also requires that tide data be expressed in terms of both chart datum and a suitable geocentric reference system such as WGS84. This is far easier on shore where the separation between these two datums is much more clearly defined.

4.3.3.2 Heave Specific Errors

Errors and usability issues in the measurement of heave data differ depending on the technique employed. Errors associated with an analogue heave compensation approach are obvious in that they rely on the human eye to pick out heave artefacts from a trace of the recorded bathymetry. This practice is almost non-existent within hydrography now but is still worth noting as it demonstrates how far vertical reference of hydrographic survey has come in a relatively short space of time.

Digital heave compensation can be split into two main categories: the industry accepted standard of the measurement of heave using inertial sensors; and the measurement of heave using GPS, which has been largely restricted to academic research.

Inertial based systems have a number of common usability issues that make life more difficult for the hydrographer. They frequently have different filter tuning settings that must be calibrated to suit the dynamics of the particular vessel they are fitted to. They can also have a setting that the hydrographer must set manually for varying sea states. Further to these complications the filter used in a real time heave algorithm has a certain transient response to large inputs which results in a 'ringing' of the output. Large inputs to the heave filter occur during vessel turns and, as such, the filter must be given time to settle after turns before it is working optimally. This adds extra length to each survey line and increases the time required for the survey. When using inertial systems to compensate for heave displacement the

accuracy of the systems is often quoted to be in the order of ± 5 centimetres or 5% of the heave displacement, whichever is the greater (VTTSS Ltd, 2005; Kongsberg, 2005). This figure relies on the filter being optimally tuned and fully settled. These errors and problems are discussed in more detail in chapter 5 after the inertial based heave algorithm developed during this project has been discussed and its performance has been analysed.

Heave measurement using the stand-alone GPS can overcome many of the issues that are present with the inertial based systems: they offer a more temporally stable heave solution, can remove the need for manual input and also potentially provide savings in cost. There are, however, drawbacks to their use, particularly the fact that they rely on a good view of the sky and that, if they are to provide equivalent accuracy to inertial based systems, they are not real time. For most hydrographic survey requirements, however, enough satellites would be available to provide an output. As for real time heave compensation of bathymetry, this is unnecessary in a practical surveying sense and only really serves to give the hydrographer confidence in the operation of the on board equipment; a near real time output could do this equally well.

4.3.3.3 General Classical Methodology Errors

The use of the classical methodology to provide vertical reference for hydrographic survey has, inherent within it, errors associated with the model of sea surface motion it uses. It is assumed that all heave motion of the vessel is contained within a particular frequency band, and that the only other influence on the vertical displacement of the vessel is tidal. Figure 4.3 shows a bode plot that demonstrates the frequency of motion that is missed when the classical methodology is implemented. Typically heave motion is considered to be all vertical vessel motion above approximately 0.03 Hz, while the highest frequency of tidal motion is in the region of 20 μ Hz (a semi-diurnal period). Any motion outside of these frequency bands will not be measured using the classical methodology.

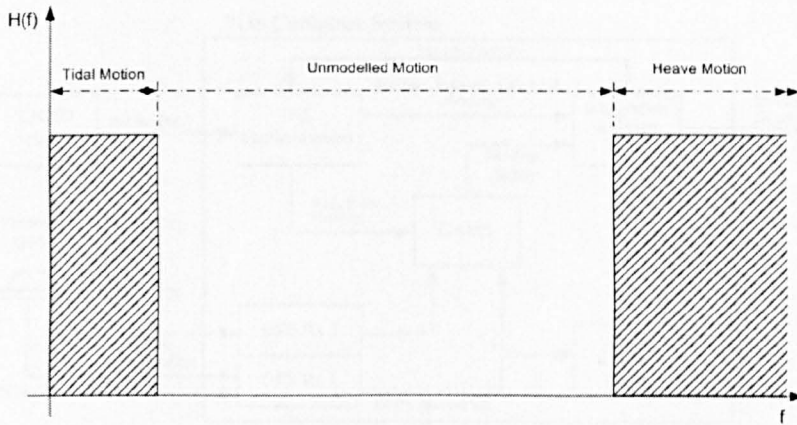


Figure 4.3: Bode plot of the frequency ranges represented in the classical method of providing vertical hydrographic survey reference

4.4 Single Water Level Correction

Many of the more modern survey reference systems fitted to hydrographic survey vessels now offer a reference based on the WGS84 ellipsoid. They are either GPS based, or GPS aided, provide an easy way to reduce bathymetry data to a global datum and compensate for vessel motion across the whole frequency spectrum. This section deals with the predominant technologies currently employed within the industry and covers the main areas of research in the field.

4.4.1 GPS-aided INS

For many years GPS and INS sensors have been coupled together in a complete system to provide accurate position and orientation data at high data rates. This has been especially useful in the survey industry and is now accepted as the ‘gold standard’ in terms of accurate survey reference data. The technique for coupling the GPS and INS sensors is well documented and based on the implementation of a Kalman Filter (Kalman, 1960; Maybeck, 1979; Gelb, 1982; Welch and Bishop, 2001; Hide, 2003). A market leader in the design, manufacture and supply of these equipments to the hydrographic survey industry is Applanix Corporation. For this reason an brief overview of the Applanix Position and Orientation System/Marine Vessels (POS/MV)

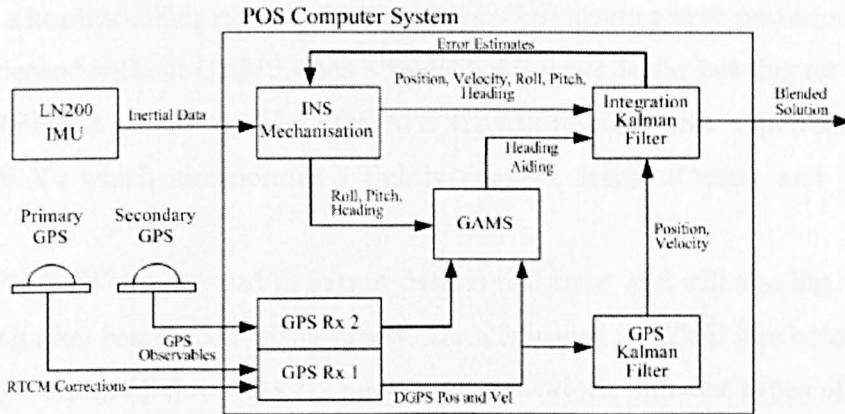


Figure 4.4: Block schematic diagram of a POS/MV 320

system follows; the principles of this system can be generally applied to many GPS-aided INS systems provided by other manufacturers.

The POS/MV is a system produced by Applanix Corporation, a company specializing in GPS-aided INS products for the survey industry and based in Toronto, Canada. The system is designed around the Applanix POS, which is the root of all Applanix systems, and uses interferometric GPS measurements to aid an inertial navigation system. It is fitted to hydrographic survey vessels to deliver a highly accurate position and orientation solution with direct applications for hydrographic survey. A POS/MV 320 consists of the following components:

- A POS Computer System (PCS)
- A Litton LN200 Inertial Measurement Unit
- A primary GPS Receiver Antenna
- A secondary GPS Receiver Antenna

These components form a loosely coupled system as shown in figure 4.4. The IMU is the primary sensor, which is aided by the differential GPS measurements obtained from the primary GPS antenna via an integration Kalman Filter (Mostafa et al., 2001). The GPS Azimuth Measurement Subsystem (GAMS) uses GPS data from both the primary and secondary GPS antennas, which are positioned on a fixed baseline, to

produce a heading aiding output. This overcomes the heading drift problems that can be experienced without GAMS when a vessel holds a particular heading for extended periods (Hide et al., 2004). The POS/MV 320 has recently been superseded by the POS/MV V4 which incorporates a tightly coupled design (Canter and Corcoran, 2004).

The POS/MV can be used to output data in real time, and will also log it for post processing after completion of the survey. Data is logged in 12MB files onto the PCS hard drive. Each of these files contains groups in which different types of data are stored (Corcoran and Pronk, 2003).

4.4.2 Interferometric GPS

As well as providing aiding data to INS sensors, interferometric GPS has also been used separately to reduce bathymetry data to a suitable datum (Scarfe, 2002; Riley et al., 2003; Terai, 2004). The principle again involves a single water level correction as opposed to the classical methodology previously discussed and has the advantage of being able to describe the vertical motion of the vessel across the entire frequency range.

4.4.3 Factors Prohibitive to the Widespread Use of Single Water Level Correction Techniques

The common theme for methods of providing vertical reference using a single water level correction is that they all involve the use of interferometric GPS. The use of this equipment brings along with it a set of usability issues that may prohibit its endemic use in the hydrographic industry. These issues, along with some others, are outlined in this section.

4.4.3.1 GPS-aided INS Specific Factors

The main factor that prohibits widespread use of GPS-aided INS systems in hydrographic survey is cost. It is widely accepted that these systems provide the best

possible reference data for hydrographic survey, but when this level of accuracy is not required the cost of the equipment cannot be justified.

Further to this factors discussed in the following subsections will also apply to GPS-aided INS systems.

4.4.3.2 Interferometric GPS Specific Factors

As explained in §3.5.3, interferometric GPS involves the use of multiple receivers, one acting as a reference. Whilst there are now networks of reference stations operated by various organisations throughout the UK such as the Ordnance Survey, in many cases the reference station must be provided by the agency undertaking the survey. This results in the need for two GPS receivers (assuming only one on the vessel), one being set up over a known point within a moderate distance of the survey site.

Anecdotal evidence suggests that the setting up and running of the reference receiver is considered by hydrographers to be a 'fiddly' and time consuming process that is prone to error. The truth of this perception can be argued either way but the fact that it exists suggests that there is a certain inertia within the industry to the take up of this technology. Added to this there are also limitations to the use of interferometric GPS offshore due to spatial decorrelation and the expense involved with the use of multiple geodetic grade receivers.

4.4.3.3 General Single Water Level Correction Methodology Factors

Generally there exists a problem with the use of single water level corrections for vertical reference of hydrographic survey; this is that they can only provide data reduced to the WGS84 geodetic reference ellipsoid. The hydrographic survey industry is currently entrenched in a system that provides charts reduced to chart datum, a natural system to do when it is considered that the important information on a chart for navigators and pilots is depth. Consequently, all bathymetry data must currently be provided reduced to chart datum as well as to the WGS84 ellipsoid (IHO, 1998), resulting in the need to have a well defined model for the separation of the geoid and the WGS84 ellipsoid. The day may be approaching when the entire industry moves over to an ellipsoidal based system but industry inertia may resist this for

some years. Until then there is always the possibility of introducing errors when modelling ellipsoidal-geoidal separation as the parameter may be clearly defined in areas of high interest such as major ports, but in many areas of the world it is not.

4.5 The International Hydrographic Organization Survey Standards

The International Hydrographic Organization (IHO) is a multi governmental organization set up in 1921 to promote safety within hydrography and coordinate the activities of the national hydrographic offices of the member states. The IHO sets out standards for four separate classifications of hydrographic survey, which are laid out in table 4.1. The sections of table 4.1 relevant to the TDD heave algorithm developed during this project relate specifically to horizontal position and depth accuracy. The parameters a and b given in the row relating to depth accuracy are used to calculate the error limits of the reduced depths:

$$Error_{depth} = \pm \sqrt{a^2 + (bd)^2} \quad (4.2)$$

where a and b are given for the order of survey and d is the depth.

The term a denotes the constant error limit and the term bd denotes the depth dependent error limits. The measurement of heave and tide, along with other less significant errors, are considered to form part of a . Errors in tidal measurement at the tide gauge site should not exceed ± 5 cm for Special order surveys and ± 10 cm for order one but transference of tidal data to the survey site can introduce errors in excess of 0.2 m in complex tidal regions (Imahori et al., 2003), which does not leave too much room for heave measurement errors in the case of Special order surveys.

It is too simplistic to say that heave measurement error limits of a nominal value will guarantee vertical reference to within the tolerances of a specific survey order as heave measurement errors must be considered alongside other constant depth errors. It can be said, however, that vertical reference for hydrographic survey using the classical method is generally concerned with surveys of order one and below; special

Order	Special	1	2	3
Examples of typical areas	Harbours, berthing areas and associated critical channels with minimum under keel clearances	Harbours, harbour approach channels, recommended tracks and some coastal areas with depths up to 100 m	Areas not described in Special Order and Order 1, or areas up to 200 m water depth	Offshore areas not described in Special Order or Orders 1 and 2
Horizontal accuracy (95% confidence level)	2 m	5 m + 5% of depth	20 m + 5% of depth	150 m + 5% of depth
Depth accuracy for reduced depths (95% confidence level)	a = 0.25 m, b = 0.0075 m	a = 0.5 m, b = 0.013 m	a = 1 m, b = 0.023 m	Same as Order 2
100% bottom search	Compulsory	Required in selected areas	May be required in selected areas	Not applicable
System detection capability	Cubic features > 1 m	Cubic features > 2 m in depths up to 40 m; 10% of depth beyond 40 m	Same as Order 1	Not applicable
Maximum line spacing	Not applicable as 100% search necessary	3 x average depth or 25 m, whichever is greater	3-4 x average depth or 200 m, whichever is greater	4 x average depth

Table 4.1: Summary of minimum standards for hydrographic surveys (IHO, 1998)

order surveys generally requiring a GPS-aided INS system. In surveys of order one and below a heave error of five to ten centimetres can be considered sufficient.

A full analysis of how heave error contributes to the overall reduced depth error is given in Hare (1995)

Chapter 5

Development of an INS Based Heave Algorithm

5.1 Introduction

From an early stage in the project it was evident that there would be a need for comparison of any GPS heave based algorithm produced to both the best reference available, and also to heave sensors currently on the market. To this end it was decided to develop Matlab code that would be able to produce a heave output equivalent to that provided by systems currently on the market from raw IMU gyro and accelerometer outputs. It was envisaged that this would provide a test platform against which to compare the GPS based heave output should a heave motion sensor not be available in the sea trials conducted, and also to allow heave to be produced from a range of IMU sensors.

Heave can be produced from raw IMU outputs using various methods, one of which is to mechanize the raw output of a strapdown IMU and incorporate a feedback damping loop to damp the vertical channel output. This process allows an estimation of the higher frequency vertical displacement of the vessel whilst removing the drift associated with the use of an INS. The feedback damping loop approach still has problems associated with its use which are evident from the frequency and transient analysis of the algorithms developed as part of this chapter. These problems were overcome in this thesis through the development of the GPS based heave algorithm which is far less susceptible to these errors and usability issues.

A heave sensing algorithm was developed that was intended to give an idea of the

accuracy of heave measurement achievable with inertial sensors and also to highlight the characteristics of heave motion sensing using inertial technologies. The algorithm developed was not intended to form a complete system or be as accurate as a commercially available heave motion sensor, but merely to be instructive as to the comparison of the GPS based heave algorithm with heave produced from inertial sensors. This chapter details the processes in the development of the INS based heave algorithm, showing the methods employed for strapdown INS mechanization used and the evolution of the damping of the vertical channel.

5.2 INS Mechanisation

It is clear from the information already given in chapter 2 that a full mechanisation of raw IMU outputs into the navigation frame is not required for heave estimation using inertial sensors; position information is not an output of an AHRS system. Instead, all that is required is the rotation of the raw accelerometer outputs measured in the body frame into the navigation frame. Velocity aiding is used in heave sensors as described in §2.5 to maintain a level platform through the sensing of the local gravity acceleration. The vertical accelerations in the navigation frame are then double integrated in a feedback damping loop to produce heave.

The heave algorithm developed during this project does not use any velocity aiding but keeps the platform level in the navigation frame through IMU gyros alone. Drift in the gyros will cause a drift in the local level as sensed by the gyros over time but the quality of the gyros over the course of the few hours for which it would be required this error was not considered significant. All aspects of full mechanisation except the resolution of horizontal velocity and position are required in the inertial heave algorithm developed, and as part of the work of the thesis a full mechanisation algorithm was developed. The entire mechanisation algorithm is included here for completeness before in depth discussion of the vertical channel damping loop.

5.2.1 Initialization and Alignment

Initialization of an INS must occur as a result of a measurement from an external sensor as described in §2.3.1. In the case of the heave algorithm developed it was

understood that the algorithm would either be used in a simulated environment where initial position and velocity were controllable, or that there would be a number of GPS receivers on board any vessel used in sea trials. In each of these cases it would be possible to provide a good estimate of initial position and velocity to the algorithm.

Alignment of an INS is discussed in §2.3.2 and ensures that an INS has a good initial estimate of attitude. This section of INS mechanisation has been omitted from this work. The reason for this, as with system initialization, is that the heave algorithm is only intended for use as a test platform and, as such, will only be used in either simulated environments or when conducting sea trials. Under simulated conditions an exact value for initial attitude can be provided and when conducting sea trials the Applanix POSRS system will be fitted to the vessel providing good estimates of attitude that can be fed to the algorithm.

As has been explained in chapter 2 AHRS units are supported by external sensors such as GPS or magnetometers, which aid initialization and alignment and maintain a level platform during operation. Algorithms to implement this aiding have not been included in the inertial based heave algorithm developed for this thesis for the reasons given above.

5.2.2 The INS Mechanisation Computation Loop

There follows a step through of the first iteration of the computation loop for INS mechanisation using the initial values passed after initialization and alignment.

5.2.2.1 Earth and Transport Rate

Earth and transport rate are both initially calculated using the position and velocity values passed to the algorithm for initialization.

Earth rate is that rotation of the earth frame with respect to the inertial frame due to rotation of the Earth on its axis and is a function of system latitude. It has been shown in equation 2.36 to be expressed in the navigation frame by

$$\omega_{ie}^n = \begin{bmatrix} \omega_{ie} \cos\lambda & 0 & -\omega_{ie} \sin\lambda \end{bmatrix}^T \quad (5.1)$$

Transport rate is the rotation of the system platform with respect to the inertial

frame caused by the travelling of the system over the Earth's surface. This has been shown in equation 2.37 to be expressed in the navigation frame as

$$\omega_{en}^n = \left[\begin{array}{ccc} \frac{v_E}{R_\lambda+h} & \frac{-v_N}{R_\phi+h} & \frac{v_E \tan \lambda}{R_\lambda+h} \end{array} \right]^T \quad (5.2)$$

These two values for Earth and transport rate can then be used to correct the raw IMU outputs for Coriolis acceleration.

5.2.2.2 Gravity Compensation

The local gravity vector is determined using a gravity model taken from Steiler and Winter (1982), which first calculates the gravity vector as a function of latitude at sea level:

$$g(0) = 9.780318(1 + 5.3024 \times 10^{-3} \sin^2 L - 5.9 \times 10^{-6} \sin^2 2L) \quad (5.3)$$

The rate of change of the gravity vector as a function of height is then calculated by

$$\frac{dg(0)}{dh} = -3.0877 \times 10^{-6}(1 - 1.39 \times 10^{-3} \sin^2 L) \quad (5.4)$$

5.2.2.3 Formation of the Navigation Frame Mechanisation Equation

The navigation frame mechanisation equation previously expressed in equation 2.42 is formed initially using the position, velocity and attitude values presented to the algorithm, and the Earth and transport rate values calculated.

A direction cosine matrix is formed from the initial attitude that allows the accelerations measured by the IMU in the body frame to be rotated into the navigation frame using equation 2.5, and Earth and transport rate are used to compute the Coriolis acceleration. These combine with the gravity vector to form the navigation frame mechanisation equation previously expressed in equation 2.42.

$$\dot{v}^n = C_n^b f^b - (2\omega_{ie}^n + \omega_{en}^n) \times v^n + g^n \quad (5.5)$$

5.2.2.4 Velocity and Position Updates

Integration of equation 5.5 will yield a velocity update that can be added to the previous velocity value to give current velocity in the navigation frame. A further integration yields a position update that can also be added to the previous position to give current position. A complication with the position update is that the navigation frame is not an ideal representation of position due to it being a flat plane tangential to the surface of the Earth. For this reason it is desirable to express system position in the geodetic frame of latitude (λ), longitude (ϕ) and height (h). The position updates can then be expressed

$$\dot{\lambda} = \frac{v_N}{R_N + h} \quad (5.6)$$

$$\dot{\phi} = \frac{v_E \sec L}{R_E + h} \quad (5.7)$$

$$\dot{h} = -v_D \quad (5.8)$$

5.2.2.5 Attitude Computation

Attitude is computed by firstly updating the quaternion elements as described in §2.4 where the quaternion propagates in accordance with

$$\dot{q} = 0.5q \cdot p_{nb}^b \quad (5.9)$$

where,

$$p_{nb}^b = \begin{bmatrix} \omega_{nb}^b \\ 0 \end{bmatrix} \quad (5.10)$$

and ω_{nb}^b are the raw attitude rate measurements recorded by the gyros of the IMU. The updated quaternion parameters are then used to compute an updated direction cosine matrix:

$$C_n^b = \begin{bmatrix} (d^2 + a^2 - b^2 - c^2) & 2(ab - dc) & 2(ac + db) \\ 2(ab + dc) & (d^2 + a^2 - b^2 - c^2) & 2(bc - da) \\ 2(ac - db) & 2(bc + da) & (d^2 + a^2 - b^2 - c^2) \end{bmatrix} \quad (5.11)$$

This is then used to compute attitude based on equation 2.5.

5.2.2.6 Subsequent Loop Iterations

The new values for system position, velocity and attitude are now fed back into the algorithm and the computation loop begins again. From this positive feedback configuration it is easy to see how drift of the output from an inertial system is of a quadratic nature as any error in the raw measurements and calculations is fed back into the next iteration of the algorithm.

5.2.3 Fourth Order Runge-Kutta Numerical Integration

Integration of the navigation frame mechanisation equation and the quaternion propagation equation must be undertaken using numerical methods because the function to be integrated is represented by numerical values (based on the raw IMU outputs). There are many methods of integrating a function numerically, some more computationally intensive than others. During the development of the INS mechanisation code the simple trapezium rule (James, 2001) was implemented but this was later replaced by the more accurate fourth order Runge-Kutta method (Kreyszig, 1988; Jeffrey, 1989).

Essentially a generalization of Simpson's rule the fourth order Runge-Kutta method of numerical integration was first demonstrated by C. Runge at the turn of the century and subsequently improved by W. Kutta. It is supposed that x and y assume the values x_n and y_n after the n^{th} integration step of the numerical integration of the function

$$\dot{y} = f(x, y) \quad (5.12)$$

Using an integration step size of h , the algorithm is given as

$$k_1 = f(x_n, y_n) \quad (5.13)$$

$$k_2 = f\left(x_n + \frac{h}{2}, y_n + \frac{k_1}{2}\right) \quad (5.14)$$

$$k_3 = f\left(x_n + \frac{h}{2}, y_n + \frac{k_2}{2}\right) \quad (5.15)$$

$$k_4 = f(x_n + h, y_n + k_3) \quad (5.16)$$

$$x_{n+1} = x_n + h \quad (5.17)$$

$$y_{n+1} = y_n + \frac{k_1 + 2k_2 + 2k_3 + k_4}{6} \quad (5.18)$$

and shows that the computation of four intermediary quantities (k_1 , k_2 , k_3 and k_4) is required before the value y_{n+1} can be calculated. It can be shown that the truncation error per step is of the order of h^5 (Collatz, 1966) making this a fourth order method. It is important to note that each integration using fourth order Runge-Kutta on sampled data will result in a solution at half the sampling rate. This is caused by the need to have measurements at $x = x_n + \frac{h}{2}$.

It is instructive to point out that the navigation frame mechanisation equation forms the function in the case at hand. When integrating to estimate velocity

$$\dot{v} = C_n^b f^b + (2\omega_{ie}^n + \omega_{en}^n) \times v^n + g^n \quad (5.19)$$

$$= f(f^n, v^n) \quad (5.20)$$

and when integrating to estimate position

$$\dot{p} = \left[\frac{v_N}{R_N + h} \frac{v_{EsecL}}{R_E + h} - v_D \right]^T \quad (5.21)$$

$$= f(f^n, p^{geo}) \quad (5.22)$$

5.3 INS Vertical Channel Damping

The position estimation from each channel of an INS (North, East and Down) will drift over time due to the positive feedback configuration inherent in the mechanisation

process (Farrell and Barth, 1999; Jekeli, 2001; Titterton and Weston, 2004). The rate of this drift will increase over time and can very quickly result in an INS output that has large position errors; the phenomenon is more evident in the vertical channel because of the gravity compensation fed back in the mechanisation.

The nature of heave motion of a vessel is such that it is only considered to occur at relatively high frequencies, nominally greater than 0.04 Hz (Godhavn, 2000), resulting in a heave output that can be considered to have a zero mean and consists of high frequency displacement away from that mean. In essence the low frequency motions measured on the vertical channel of the INS can be filtered out, a process which also removes the drift on that channel. There are various ways to achieve this; one technique, employed in this thesis, is to include a feedback damping loop on the vertical channel of the INS. This section details the processes used in the implementation of a third order feedback damping loop into the vertical channel of the INS mechanisation software.

5.3.1 The Baro-inertial Altimeter

For decades the avionics industry has used a damped INS output to improve the accuracy with which they can measure vertical velocity. This involves the use of a third order feedback damping loop, using the barometric altitude from the air data computer as a reference, a system called a baro-inertial altimeter.

The baro-inertial altimeter recognizes the long term instability of INS measurements and attempts to mitigate the errors associated with this by integrating the INS with a barometric altitude reference input. The inclusion of the long term stable barometric measurements results in a system that incorporates the short term advantages of INS without the long term drift. A full explanation of the operation of the system is given in Blanchard (1971); Siouris (1993); Kayton and Fried (1997). The basic principle is that an error signal is generated which is the difference between the altitude derived from the INS and the barometric altitude. This error signal is then fed back through gains to provide acceleration and velocity corrections which filter out low frequency motion and drift.

5.3.1.1 A Heave Filter Based on the Baro-inertial Altimeter

Heave motion is predominantly oscillatory in nature and so produces a time series that is assumed to have zero mean. Using this assumption a filter can be designed based on the baro-inertial altimeter to measure vertical heave displacement.

A filter of this kind, developed as part of the work of this project, was used in a paper concerning structural health monitoring (Hide et al., 2005). The motion experienced by large structures is similar in many respects to the heave motion of a vessel and so damped INS outputs lend themselves very well to this field.

A block schematic of a third order feedback damping loop used in a baro-inertial altimeter is given in figure 5.1. The reference input to the loop would be barometric altitude in a baro-inertial loop, but for heave motion sensing this is held at zero. The error signal is generated between the reference and the INS derived height output (h) to give

$$err = h - ref \quad (5.23)$$

In the case of the heave measurement feedback loop, the reference was zero so the error signal fed back is simply h . The gain C_4 is used to account for altimeter lag in the baro-inertial altimeter caused by the dynamic lag of the pressure transducer. This is unnecessary when the loop is configured for heave measurement as no pressure measurements are required and consequently C_4 was set to zero. Values for each of the feedback gains C_1 , C_2 and C_3 were taken from Siouris (1993):

$$C_1 = \frac{3}{\tau} \quad (5.24)$$

$$C_2 = 2\omega_s^2 + \frac{3}{\tau^2} \quad (5.25)$$

$$C_3 = \frac{1}{\tau^3} \quad (5.26)$$

where τ is the loop time constant and can be set by the user and ω_s is the Schuler frequency.

The vertical accelerations are input on the left hand side of the loop and are integrated twice at the blocks labeled $1/s$ to produce vertical velocity and position. A new

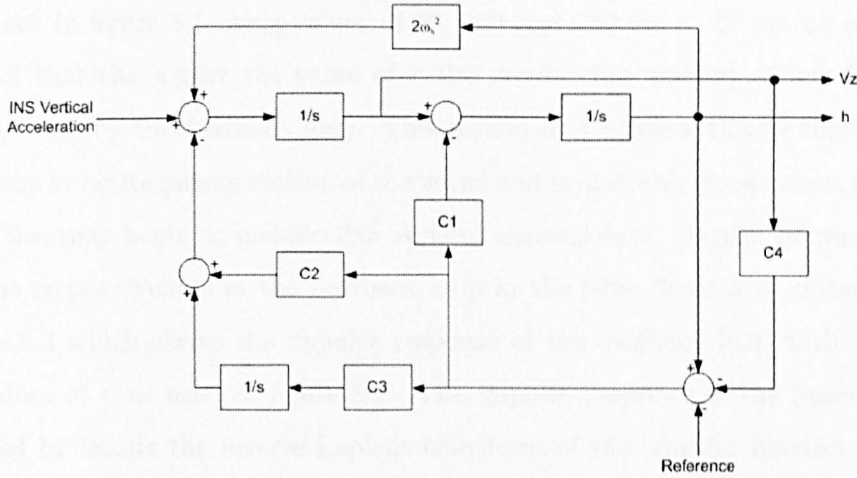


Figure 5.1: Block schematic diagram of a third order feedback damping loop

gravity calculation is provided by $2\omega_s^2$ and is fed back to the incoming accelerations. The error signal is fed back through gain C_1 to correct the velocity, and through the gains C_2 and C_3 and an integration step to correct the acceleration.

5.3.1.2 Frequency and Transient Analysis of the Baro-inertial Altimeter Based Heave Filter

The error signal and the gains that form the feedback damping loop correct the accelerations and velocity that are calculated in the vertical channel of the INS. The result of this feedback configuration is a system which behaves differently when subjected to signals of varying frequencies. The calculation of C_1 , C_2 and C_3 are such that they produce three poles at the complex frequency

$$s = -\frac{1}{\tau} \quad (5.27)$$

where s is the Laplace operator (Lidner, 1999). This results in a transfer function of

$$H(s) = \frac{1}{(s + \frac{1}{\tau})^3} \quad (5.28)$$

This transfer function can be used to produce plots that demonstrates the frequency response of the feedback damping loop with varying values of time constant (τ). Figure 5.2 shows the frequency and phase response of the third order feedback damping

loop shown in figure 5.1 using values of 50, 100 and 200 for τ . It can be seen from figure 5.2 that the higher the value of τ the greater the amount of low frequency motion passed by the feedback loop. This results in a heave estimate that includes more of the lower frequency motion of the vessel and is desirable except that, if pushed too far, this may begin to include INS vertical channel drift. Higher values of τ also affect the responsiveness of the feedback loop in the time domain as demonstrated in figure 5.3 which shows the impulse response of the feedback loop with the same three values of τ as used in figure 5.2. The impulse response of the heave filter is calculated by taking the inverse Laplace transform of the transfer function given in equation 5.28.

$$L[H(s)] = L\left[\frac{1}{\left(s + \frac{1}{\tau}\right)^3}\right] \quad (5.29)$$

$$= 0.5t^2e^{-\frac{t}{\tau}} \quad (5.30)$$

With a larger value of τ the output of the feedback loop takes longer to settle and so is less responsive to higher frequency inputs. It is also noted from figure 5.3 that the impulse response shows the loop to be over damped. The damping of the INS heave filter based on the baro-inertial altimeter is not currently configurable. This results in a heave filter that cannot be adequately tuned for different sea states and so may lack some flexibility in terms of heave measurement.

5.3.1.3 Redesign of the Heave Filter to Incorporate a Damping Coefficient

The short coming associated with the lack of damping control led to the redesign of the heave filter based on a transfer function seen in Weiss and DeVries (1977). This work shows a heave filter transfer function that incorporates a damping coefficient, ζ :

$$H(s) = \frac{1}{(s + \alpha)(s^2 + s\zeta\omega_n s + \omega_n^2)} \quad (5.31)$$

Where α is the real root s^{-1} and ω_n is the natural frequency in rads/s which is related to the time constant by $\omega_n = 2\pi/\tau$.

This transfer function allows the recalculation of the feedback gains C_1 , C_2 and C_3 incorporating ζ and setting $\omega_n = \alpha$.

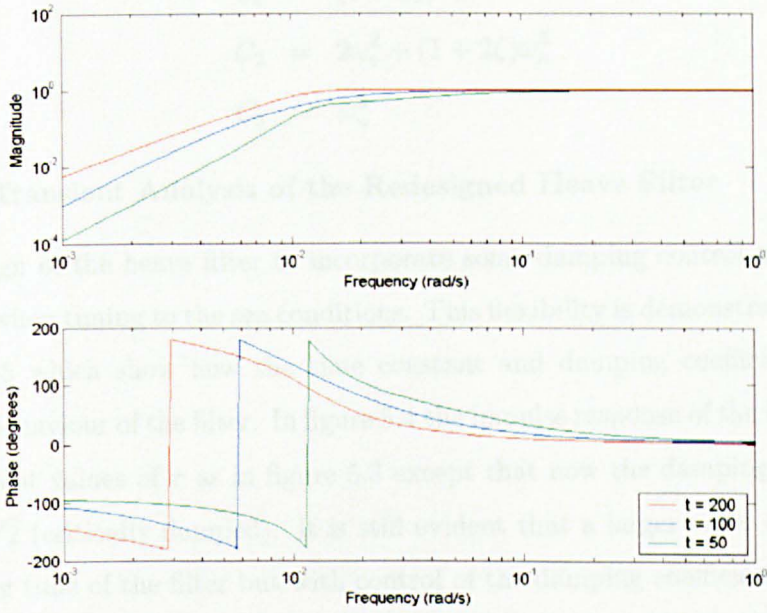


Figure 5.2: Frequency and phase response of baro-inertial altimeter with varying time constant

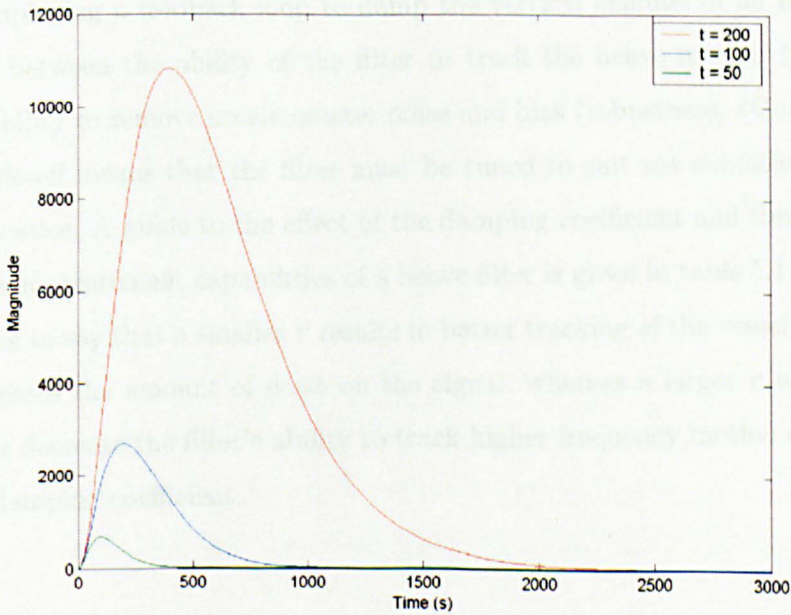


Figure 5.3: Impulse response of baro-inertial altimeter with varying time constant

$$C_1 = (1 + 2\zeta)\omega_n \quad (5.32)$$

$$C_2 = 2\omega_s^2 + (1 + 2\zeta)\omega_n^2 \quad (5.33)$$

$$C_3 = \omega_n^3 \quad (5.34)$$

5.3.1.4 Transient Analysis of the Redesigned Heave Filter

The redesign of the heave filter to incorporate some damping control allows greater flexibility when tuning to the sea conditions. This flexibility is demonstrated in figures 5.4 and 5.5 which show how the time constant and damping coefficient alter the transient behaviour of the filter. In figure 5.4 the impulse response of the filter is shown with different values of τ as in figure 5.3 except that now the damping coefficient is set to $1/\sqrt{2}$ (critically damped). It is still evident that a larger value of τ increases the settling time of the filter but with control of the damping coefficient this settling time is considerably reduced. Figure 5.5 shows the effect of the damping coefficient on filter settling time and shows that the larger the value of ζ the greater the amount of damping provided.

5.3.2 Heave Filter Tuning

When employing a feedback loop to damp the vertical channel of an INS there is a trade-off between the ability of the filter to track the heave motion (performance) and its ability to remove accelerometer noise and bias (robustness) (Godhavn, 2000). This trade-off means that the filter must be tuned to suit sea conditions and vessel characteristics. A guide to the effect of the damping coefficient and time constant on the heave measurement capabilities of a heave filter is given in table 5.1. Generally, it is possible to say that a smaller τ results in better tracking of the vessel heave motion but increases the amount of noise on the signal, whereas a larger τ will reduce the noise but decrease the filter's ability to track higher frequency motion and vice-versa for the damping coefficient.

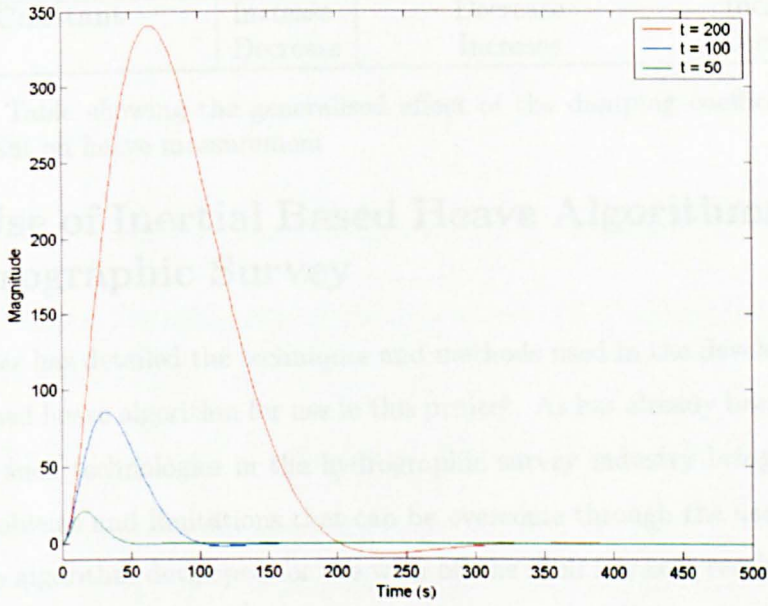


Figure 5.4: Impulse response of redesigned heave filter with varying time constant

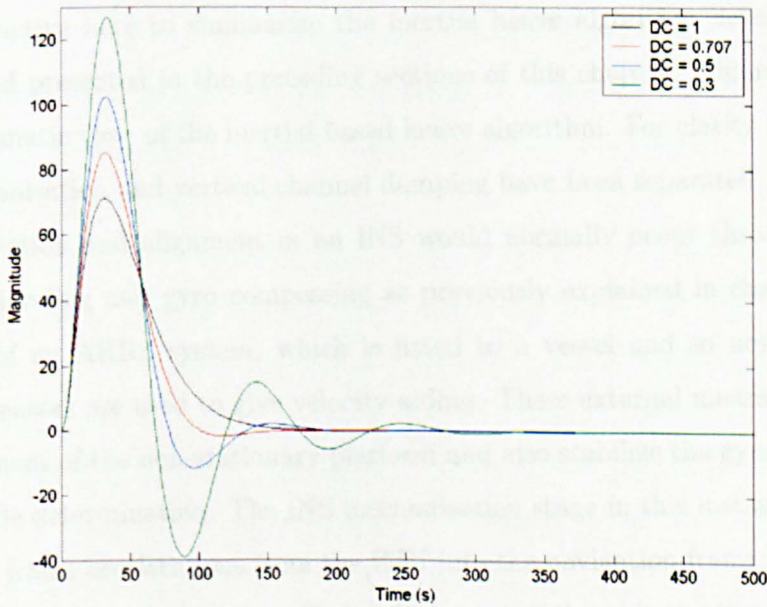


Figure 5.5: Impulse response of redesigned heave filter with varying damping coefficient

Heave Filter Parameter		Steady State Error	Settling Time
Damping Coefficient	Increase	Increase	Decrease
	Decrease	Decrease	Increase
Time Constant	Increase	Decrease	Increase
	Decrease	Increase	Decrease

Table 5.1: Table showing the generalised effect of the damping coefficient and the time constant on heave measurement

5.4 Use of Inertial Based Heave Algorithms in Hydrographic Survey

This chapter has detailed the techniques and methods used in the development of an inertial based heave algorithm for use in this project. As has already been mentioned, the use of such technologies in the hydrographic survey industry brings along with it some problems and limitations that can be overcome through the use of the novel GPS heave algorithm developed for use with off the shelf low cost receivers.

This section discusses the problems related to the use of inertial technologies for heave measurement with specific reference to the low cost GPS algorithm developed during the PhD.

5.4.1 Summary of Inertial Heave Algorithm

It is instructive here to summarize the inertial heave algorithm developed for the project and presented in the preceding sections of this chapter. Figure 5.6 shows a block schematic view of the inertial based heave algorithm. For clarity the process of INS mechanisation and vertical channel damping have been separated.

Initialization and alignment in an INS would normally occur through a process of coarse leveling and gyro compassing as previously explained in chapter 2 but in the case of an AHRS system, which is fitted to a vessel and so never stationary, external sensors are used to give velocity aiding. These external measurements allow the alignment of the non-stationary platform and also stabilize the gyro outputs used for attitude determination. The INS mechanisation stage in this instance rotates the raw body frame accelerations from the IMU into the navigation frame before vertical channel damping is undertaken. Heave filter tuning through the time constant and

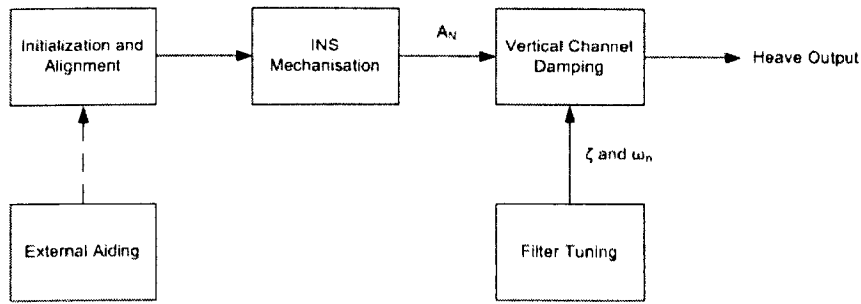


Figure 5.6: Block schematic diagram of the inertial heave algorithm

damping coefficient can change the characteristics of the heave output and are altered to suit vessel conditions.

5.4.2 Turn Induced Heave and Filter Transient Behaviour

The transient response of the heave algorithm has been assessed in §5.3.1.2 and the plots of the impulse response of the heave filter seen in figures 5.4 and 5.5 demonstrate that the heave filter has a certain transient response to large inputs. Dependent on the filter tuning parameters the heave output will ‘ring’ following a large input and so will require time to settle.

When a hydrographic survey vessel makes a turn at the end of a survey line a large input to the heave filter is generated, which causes a transient response similar to that seen in figures 5.4 and 5.5. The result of this is that the inertial heave sensor must be given time to settle again before the output can be considered accurate with settling times varying between 20 seconds and over $1\frac{1}{2}$ minutes dependent on the system used (Parker and Mallace, 2006).

The settling time of heave filters is of major importance to the hydrographic survey industry because they add directly to the length of time it takes for hydrographers to complete a survey. If a heave filter takes a minute to settle after a turn, this will add more than 2 minutes to each survey line which, when multiplied by the number of survey lines in the entire survey and the cost of putting a vessel to sea, can incur large costs for the survey company. In addition, a long run in to survey lines may not be possible if the survey is to be conducted in a confined space. The GPS velocity based heave algorithm developed for use on low cost GPS receivers overcomes

this stability limitation of inertial based heave sensors because it does not employ a feedback damping loop. Instead, a high pass filter is employed to remove the drift seen on the GPS based heave output as explained in chapter 6. This does result in a delay on the heave output but this would not pose a problem in the survey industry as there is no compelling requirement for heave data in real time.

5.4.3 Heave Filter Tuning

Filter tuning, as described in §5.3.2, can have a significant effect on the output seen from an inertial based heave filter. The heave filter must be tuned during installation so as to be compatible with vessel dynamic behaviour and in addition the user is expected to make an assessment of the sea state during the survey and set the filter tuning parameters accordingly. This is something of a black art and incorrect parameters can easily be set. Moreover, the burden placed on the user to set the filter tuning parameters can often be overlooked, the settings simply remaining in a given configuration. Both these scenarios can lead to significant errors in the heave compensation for a survey.

The problem of heave filter tuning is surmounted when the GPS velocity based heave algorithm developed during this PhD is used because sea state and vessel dynamic characteristics play no part in its determination of heave. There are no transients experienced by the GPS algorithm as it does not incorporate a feedback loop. This results in the same level of accuracy regardless of the vessel used or the sea conditions experienced.

5.4.4 Cost Implications of Inertial Heave Systems

As well as the cost implications already covered as part of the inertial heave algorithms stability limitations, there is a large cost involved in the use of inertial technologies for heave measurement based solely on their physical cost. Anecdotal evidence suggests that prices for inertial based heave sensors range from £12,000 to £25,000. When this is compared to the few hundred pounds that a low cost GPS receiver may cost, the financial savings become obvious. It is acknowledged, however, that heave measurement using inertial technologies is usual only one output of an AHRS system

that will also provide heading and attitude information for echo sounder beam steering a feature that could not be provided by a single GPS receiver but could be possible using multiple receivers all calculating TDD velocity.

Chapter 6

Development of a GPS Velocity Based Heave Algorithm

6.1 Introduction

There are a number of problems associated with the measurement of heave using inertial technologies, mainly surrounding usability, cost and long term instability. These can lead to inaccuracies in the measured heave and can also increase the time required to complete an offshore survey. These problems can largely be overcome through the use of the new heave algorithm developed for this project based on the carrier phase pseudo-ranges recorded using a U-Blox Antaris low cost GPS receiver. This method does not suffer from the same error sources as velocities derived from an INS, and can also be said to provide a much more stable heave output.

A heave algorithm was developed which extracted a highly accurate velocity estimate from a stand-alone GPS receiver using temporally differenced carrier phase pseudo-ranges. These velocities were then integrated to produce relative position, which, in the vertical channel, can provide an estimate of vessel heave. Drift, which grew over time, was evident on the relative position data produced in this way due to bias errors in the estimated velocity. A high pass filter was designed that would remove this drift but allow motion in the heave frequency band to remain.

The new heave algorithm developed during this research is the first to use a double difference approach to temporally differenced carrier phase velocity estimation. This approach calculates a first difference between observations across adjacent epochs from the same satellite and a second difference that removes the receiver clock by

differencing observations between satellites. It is the first algorithm that is specifically designed for use with commercially available low cost GPS receivers that record the carrier phase pseudo-range observable, and to have cycle slip handling based on the least squares residuals and a weighting scheme that takes advantage of the signal-to-noise ratio of each observation.

Strong advantages are available to the hydrographic survey industry through the use of the newly developed GPS based heave algorithm, not least reduced cost and reduced operator burden as there is no requirement to set time constants and damping factors as with inertial based heave sensors. This chapter shows the development of this GPS velocity based heave algorithm and gives details of all the algorithms, methods and techniques used when estimating heave in this way.

6.2 Velocity From Time-Differenced Carrier Phase Pseudo-range

The estimation of velocity from GPS can be undertaken using various methods, some of which are discussed in §3.6. The method used to produce the GPS based heave algorithm developed as part of this project is time differenced carrier phase pseudo-range (Itani et al., 2000; Serrano et al., 2004b; van Graas and Soloviev, 2004), a method often referred to as temporal differencing. This is currently the most accurate velocity estimation method to utilize only a single, stand-alone, GPS receiver because it is based on the carrier phase pseudo-range observable which contains less noise than the pseudo-range rate observable.

This section outlines a process of temporal differencing that actually implements a second difference of the carrier phase pseudo-range equation between two satellites and derives all of the equations required. This method will remove the receiver clock error term and, due to its nature, is termed temporal double differencing (TDD).

6.2.1 The Temporal Double Difference Observation Equation

Derivation of the TDD observation equation begins with the carrier phase pseudo-range observation equation derived in §3.3.2 with time frames removed for increased clarity of the TDD concept.

$$\phi_r^s = \frac{f}{c}\rho_r^s - f[\delta\tau_r - \delta t^s] + N_r^s + I + T + \epsilon \quad (6.1)$$

The first difference, that between observations from a single satellite recorded at adjacent epochs, results in the removal of the integer ambiguity term, N^s from 6.1.

$$\begin{aligned} \phi_r^{s1}(t_1, t_2) &= \phi_r^{s1}(t_2) - \phi_r^{s1}(t_1) \\ &= \frac{f}{c}\rho_r^{s1}(t_1, t_2) - f\delta\tau_r(t_1, t_2) + \epsilon \end{aligned} \quad (6.2)$$

Equation 6.2 describes the single differenced observations taken across two epochs. The integer ambiguity term, N^s , has been differenced away, the atmosphere is compensated for through the use of algorithms explained in §6.2.3 and the change in range and receiver clock drift terms remain. The satellite clock drift term is calculable from the GPS navigation message and is considered known.

The second difference occurs between two single difference equations generated from observations from separate satellites:

$$\begin{aligned} \phi_r^{s1s2}(t_1, t_2) &= \phi_r^{s2}(t_1, t_2) - \phi_r^{s1}(t_1, t_2) \\ &= \frac{f}{c}\rho_r^{s1s2}(t_1, t_2) + \epsilon \end{aligned} \quad (6.3)$$

In equation 6.3 the receiver clock drift term, $\delta\tau_r(t_1, t_2)$, is differenced away and ϵ is a combined error term that covers all remaining satellite, receiver and multipath errors.

6.2.2 The TDD Processing Algorithm

The algorithm described in the following sections has been implemented in Matlab and is largely based on van Graas and Soloviev (2004), although that work deals only with temporal differencing as opposed to the temporal double differencing used in this thesis. This section derives the TDD velocity algorithm from the observation equations given in §6.2.1.

Defining the necessary terms:

$$\begin{aligned} \Psi &= \text{ECEF XYZ position of satellite} \\ \psi &= \text{ECEF XYZ position of receiver} \end{aligned}$$

$$\begin{aligned}\rho &= \text{satellite to receiver range} \\ e &= \text{line of sight unit vector}\end{aligned}$$

In addition, t_1 and t_2 , when they appear in parenthesis after one of the terms defined above, denote the epoch from which the term originated.

The satellite to receiver range can be expressed as the dot product of the line of sight unit vector and the difference of satellite and receiver position:

$$\rho(t_1) = e(t_1) \cdot (\Psi(t_1) - \psi(t_1)) \quad (6.4)$$

Therefore, the single difference of the satellite receiver range as per equation 6.2 can be expressed as

$$\rho(t_1, t_2) = e(t_2) \cdot (\Psi(t_2) - \psi(t_2)) - e(t_1) \cdot (\Psi(t_1) - \psi(t_1)) \quad (6.5)$$

$$= e(t_2) \cdot \Psi(t_2) - e(t_1) \cdot \Psi(t_1) - e(t_2) \cdot \psi(t_2) + e(t_1) \cdot \psi(t_1) \quad (6.6)$$

The receiver position at t_2 , $\psi(t_2)$, can be expressed in terms of the receiver position at t_1 and a correction term.

$$\psi(t_2) = \psi(t_1) + \delta\psi \quad (6.7)$$

Substituting this into equation 6.6 yields

$$\begin{aligned}\rho(t_1, t_2) &= \\ &e(t_2) \cdot \Psi(t_2) - e(t_1) \cdot \Psi(t_1) - e(t_2) \cdot \psi(t_1) \\ &+ e(t_1) \cdot \psi(t_1) - e(t_2) \cdot \delta\psi\end{aligned} \quad (6.8)$$

In equation 6.8, $e(t_2) \cdot \Psi(t_2) - e(t_1) \cdot \Psi(t_1)$ represents the change in range caused by satellite motion over the epoch and is analogous to satellite velocity along the line of sight vector when data is collected at 1 Hz. Also, $e(t_2) \cdot \psi(t_1) + e(t_1) \cdot \psi(t_1)$ represents

the change in satellite to receiver geometry over the epoch. This allows equation 6.8 to be rewritten as

$$\rho(t_1, t_2) = \Psi(t_1, t_2) - geo(t_1, t_2) - e(t_2) \cdot \delta\psi \quad (6.9)$$

Equation 6.9 can now be substituted into equation 6.2 to yield

$$\phi_r^{s1}(t_1, t_2) = \frac{f}{c} \left[\Psi^{s1}(t_1, t_2) - geo^{s1}(t_1, t_2) - e(t_2) \cdot \delta\psi \right] - f\delta\tau_r(t_1, t_2) + \epsilon \quad (6.10)$$

If equation 6.10 is produced for two satellites then a further difference can be conducted that will remove the receiver clock drift term $f\delta\tau_r(t_1, t_2)$ resulting in

$$\begin{aligned} \phi_r^{s1s2}(t_1, t_2) &= \phi_r^{s2}(t_1, t_2) - \phi_r^{s1}(t_1, t_2) \\ &= \frac{f}{c} \left[\Psi^{s1s2}(t_1, t_2) - geo^{s1s2}(t_1, t_2) - e^{s1s2}(t_2) \cdot \delta\psi \right] + \epsilon \end{aligned} \quad (6.11)$$

which is the TDD observation equation.

Collecting together the known terms to the right hand side and the unknown terms to the left hand side of equation 6.11 yields

$$-e^{s1s2}(t_2) \cdot \delta\psi + \epsilon = \phi_r^{s1s2}(t_1, t_2) - \frac{f}{c} \left[\Psi^{s1}(t_1, t_2) - geo^{s1}(t_1, t_2) \right] \quad (6.12)$$

For simplification the following shorthand representations are used

$$\begin{aligned} \Delta\phi &= \phi_r^{s1s2}(t_1, t_2) - \frac{f}{c} \left[\Psi^{s1}(t_1, t_2) - geo^{s1}(t_1, t_2) \right] \\ e &= e^{s1s2}(t_2) \end{aligned}$$

A system of equations can then be formed for $n + 1$ satellites using the algorithm set out above that can be expressed in matrix form as

$$\underline{l} = \underline{A}\underline{x} \quad (6.13)$$

where

$$\underline{l} = \begin{bmatrix} \Delta\phi_1 \\ \Delta\phi_2 \\ \vdots \\ \Delta\phi_n \end{bmatrix} \quad (6.14)$$

$$\underline{A} = \begin{bmatrix} e_1 \\ e_2 \\ \vdots \\ e_n \end{bmatrix} \quad (6.15)$$

$$\underline{x} = \begin{bmatrix} \delta\psi_x \\ \delta\psi_y \\ \delta\psi_z \end{bmatrix} \quad (6.16)$$

Least squares can then be used to solve for \underline{x} which is the average receiver velocity over the epoch.

6.2.3 Specific Models and Techniques Used in the TDD Velocity Algorithm

This section describes each of the various models and techniques used within the TDD velocity algorithm in more detail.

6.2.3.1 Satellite Ephemeris Calculation

In order to process any of the observations recorded by the GPS receivers, satellite position must first be calculated. The TDD algorithm did this through the use of the navigation message transmitted by each satellite. Raw observation data collected by a GPS receiver was first converted into RINEX v2.1 files, an observation file and a navigation file. The navigation file contained all the information required to calculate satellite ephemeris. Calculation of satellite ephemeris was conducted using the algorithms laid out by the GPS JPO (1997) in the GPS interface control document.

To calculate satellite velocity for use in the estimation of user velocity, satellite positions from adjacent epochs were differenced, which can achieve satellite velocities with an error of ± 1 mm/s (Zhang et al., 2006).

6.2.3.2 Stand-alone GPS Position

Once satellite ephemeris was calculated and the position of each satellite known for a given time, stand-alone GPS position was then estimated using the equations discussed in §3.5.1. Calculation of receiver stand-alone position was important in the TDD algorithm for the formulation of the user to satellite unit vector. Stand-alone position was sufficient for the calculation of this vector due to the scales involved; the GPS satellites were upwards of 20,000 km away from the receiver and so a receiver position accuracy of around 10 m had little effect on the overall unit vector, which was calculated by

$$e_r^s = \frac{\Psi^s - \psi_r}{|\Psi^s - \psi_r|} \quad (6.17)$$

where e_r^s is the receiver to satellite unit vector, Ψ^s is satellite position and ψ_r is receiver position.

6.2.3.3 Tropospheric Correction

Tropospheric correction was provided for both the stand-alone position algorithm and the TDD velocity algorithm through the STANAG (1990) tropospheric model. The algorithm for tropospheric delay mitigation is given below; the part of the algorithm relating to altitudes between 0 and 1 km only was coded into the algorithm because of the intended application area.

The tropospheric range error estimated by STANAG (1990) can be written as

$$R(h, \theta) = f(\theta)\Delta R(h) \quad (6.18)$$

where

$$\begin{aligned} R(h, \theta) &= \text{total range error in metres} \\ \Delta R(h) &= \text{range error as a function of altitude in metres} \end{aligned}$$

h = altitude above mean sea level in metres
 θ = satellite elevation angle
 $f(\theta)$ = range error factor (mapping function) as a function of elevation angle

The mapping function $f(\theta)$ can be defined as

$$f(\theta) = \frac{1}{\sin\theta + \frac{0.00143}{\tan\theta + 0.0455}} \quad (6.19)$$

for $\theta < 90$, and $f(\theta) = 1$ for $\theta = 90$. Also

$$\Delta R(h) = \left[\int_{h=h_u}^{h=1km} (N_s + h\Delta N) dh + 1430 + 732 \right] \times 10^{-3} \quad (6.20)$$

$$= \left[(N_s + 0.5\Delta N^2) - (N_s h_u + 0.5\Delta N h_u^2) + 1430 + 732 \right] \times 10^{-3} \quad (6.21)$$

where h_u is the receiver altitude in kilometres, N_s is the surface refractivity index at mean sea level and $\Delta N = -7.32 \exp^{(0.005577N_s)}$. The global mean value for N_s is 324.8 but a recorded value can also be used.

In the case of stand alone position this correction was applied directly to the code pseudo-ranges before processing. When used in the TDD velocity algorithm the correction was scaled to L1 cycles through

$$\Delta R_\phi(h) = \frac{\Delta R(h)}{\lambda_{L1}} \quad (6.22)$$

where λ_{L1} is the wavelength of the L1 frequency transmission. This correction was then applied to the raw carrier phase pseudo-ranges before differencing.

6.2.3.4 Ionospheric Correction

Ionospheric corrections were applied to the algorithm in two separate ways, dependent on the mode of data collection. For dual frequency receivers the dual frequency data was used to remove almost all of the ionospheric delay while for single frequency receivers the Klobuchar (1996) ionospheric model was used.

The dual frequency data was corrected for ionospheric delay using observations on both the L1 and L2 frequencies (Parkinson and Spilker, 1996a; GPS JPO, 1997; Misra and Enge, 2004). The equation for this when using code pseudo-ranges was given in equation 3.15 and this was used when estimating stand-alone position. In the TDD velocity algorithm, however, carrier phase pseudo-range measurements were used and, in this case, the equation can be represented as below.

$$I_{\phi L1} = \frac{\phi_{L1} f_1 f_2 - \phi_{L2} f_2^2}{f_2^2 - f_1^2} \quad (6.23)$$

Use of dual frequency data removed almost all of the ionospheric delay that appeared on the carrier phase pseudo-range observable on L1 although some residual effects still remained. There was also some component of this correction that was affected by receiver noise. Receiver noise was present on the carrier phase pseudo-range observable and so was also present on $I_{\phi L1}$. This manifested as high frequency changes in the ionospheric delay, a notion which is empirically unsound. $I_{\phi L1}$ was therefore filtered through a low pass filter that removed much of the noise. This process introduced a delay in the output of the TDD velocity algorithm through the group delay of the filter, but this was considered unimportant since there was to be a filter used to remove the drift from the eventual heave output, which will introduce a larger group delay as described in §6.3. The low pass filter used was merely a running average which took the mean of $I_{\phi L1}$ for 24 epochs either side of the current epoch. The smoothed dual frequency ionospheric correction had reduced noise and so produced a less noisy TDD velocity output.

Ionospheric correction for single frequency data was provided by the Klobuchar (1996) ionospheric model. This used a set of parameters, α and β , which each contained four elements and were transmitted in the GPS navigation message. The

algorithm used for this is given below.

The earth centred angle, ψ , was first calculated:

$$\psi = \frac{0.0137}{(\theta + 0.11)} - 0.022 \quad (6.24)$$

where θ is the satellite elevation angle.

Then the subionospheric latitude, λ_l could be computed:

$$\lambda_l = \lambda + \psi \cos A \quad (6.25)$$

where λ is the user receiver latitude and A is the satellite azimuth. Here the maximum range of λ_l is ± 0.416 such that if $\lambda_l > 0.416$, then $\lambda_l = 0.416$ and if $\lambda_l < -0.416$, then $\lambda_l = -0.416$.

The subionospheric longitude, ϕ_l , was computed next:

$$\phi_l = \phi + \left(\frac{\psi \sin A}{\cos \lambda_l} \right) \quad (6.26)$$

where ϕ is user receiver longitude.

The geomagnetic latitude, λ_m , of the subionospheric location looking toward each GPS satellite could then be calculated:

$$\lambda_m = \lambda_l + 0.064 \cos(\phi_l - 1.617) \quad (6.27)$$

Then local time, t_l at the subionospheric point:

$$t_l = 4.32 \times 10^4 \phi_l + \text{GPS time} \quad (6.28)$$

Now the slant factor, F , was calculated:

$$F = 1.0 + 16.0 \times (0.53 - \theta)^3 \quad (6.29)$$

Then, the ionospheric time delay, T_{iono} was found by first computing the period of model (PER) and subsequently x :

$$PER = \sum_{n=0}^3 \beta_n \lambda_m^n \quad (6.30)$$

$$x = \frac{2\pi(t_l - 50400)}{PER} \quad (6.31)$$

Then T_{iono} could be computed from either

$$T_{iono} = F(5 \times 10^{-9}) \quad (6.32)$$

for $|x| > 1.57$. Or

$$T_{iono} = F \left[5 \times 10^{-9} + \sum_{n=0}^3 \alpha_n \phi_m^n \times \left(1 - \frac{x^2}{2} + \frac{x^4}{24} \right) \right] \quad (6.33)$$

The terms α and β in equations 6.33 and 6.30 respectively are those parameters transmitted in the GPS navigation message.

As with tropospheric delay mitigation, this correction was applied directly to code pseudo-ranges when stand-alone position was required. For the TDD velocity algorithm the correction was scaled to L1 cycles, as described in equation 6.22 and applied before differencing.

6.2.3.5 Correction for Satellite Loss

The nature of TDD velocity requires that two adjacent epochs of data are available for each satellite to be used in the algorithm. If a satellite was lost below the elevation mask then it was also removed from the observations of the previous epoch and as such played no part in the estimation of TDD velocity. A similar technique was applied to new satellites that appeared above the elevation mask in that they could not be used in the TDD velocity algorithm until at least two adjacent epochs of data were available.

6.2.3.6 Cycle Slip Handling

The majority of cycle slips that may occur in the measurement of the carrier phase pseudo-range observable are handled inherently as part of the TDD algorithm itself. In order to difference the carrier phase pseudo-range observable across adjacent epochs as described above, there had to be two consecutive epochs of data available to the algorithm. When in the case of a particular satellite there were not consecutive observations, that satellite's data was discarded and not included in the algorithm for that epoch. This applied when a satellite's signal was lost for any reason and so did not appear in the RINEX file, and also when it was regained and consequently reappeared. Through this system the majority of cycle slips, which were caused through satellite signal loss, were prevented from having an impact on the TDD velocity solution.

In addition to the cycle slip immunity offered by the TDD velocity algorithm, a process of least squares analysis was developed that would remove any 'bad' observations that had been subject to slips and had introduced an error in the TDD velocity estimation. After TDD processing the least squares residuals were analysed and their mean value calculated. If the residual of a particular observation was seen to differ from the mean of the residuals by a sufficient amount then this observation was removed from the system of equations and the least squares estimation computed again.

Under the majority of circumstances this algorithm was sufficient to remove the observation containing the cycle slip but, because the TDD algorithm differences carrier phase pseudo-ranges from separate satellites, cycle slips were not always removed in this way. In the TDD algorithm a reference satellite is chosen, the observations of which are used to difference with the observations from the other usable satellites. If the cycle slip occurred on the observation from the reference satellite then all residuals would be affected. In this instance the reference satellite observations were removed from the algorithm, a new reference satellite was selected and the least squares estimation computed again with the new reference satellite.

On rare occasions even this second attempt to provide cycle slip immunity was not sufficient and under these circumstances it was considered that cycle slips had

occured on multiple, possibly all, channels of the receiver. Algorithms exist to repair these errors in carrier phase pseudo-range data but they have not been investigated as part of this research. Instead, the epochs where this has occurred have been removed from the data set.

6.2.3.7 Carrier-to-Noise Density Weighting Scheme

Weighting schemes can be applied to the least squares processing of GPS observations in order to weight more heavily any high quality observations and decrease the influence of poor quality observations. These weighting schemes can improve the quality of the position and velocity outputs produced from receiver raw observations, particularly in the case of low cost receivers such as the U-Blox Antaris where tracking loop componentry is of a low quality. In the case of low cost GPS receivers the thermal noise and noise introduced by the code and carrier tracking loops due to low quality componentry can be much more significant than that seen in higher grade dual frequency receivers.

The use of the U-Blox Antaris low cost receiver in this thesis has necessitated the development of a weighting scheme to better handle the raw carrier phase pseudo-range observables. Weighting schemes have been suggested based upon both satellite elevation angle and observation signal-to-noise ratio (Collins and Langley, 1999) but analysis of the stand-alone position and TDD velocity residuals from the least squares estimation using the U-Blox receiver suggested a strong correlation between poor quality observations and carrier-to-noise density, C/N_0 . For this reason, and because they are considered to be potentially more powerful, it was decided to employ a weighting scheme based upon the carrier-to-noise density of each observation. Collins and Langley (1999) implemented a weighting scheme based upon the approximation of the formula for calculating carrier tracking loop noise given in Langley (1997).

$$\sigma_{L1} = \sqrt{\frac{B}{c/n_0}} \cdot \frac{\lambda_{L1}}{2\pi} \quad (6.34)$$

where σ_{L1} is the error on the carrier phase measurement (m), B is the carrier tracking loop bandwidth (Hz), c/n_0 is the carrier-to-noise density expressed as a ratio ($=10^{\frac{C/N_0}{10}}$ in dB-Hz) and λ_{L1} is the L1 carrier wavelength.

To be able to implement this formula as a weighting scheme it was required that the carrier-to-noise density be recorded by the receiver to be used. The U-Blox Antaris receiver does record this value and by removing those elements which were constant at a particular epoch a function was arrived at that would provide the weighting scheme for the U-Blox Antaris GPS observations.

$$\frac{1}{w^s} = \sqrt{\frac{1}{10^{\frac{C/N_0}{10}}}} \quad (6.35)$$

where w^s is the weighting factor for a given satellite. All the values of w^s were then normalised and formed into a diagonal matrix which was used to weight the least squares estimation.

6.3 The TDD Heave Algorithm

The velocities produced by the TDD velocity algorithm were integrated in the vertical channel in order to produce relative vertical position, which could be directly compared to the heave output from an inertial based heave sensor. Bias errors in the vertical velocity resulted in a drift of the relative vertical position with time, however, and these drift errors had to be removed to improve the accuracy of the TDD heave algorithm output.

A high pass filter was designed that removed all the drift yet left a zero meaned relative vertical position output within the required heave frequency band (> 0.03 Hz). The filter is a linear phase finite impulse response filter designed using the Parks-McClellan algorithm (IEEE, 1979) within the filter design and analysis tool in Matlab. The order of the filter was 276 and was a result of the design algorithm employed within Matlab based on the design criteria requested in the filter design and analysis tool, which are listed below and illustrated in figure 6.1.

- F_s 1 Hz
- F_{stop} 0.02 Hz
- F_{pass} 0.03 Hz
- A_{pass} 1 dB

- A_{stop} -80 dB

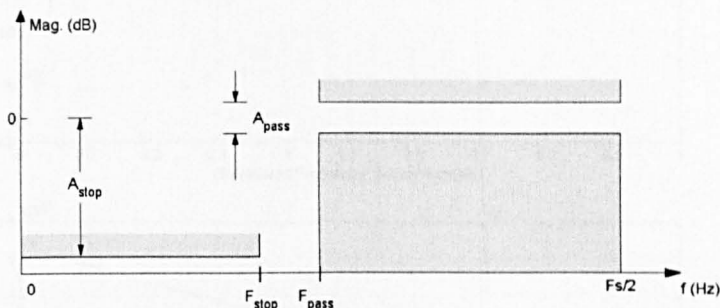


Figure 6.1: High pass filter design criteria required by Matlab filter design and analysis tool

The order of the filter was not considered an important factor when designing the heave filter as the TDD heave algorithm was always intended to be a near real time system. Increasing the performance of the filter in terms of its design criteria would have the effect of increasing the filter order and, hence, the filter group delay. The transfer function of the heave filter is shown in figure 6.2. It had a -3dB cut-off frequency of 0.03 Hz and imparted a group delay of 138 samples on the heave output data when GPS observables were recorded at 1 Hz.

The heave filter designed was used to remove all the drift from the relative position output gained from the integration of the TDD velocities and the bias errors associated with it.

A block schematic diagram of the full TDD heave algorithm is included here at figure 6.3 showing the entire process from raw GPS data collection through to heave output.

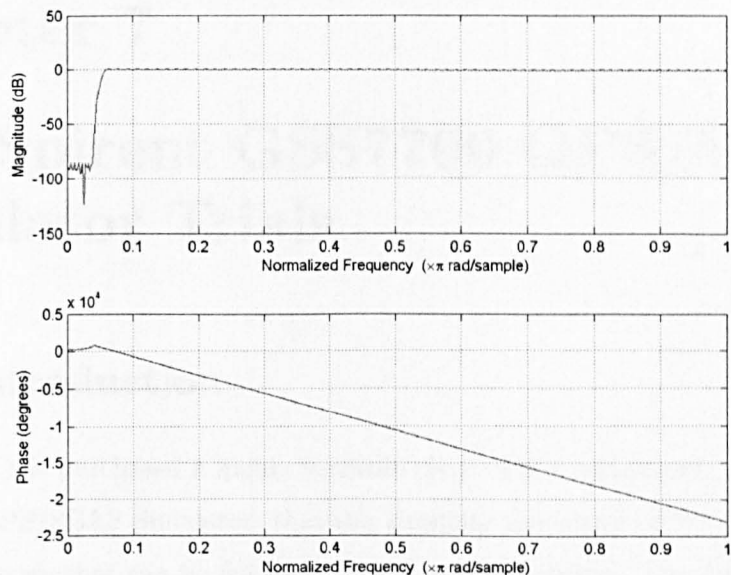


Figure 6.2: Frequency and phase response of high pass heave filter

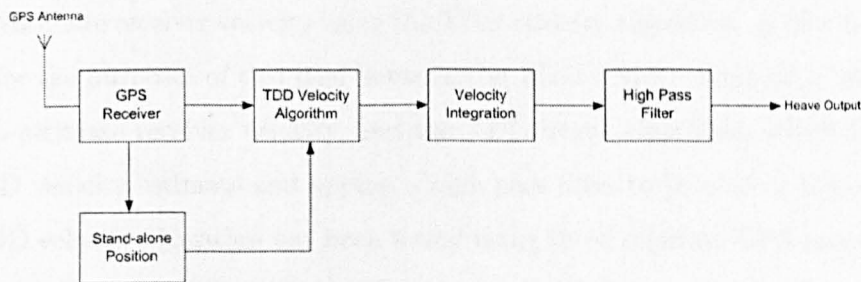


Figure 6.3: Block schematic diagram of the TDD heave algorithm

Chapter 7

The Spirent GSS7700 GPS/SBAS Simulator Trials

7.1 Introduction

The IESSG has purchased a highly versatile piece of test equipment, called a Spirent GSS7700 GPS/SBAS Simulator, that can simulate the entire GPS constellation and generate signals that can be fed directly into a GPS receiver. The Spirent simulator simulates the GPS signals transmitted by each of the GPS satellites as they would be received by a GPS receiver that was undergoing the dynamics laid out in the simulator scenario. As such, the Spirent simulator provides an excellent platform from which to test different GPS receivers against one another and has been used extensively during the development and testing of the TDD velocity algorithm discussed in chapter 6.

A trial was developed to assess the quality of the phase pseudo-range observable recorded with a commercially available low cost GPS receiver, and its ability to be used to estimate receiver velocity using the TDD velocity algorithm. A distinction was drawn for the purposes of this trial between the TDD velocity algorithm, which uses TDD to estimate receiver velocity, and the TDD heave algorithm, which integrates the TDD velocity estimate and applies a high pass filter to produce a heave output. The TDD velocity algorithm has been tested using three separate GPS receivers: one low cost and two dual frequency. They have each been used to collect simulated raw GPS observables under varying simulated dynamic conditions and the use of the Spirent simulator allowed the extraction of truth data that meant a highly accurate assessment of receiver performance was possible. The TDD heave algorithm has been

tested using a simulated marine scenario with dynamics close to those experienced under real marine conditions.

This trial was the first to assess the performance of the TDD velocity and heave algorithms using commercially available low cost GPS receivers under the controlled conditions of a simulated environment. It has allowed an accurate assessment of the ability of low cost receivers to provide a quality phase pseudo-range observable and helped develop an understanding of the likely error sources, information vital to the continued development of low cost receivers for accurate position and velocity applications. This work expanded on the work already conducted in the estimation of precise GPS velocity based on time differenced carrier phase pseudo-ranges using a similar simulator (Ryan et al., 1997), which has tested a temporally differenced carrier phase pseudo-range based velocity technique under various dynamics using higher grade GPS receivers.

This chapter discusses the Spirent GSS7700 GPS/SBAS Simulator and the particular elements used in this project, the trial conducted on the simulator and goes on to present the results of the trial.

7.2 The Spirent GSS7700 GPS/SBAS Simulator

The Spirent GSS7700 GPS/SBAS Simulator is a tool that provides a comprehensive development and testing environment for satellite navigation hardware (Spirent, 2006). The Spirent simulator can simulate the environment experienced by a GPS receiver while on a static or kinematic platform. The GPS transmitted signals can be simulated and fed directly into an existing GPS receiver via an RF cable as though that receiver were undergoing a set of predetermined vehicle dynamics, with full control over a number of error sources.

The Spirent simulator can be considered to consist of two elements, a brief description of both is given in the following two subsections.

7.2.1 Simulator Hardware

The hardware purchased by the IESSG consists of two RF signal generators, a PC and a pre-amp unit. A picture of the setup used in the simulator trial is given in

figure 7.1 and shows each of the main hardware elements required.

The signal generators generate and transmit the simulated GPS signals that will be received at the receiver. Essentially, they convert the calculated pseudo-ranges into the correct GPS messages from each satellite in view; the PC is used to configure the signal generators using the SimGEN software explained in §7.2.2; and the pre-amp has been designed to simulate the pre-amps that are found in many GPS antennas.

7.2.2 Simulator Software

SimGEN is the software that is provided as a development environment for the designed simulations, termed scenarios. A set of description or source files go together to define the scenario. The principle description files used during the simulator trial were the motion file, which describes the motion of the receiver to be simulated, and an atmosphere file that define what atmospheric effects are to be modelled. Navigation data to describe satellite orbits can also be provided to the simulator so as to simulate a particular date as accurately as possible.

The software uses the description files to run models that calculate such parameters as pseudo-range, atmospheric delays and satellite position. Each of these parameters can be output by the simulator, providing an excellent testbed for development of any GPS navigation software.

7.2.3 Simulator Setup and Error Models

The Spirent simulator is tremendously versatile and gives the user complete control over many of the error sources and accuracy parameters of the space section of the GPS. For much of the trial all the error models that can be implemented using the Spirent simulator were turned off as the simulator trial was primarily focussed on isolating receiver based errors. Where atmospheric modelling was required the STANAG (1990) model was used to impart tropospheric error on the simulated signals and the Klobuchar (1996) model was used for ionospheric delay modelling. All other models and error sources were turned off for the simulator trial but in future tests the Spirent simulator could prove a powerful tool in the assessment of the impact of various space segment based error sources on TDD velocity estimation using low cost

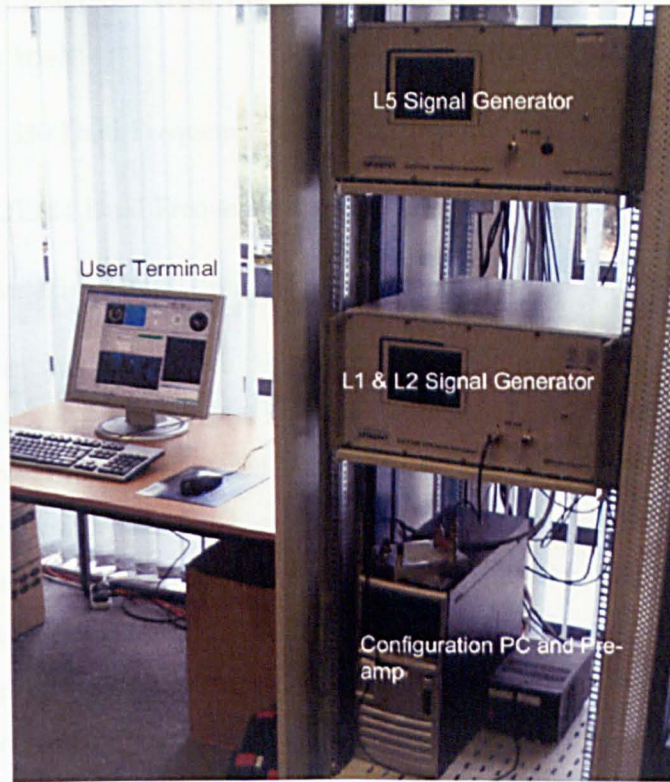


Figure 7.1: Spirent GNSS Simulator

receivers.

Satellite orbit information was provided to the simulator from a global RINEX v2.1 navigation file for the simulated trial date downloaded from the CORS website (National Geodetic Survey, 2007). This allowed a realistic simulation of the actual conditions experienced on the day in terms of satellite availability. Satellite clock offsets and drifts were also contained within the navigation file and modeled as such within the simulator.

7.3 Trial Methodology

The simulator trial was designed to test both the TDD velocity and heave algorithms developed as part of the project, and the effect of the use of low cost receivers compared to geodetic grade receivers. The hardware simulator, unlike software simulators, produces simulated GPS signals that can be fed directly into real GPS receivers. This allows a thorough assessment of receivers against each other as the errors introduced

by each can be isolated. With this in mind three separate types of receiver were selected for the trials:

- Leica SR 530 Dual Frequency Receiver
- Novatel OEM4 Dual Frequency Receiver
- U-Blox Antaris LEA-4T Single Frequency Receiver

Each receiver was selected to represent a different section of the GPS receiver market: the Leica SR 530 is a dual frequency geodetic receiver that is primarily used in the land survey industry to record static observations, the Novatel OEM4 is another dual frequency receiver that has been designed for the navigation market, and the U-Blox Antaris is a single frequency low cost receiver that can record the carrier phase pseudo-range observable.

Three scenarios were programmed into the Spirent simulator to test each receiver under different dynamic conditions. Four trials were then designed that would effectively test each receiver and also demonstrate the operability and limitations of the TDD velocity and heave algorithms. An arbitrary date of 24 January 2006 was selected to be the trial date for all simulator trials and the ephemeris data for that date, downloaded from National Geodetic Survey (2007), was loaded into each of the three scenarios.

An auxiliary trial, trial 5, is also included here although it did not involve the use of the Spirent simulator but rather the collection of real GPS data.

7.3.1 The Simulated Scenarios

Three scenarios were developed and programmed into the Spirent simulator. These were designed to test the algorithm under different dynamics and are outlined below.

7.3.1.1 Static

The static scenario simulated a static GPS receiver at the same location as a real GPS antenna sited on the turret of the IESSG building. The position of the simulated receiver was programmed into SimGEN as

- Latitude: 52° 56' 26.49612''*N*
- Longitude: 1° 11' 32.32482''*W*
- Height: 98.47 m

7.3.1.2 Marine

A marine scenario was developed that was intended to deliver the most realistic simulation of the intended algorithm environment. A motion file was programmed into the simulator using SimGEN. The motion file held the vessel static, in the same position as simulated for the static scenario, for a period of 650 s so that each of the GPS receivers used would have sufficient time to lock on to all the satellites before and simulated motion began. The scenario then took the simulated vessel from the start position in a straight line in a north-westerly direction for a further 1,150 s. Over the course of the simulation four separate sea states of varying severity were simulated. SimGEN only allows for sinusoidal heave motion within the sea state file and so realistic heave motion cannot be simulated but the principles of heave motion remain the same. Therefore, during the marine scenario the TDD velocities computed using the three separate receivers were used to create a heave plot of vertical motion, which was compared directly to heave derived from true vertical motion.

A plan view of the trajectory of the marine scenario is shown in figure 7.2 and the height profile can be seen in figure 7.3. Whilst the height profile plot in figure 7.3 does not clearly show the frequency of the heave in each of the separate sea state zones the details of each sea state are given in table 7.1. In addition to the trajectory of the marine scenario, it is also necessary to include the velocity profile, seen in figure 7.4, which shows the changes in North, East and Down velocity with time during the scenario.

Sea State	Wave Height (m)	Wave Frequency (Hz)
1	1.5	0.4
2	1.5	0.2
3	1.5	0.1
4	1.5	0.05

Table 7.1: Table of sea states used in simulated marine scenario

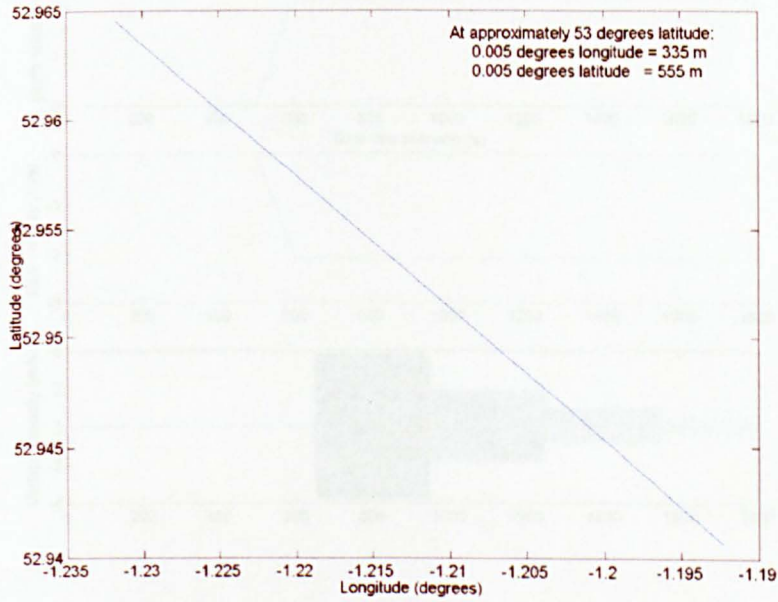


Figure 7.2: Plan view of simulated marine scenario trajectory

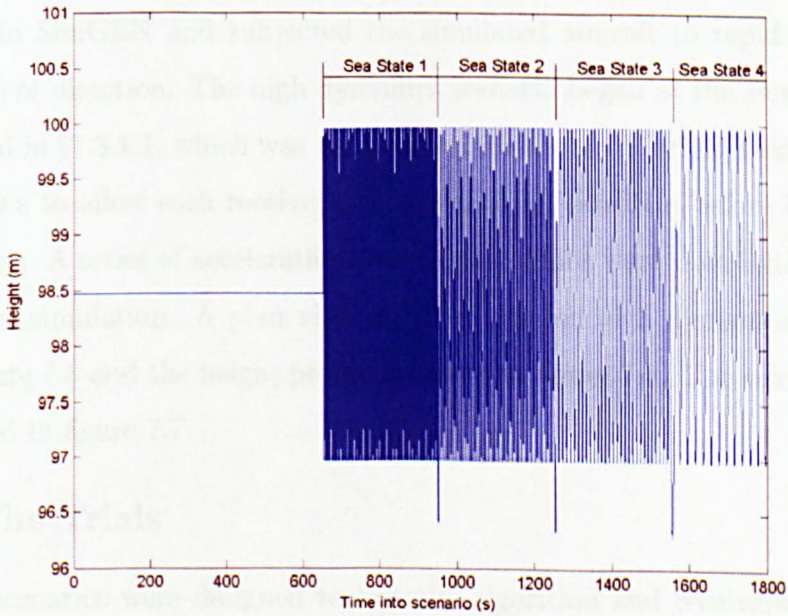


Figure 7.3: Height profile of simulated marine scenario

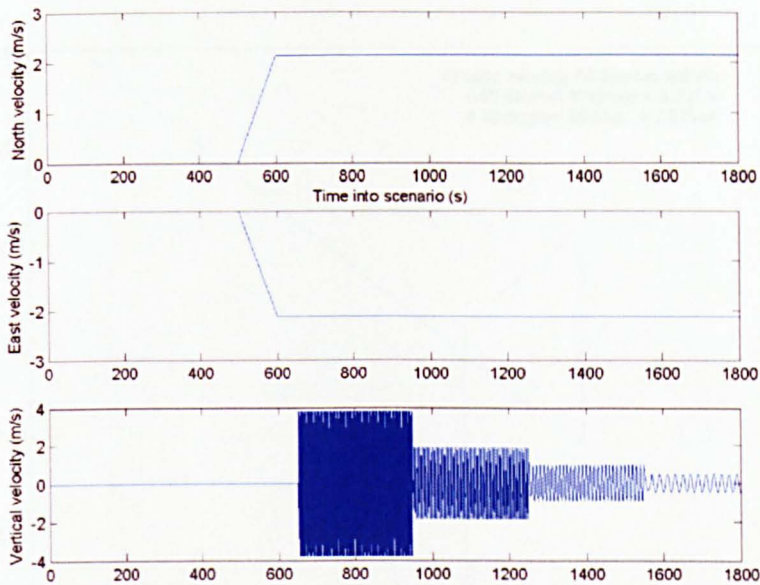


Figure 7.4: Velocity profile of simulated marine scenario

7.3.1.3 High Dynamics

In order to test the dynamic stress performance of the signal tracking loops on each receiver a high dynamic scenario was designed. This used the aircraft vehicle model within SimGEN and subjected the simulated aircraft to rapid accelerations and changes of direction. The high dynamics scenario began at the same position as that detailed in §7.3.1.1, which was the position for the static trial. This position was held for 300 s to allow each receiver to lock on to all satellites before high dynamic motion began. A series of accelerations, turns and climbs were then initiated over the course of the simulation. A plan view of the simulated high dynamics trajectory is given in figure 7.5 and the height profile is shown in figure 7.6. The velocity profile is also included in figure 7.7.

7.3.2 The Trials

The three scenarios were designed to test the algorithm and receivers under different dynamics; a series of trials were developed to isolate receiver based errors and demonstrate the functionality of the TDD velocity and heave algorithms. The trials

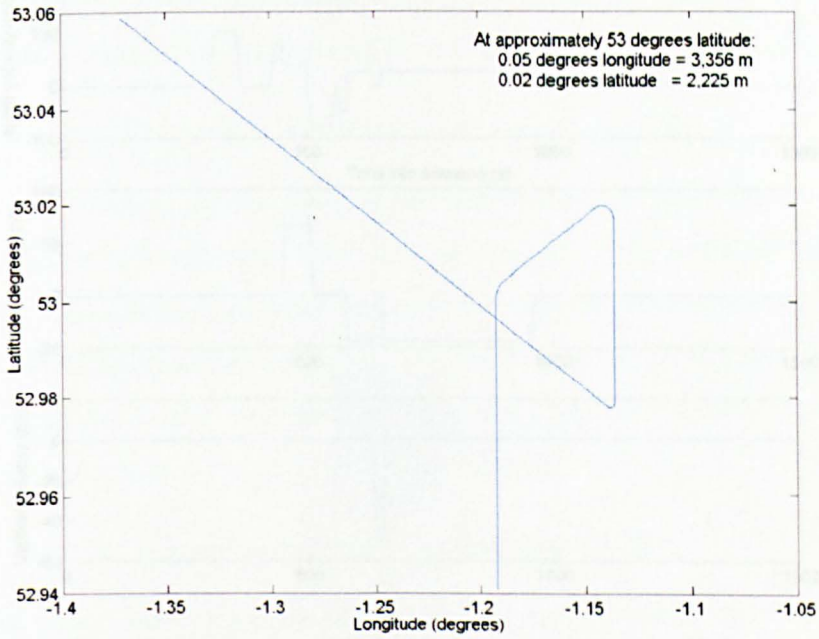


Figure 7.5: Plan view of simulated high dynamics scenario

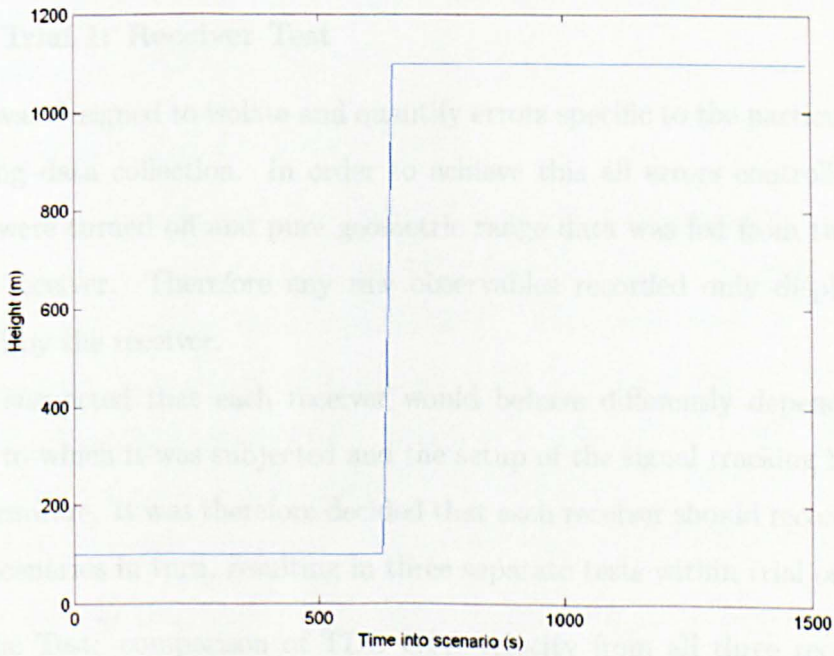


Figure 7.6: Height profile of simulated high dynamics scenario

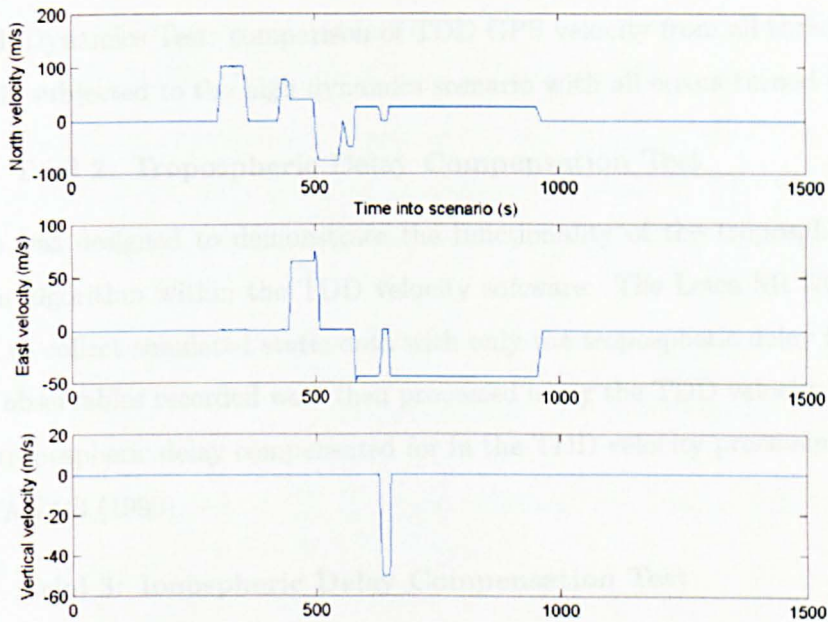


Figure 7.7: Velocity profile of simulated high dynamics scenario

are numbered one to five and each had a specific objective, which is set out in the following subsections.

7.3.2.1 Trial 1: Receiver Test

Trial one was designed to isolate and quantify errors specific to the particular receiver used during data collection. In order to achieve this all errors controllable within SimGEN were turned off and pure geometric range data was fed from the simulator into each receiver. Therefore any raw observables recorded only displayed errors introduced by the receiver.

It was suspected that each receiver would behave differently dependent on the dynamics to which it was subjected and the setup of the signal tracking loops within receiver firmware. It was therefore decided that each receiver should record data from all three scenarios in turn, resulting in three separate tests within trial one.

- Static Test: comparison of TDD GPS velocity from all three receivers while subjected to the static scenario with all errors turned off.
- Marine Test: comparison of TDD GPS heave from all three receivers while

subjected to the marine scenario with all errors turned off.

- High Dynamics Test: comparison of TDD GPS velocity from all three receivers while subjected to the high dynamics scenario with all errors turned off

7.3.2.2 Trial 2: Tropospheric Delay Compensation Test

Trial two was designed to demonstrate the functionality of the tropospheric delay correction algorithm within the TDD velocity software. The Leica SR 530 receiver was used to collect simulated static data with only the tropospheric delay turned on. The raw observables recorded were then processed using the TDD velocity algorithm and the tropospheric delay compensated for in the TDD velocity processing software using STANAG (1990).

7.3.2.3 Trial 3: Ionospheric Delay Compensation Test

Trial three was similar in nature to trial two except that trial three was designed to demonstrate the functionality of the ionospheric delay correction algorithm within the TDD velocity processing software. The Leica SR 530 receiver was again used to collect simulated static data, this time with only the ionospheric delay turned on. The raw observables were then processed using the TDD velocity algorithm, firstly using only L1 data with the Klobuchar model, then using dual frequency data with dual frequency ionospheric correction.

7.3.2.4 Trial 4: Full Simulation Test

Trial four was the final trial to be conducted using the Spirent simulator and brought together all the previous trials by recording data from both the static and marine scenarios on all receivers with tropospheric and ionospheric delay turned on. This constituted the most realistic trial conducted with the simulator and was a natural final step before collecting real GPS data. The high dynamic scenario was neglected for this trial because it was designed to test the dynamic performance of the signal tracking loops in each receiver and this had already been completed in trial one.

7.3.2.5 Trial 5: Real Static Data

After completion of the Spirent simulator trial it was decided that a good intermediate step between that and the Plymouth sea trial would be to collect real static GPS data using each receiver and subsequently process the data using the TDD velocity algorithm. Static GPS data were collected simultaneously using all three GPS receivers from antennas placed on the turret of the IESSG building. The antennas used for the trial were

- Leica SR 530 - Leica 503 choke ring geodetic antenna
- OEM4 - Novatel GPS-600 Pinwheel antenna
- U-Blox - U-Blox ANN-MS-0-005 patch antenna

The trial began at 09:30 UTC 17 March 2007 and an hour of static data were collected.

7.4 Trial Results

Each of the trials described in §7.3 were conducted and the raw data collected were processed using the TDD velocity algorithm implemented in Matlab. The resulting velocities have been compared with the truth data, which was extracted from the Spirent simulator software, SimGEN. Throughout this set of trials all velocities output from the TDD algorithm have been presented although only vertical velocity is of use when considering the TDD heave algorithm. The following subsections present the results from the Spirent simulator trials.

7.4.1 Trial 1

Trial one was primarily designed to isolate and quantify all errors that are specific to the receiver used, but also served as an adequate test of the TDD velocity and heave algorithms. As previously discussed, there were three separate sections to trial one: static test, marine test and high dynamics test.

7.4.1.1 Static Scenario

Static data simulated by the Spirent simulator was collected using three GPS receivers of varying grades: Leica SR 530, Novatel OEM4 and U-Blox Antaris. The raw data

collected were then converted into RINEX v2.1 files ready for processing through the TDD velocity algorithm. The velocities output by the algorithm are shown in figures 7.8, 7.9 and 7.10 for Leica SR 530, Novatel OEM4 and U-Blox Antaris respectively. The data collected was from a static scenario and the plots of TDD velocity can therefore also be considered error plots. The error can be shown to be normally distributed and so the standard deviation of the error is presented in table 7.2; the mean of the error experienced during the static scenario was at the micrometre or tens of micrometer level and so was considered negligible and not included in the results of table 7.2.

Table 7.2 shows that the U-Blox receiver performed to the same standard as both the dual frequency receivers when in a static environment. The figures presented in the table show standard deviation and mean error values for the U-Blox receiver of the same order as for the Leica and the Novatel. These results were slightly unexpected considering the difference in cost between the receivers but were thought to probably be an artefact of the tracking loop algorithms employed in the U-Blox receiver. It is accepted that the Leica and Novatel will most likely utilize higher grade componentry within the receiver, but when static the U-Blox receiver may be able to use the lack of dynamics to alter the bandwidth of its tracking loops. This analysis is largely conjecture but it is certainly safe to say from these results that, under static error free conditions, the U-Blox receiver can perform at least as well as the Leica and Novatel receivers.

Receiver Type	1σ Standard Dev. (mm/s)		
	North	East	Down
Leica SR 530	0.8	0.7	2.0
OEM4	0.7	0.6	1.6
U-Blox	0.8	1.0	3.4

Table 7.2: Results of static test of TDD velocity algorithm using error free simulated data

7.4.1.2 Marine Scenario

The marine scenario was designed to test the TDD heave algorithm in an environment that would be as close as possible to the intended environment of use. Error free data

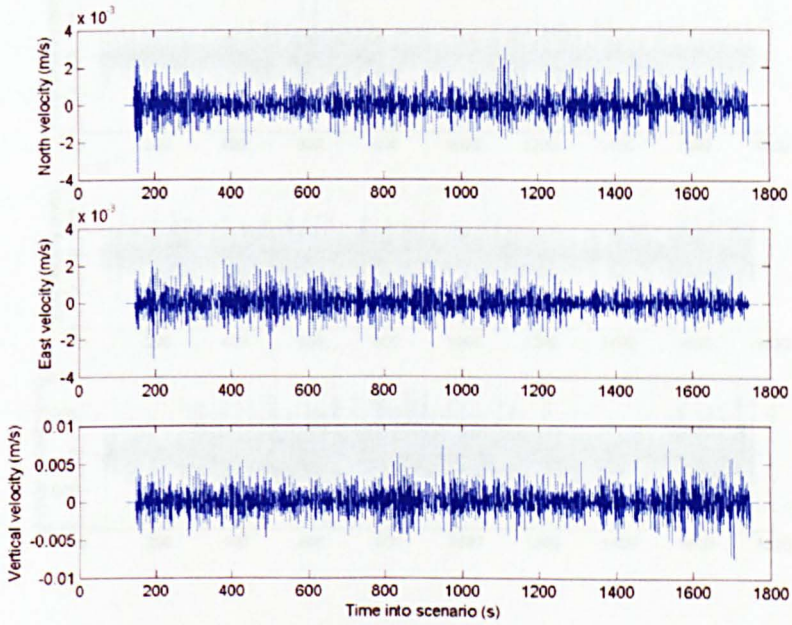


Figure 7.8: Leica SR 530 dual frequency receiver TDD velocity from simulated static

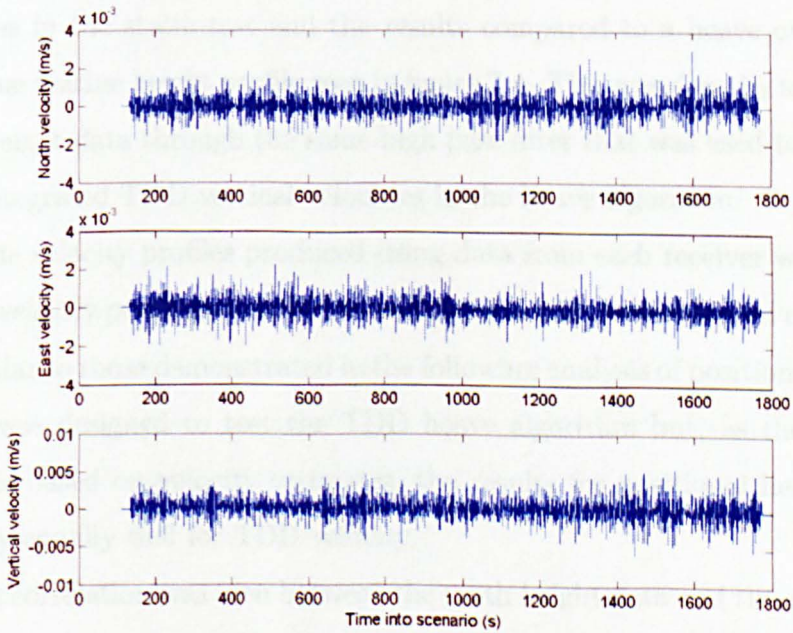


Figure 7.9: Novatel OEM4 dual frequency receiver TDD velocity from simulated static data

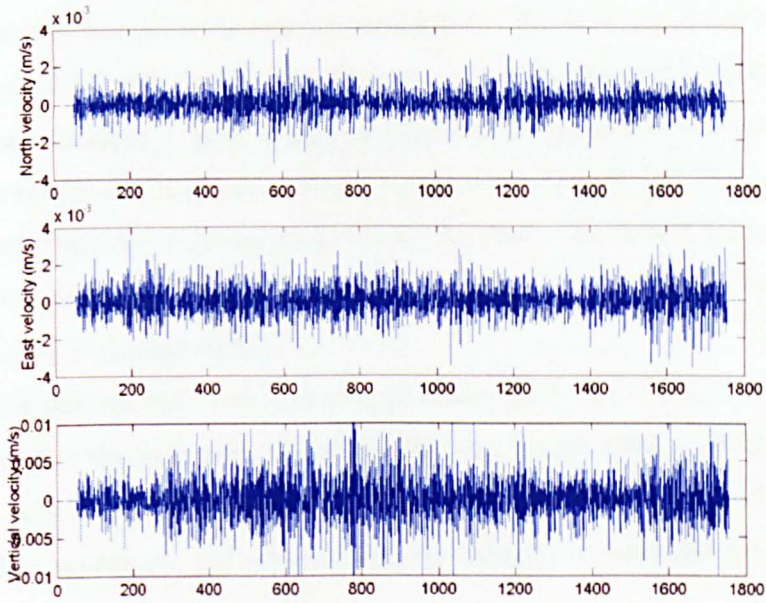


Figure 7.10: U-Blox Antaris single frequency receiver TDD velocity from simulated static data

were once again collected using the same three receivers, this time being subjected to a simulated marine environment. These data were then processed using the TDD heave algorithm as in the static test and the results compared to a heave output created from the true marine height profile seen in figure 7.4. This was done by simply passing the truth height data through the same high pass filter that was used to remove drift from the integrated TDD vertical velocities in the heave algorithm.

When the velocity profiles produced using data from each receiver were compared to the true velocity profiles extracted from SimGEN, the results showed characteristics largely similar to those demonstrated in the following analysis of positional heave data. This trial was designed to test the TDD heave algorithm but, as the TDD heave algorithm is based on velocity estimates, the results for positional heave expressed below apply equally well for TDD velocity.

A strong correlation was seen between the truth height data and the relative height data produced through the integration of TDD velocities. Figure 7.11 shows the difference plot of the true height and integrated TDD velocity using Leica SR 530 dual frequency data; the bias of 98.470 m on the truth height was removed for this

comparison. The results in figure 7.11 clearly show the drift on the integrated TDD velocity caused by bias errors in velocity estimation. This drift was removed by passing the integrated TDD velocity through the high pass filter designed for the TDD heave algorithm and detailed in §6.3. Figure 7.12 shows a comparison between high pass filtered true height and high pass filtered integrated Leica SR 530 TDD velocity and it can be seen that the drift was removed by the filter; the results gained from data collected with the Novatel OEM4 and U-Blox Antaris GPS receivers can be seen in figures 7.13 and 7.14 respectively.

A bias was seen on the error plot of approximately 6 mm, which was caused by a residual left after the high pass filtering of the true height data. The high pass filter has a finite stop band attenuation of -80 dB and so a residual height will remain after filtering. This hypothesis was proven using the formula to calculate gain in dB:

$$A = 20 \log \left(\frac{S_1}{S_2} \right) \quad (7.1)$$

where A is the gain in dB and S_1 and S_2 are the levels of the signals. Setting the values of $S_2 = 98.470$ m and $S_1 = 6$ mm yields a gain of -84 dB, which is very close to the stop band attenuation of the high pass filter.

It can be seen from the error plots in figures 7.12, 7.13 and 7.14 that, when subjected to a dynamic scenario, the Leica and Novatel receivers clearly outperformed the U-Blox receiver with errors which appeared over an order of magnitude smaller under visual inspection. It was also noted that the areas which contained the largest error on all the vertical velocity error plots coincided with the time when the receiver was subjected to the highest frequency of motion. Table 7.3 shows the errors in the TDD heave from each receiver when subjected to the various sea states during the trial.

The high level of performance of the Novatel and Leica dual frequency receivers suggested that there was no catastrophic failure in the TDD heave algorithm. It was therefore assumed that the large errors seen in the results of the U-Blox receiver were caused by the receiver itself and, more specifically, the receiver tracking loops. The results in table 7.3 show that the errors in the TDD heave from the U-Blox receiver were much greater than those seen in the Leica and Novatel receivers during sea state one yet they quickly reduced to levels of a similar magnitude when the frequency

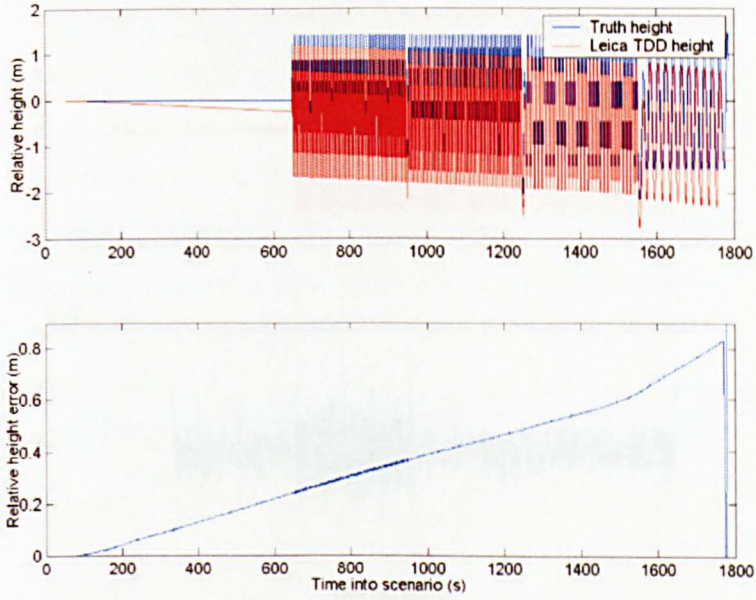


Figure 7.11: Leica SR 530 integrated TDD position drift error from the marine scenario

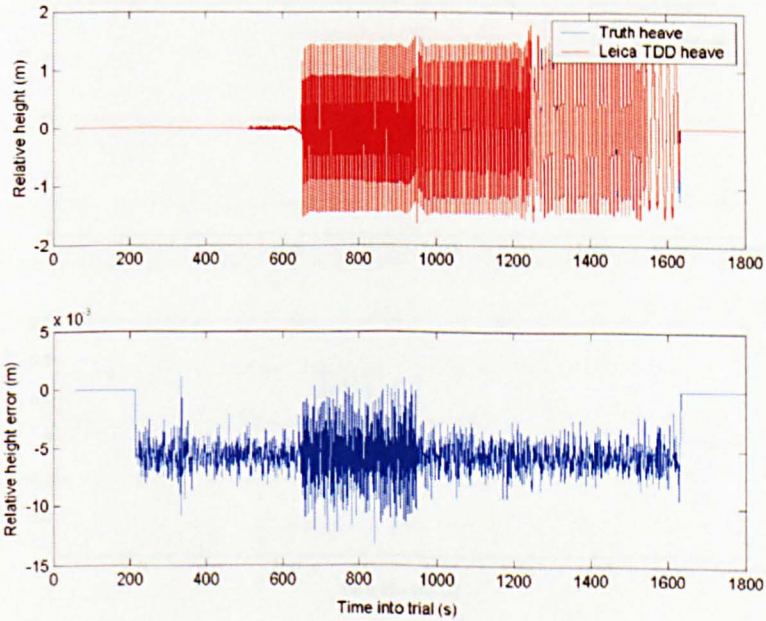


Figure 7.12: Leica SR 530 TDD heave error from the marine scenario

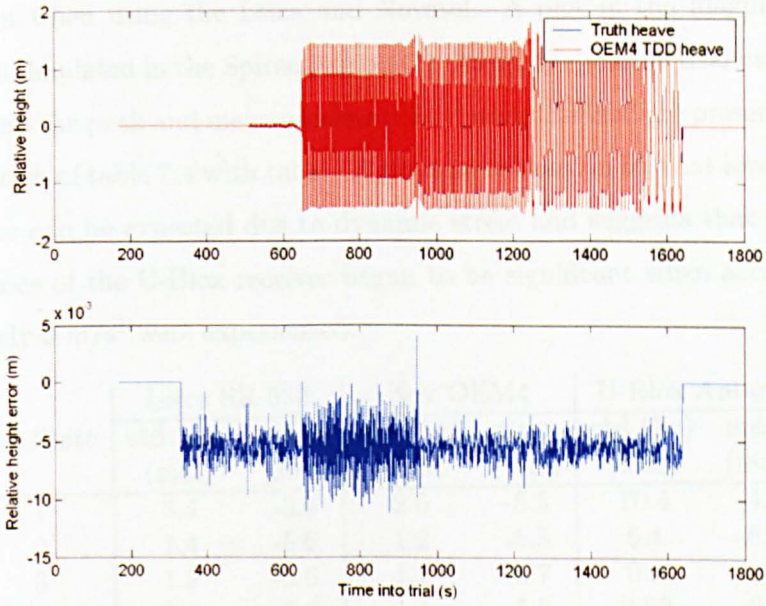


Figure 7.13: Novatel OEM4 TDD heave error from the marine scenario

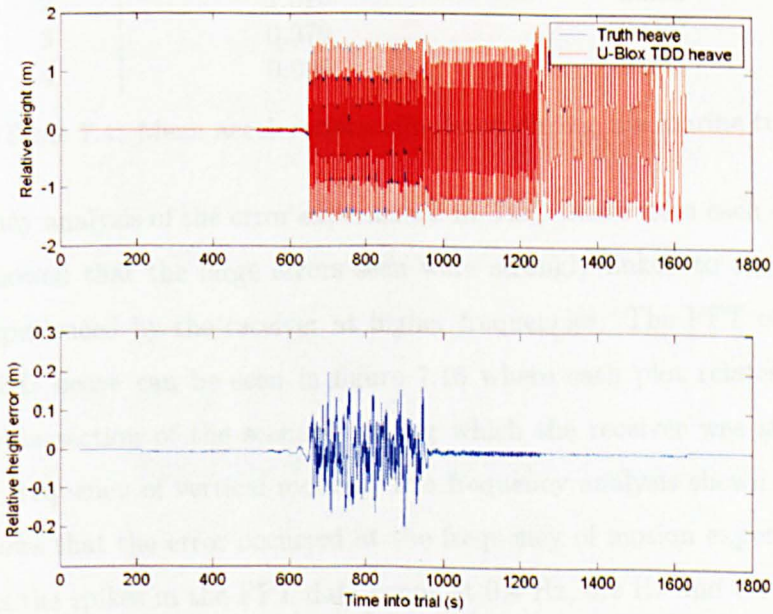


Figure 7.14: U-Blox Antaris TDD heave error from the marine scenario

of motion was decreased during the remaining sea states. The TDD heave errors experienced by the U-Blox receiver during sea states three and four were no different to those seen when using the Leica and Novatel. A plot of the magnitude of the accelerations simulated in the Spirent simulator during the marine trial can be seen in figure 7.15 and the peak and mean accelerations during the trial are presented in table 7.4. Correlation of table 7.4 with table 7.3 gives an indication of what level of receiver induced error can be expected due to dynamic stress and suggests that degradation of performance of the U-Blox receiver began to be significant when accelerations of approximately 3 m/s^2 were experienced.

Sea State	Leica SR 530		Nov OEM4		U-Blox Antaris	
	std (1σ) (mm)	mean (mm)	std (1σ) (mm)	mean (mm)	std (1σ) (mm)	mean (mm)
1	3.4	-5.6	2.6	-5.5	70.4	-4.4
2	1.4	-5.6	1.2	-5.5	6.4	-6.2
3	1.2	-5.6	1.1	-5.7	0.9	-5.60
4	1.4	-5.6	1.4	-5.9	0.82	-5.6

Table 7.3: Receiver induced heave errors for each section of the simulated marine scenario

Sea State	Mean Acceleration (m/s^2)	Peak Acceleration (m/s^2)
1	5.993	9.457
2	1.510	3.600
3	0.379	0.922
4	0.095	0.232

Table 7.4: Mean accelerations simulated during the marine trial

Frequency analysis of the error experienced in TDD heave from each of the U-Blox receiver showed that the large errors seen were strongly linked to the frequency of motion experienced by the receiver at higher frequencies. The FFT of the error in U-Blox TDD heave can be seen in figure 7.16 where each plot relates to the FFT of a separate section of the scenario during which the receiver was subjected to a particular frequency of vertical motion. The frequency analysis shown in figure 7.16 clearly shows that the error occurred at the frequency of motion experienced by the receiver as the spikes in the FFT data occur at 0.4 Hz, 0.2 Hz and 0.1 Hz, the same frequencies of motion used in the marine scenario. Once frequency of motion has

dropped to 0.05 Hz the power in the error signal at that frequency appears to have dropped below the noise level and so has little effect on the error. It can also be seen in the figure 7.16 that the Gaussian noise was of a greater magnitude when the receiver experienced the higher frequencies of motion.

It was clear from these results that the errors introduced by the U-Blox receiver when in motion were far larger than those introduced by either the Leica or the Novatel. These errors included a Gaussian component and a component that occurred at the frequency of motion with both components seen regardless of the receiver used. The largest errors occurred when the receiver was subjected to the highest frequencies of motion (in this trial a sinusoidal motion at 0.4 Hz saw the largest magnitude of error) and consequently when the signal tracking loops within the receiver are placed under the most dynamic stress. It was the dynamic stress that was thought to cause that error in the heave estimate which occurs at the frequency of motion. The extra dynamic stress on the carrier tracking loop was handled more easily in the receivers with higher grade componentry than in the U-Blox. It is believed that the relatively sluggish dynamic performance of the U-Blox receiver caused a significant lag in the output of the carrier tracking loop, and resulted in the heave error at the frequency of motion. Also, as discussed in §3.3.4, it was thought that the increased receiver dynamics resulted in an increase in carrier tracking loop bandwidth in order to track the GPS signals, which had an adverse effect on carrier tracking loop noise.

The true cause of the dynamic stress error at the firmware level is difficult to appreciate fully but it can certainly be surmised from the results obtained that higher accelerations, which place the receiver tracking loops under greater dynamic stress, cause errors in the U-Blox receiver that can be more than an order of magnitude greater than those seen in either of the dual frequency receivers.

7.4.1.3 High Dynamic Scenario

The high dynamic scenario was designed to place the signal tracking loops under far greater dynamic stress than in the marine test. This would endorse the findings of the marine test and give an idea of the magnitude of error that may occur when using the TDD velocity algorithm in more dynamic applications.

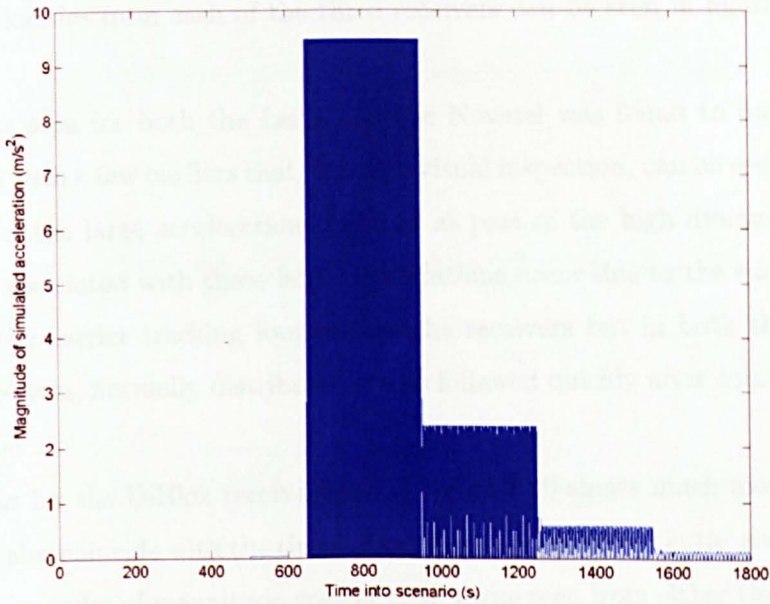


Figure 7.15: Magnitude of simulated vessel acceleration during the marine trial

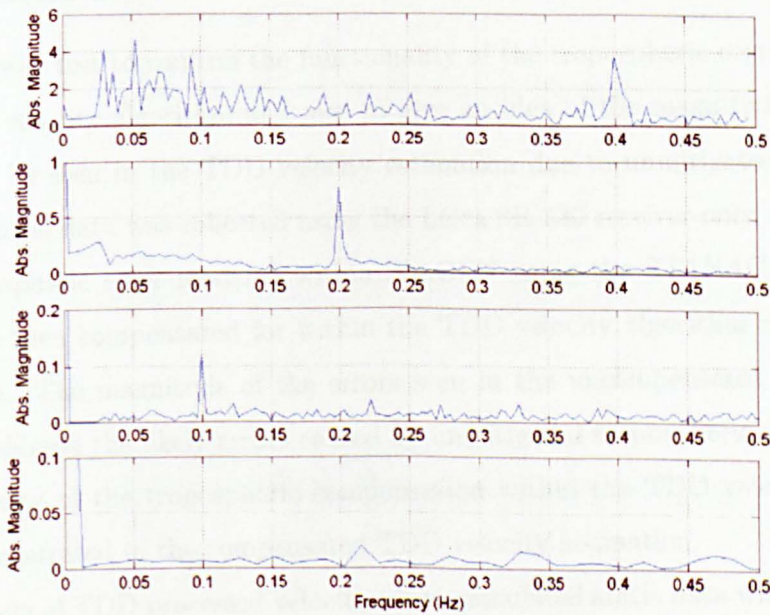


Figure 7.16: Frequency analysis of error in U-Blox Antaris TDD velocity during marine trial

The TDD velocities calculated using the raw observables from each receiver were compared to the velocities extracted from the simulator truth file. The error plots based on velocities from each of the three receivers can be seen in figures 7.17, 7.18 and 7.19.

The error seen for both the Leica and the Novatel was found to have a normal distribution with a few outliers that, through visual inspection, can be seen to coincide with some of the large accelerations induced as part of the high dynamics scenario. The errors associated with these large accelerations occur due to the excessive stress placed on the carrier tracking loop within the receivers but in both the Leica and Novatel receivers, normally distributed errors followed quickly after constant velocity was resumed.

The error for the U-Blox receiver seen in figure 7.19 shows much more prominent errors that also coincide with the times of the large accelerations in the scenario, which are around an order of magnitude greater than those seen from either the Leica or the Novatel. During the periods of the scenario when constant velocity was experienced the error in the U-Blox receiver is normally distributed but the time required for this is greater than with the higher grade receivers.

7.4.2 Trial 2

Trial two was test to confirm the functionality of the tropospheric correction used in the TDD velocity algorithm and also to give an idea of the magnitude of the error that may be seen in the TDD velocity estimation due to unmitigated tropospheric effects. Static data was collected using the Leica SR 530 receiver only, this time with the tropospheric error modeled within SimGEN using the STANAG (1990). This error was then compensated for within the TDD velocity algorithm using the same algorithm. The magnitude of the errors seen in the uncompensated TDD velocity solution showed the likely errors caused by unmitigated tropospheric effects, and the functionality of the tropospheric compensation within the TDD velocity algorithm was demonstrated in the compensated TDD velocity estimation.

Two sets of TDD processed velocities from simulated static data with tropospheric error modeling turned on and collected using a Leica SR 530 can be seen in figures

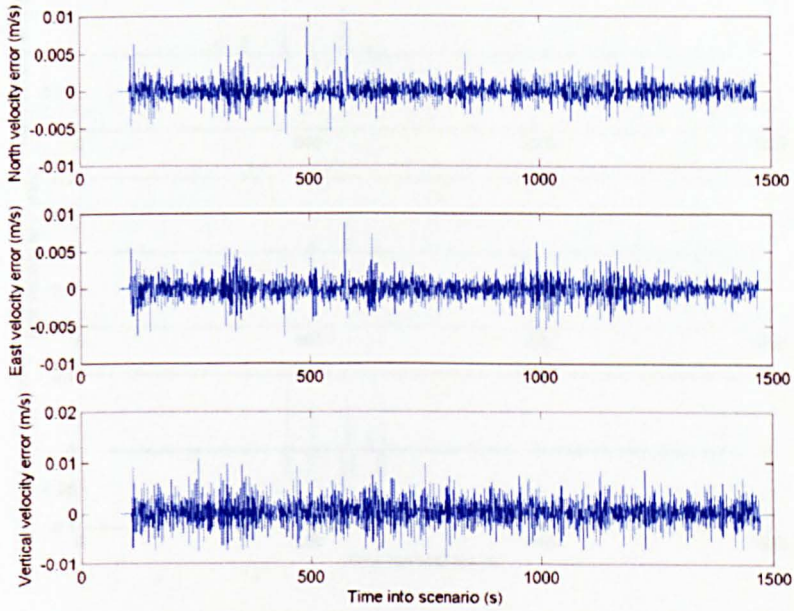


Figure 7.17: Leica SR 530 dual frequency receiver induced velocity error from simulated high dynamics data

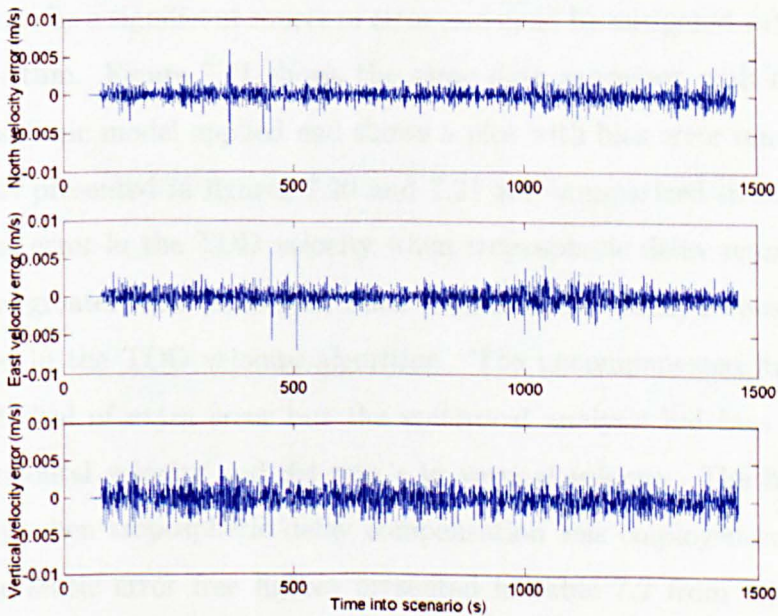


Figure 7.18: Novatel OEM4 dual frequency receiver induced error from simulated high dynamics data

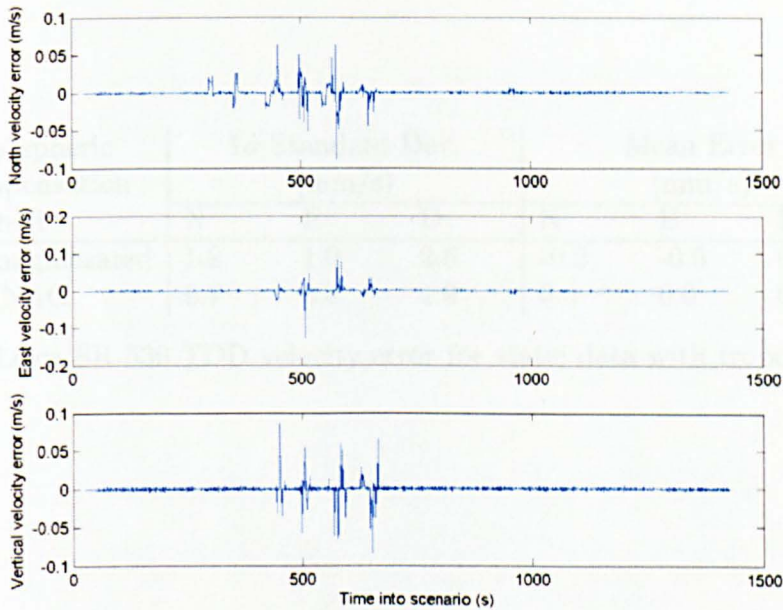


Figure 7.19: U-Blox Antaris single frequency receiver induced error from simulated high dynamics data

7.20 and 7.21. Figure 7.20 shows the velocities with no tropospheric correction applied during processing and it is clear from these plots that the rate of change of the troposphere can be a significant source of error and must be mitigated within the TDD velocity algorithm. Figure 7.21 shows the same data processed with the STANAG (1990) tropospheric model applied and shows a plot with bias error removed.

The results presented in figures 7.20 and 7.21 are summarized in table 7.5. The figures for the error in the TDD velocity when tropospheric delay remained uncompensated were greater than those seen when the STANAG (1990) tropospheric model was employed in the TDD velocity algorithm. The uncompensated figures did not show a great deal of extra error but the statistical analysis hid bias errors of ± 2 mm/s in horizontal velocity and ± 4 mm/s in vertical velocity. The figures for the TDD velocity when tropospheric delay compensation was employed compared very well with the static error free figures presented in table 7.2 from trial one. This was expected as the TDD algorithm employed the same tropospheric model as the simulator but did prove the functionality of this algorithm employed in the Matlab code.

Tropospheric Compensation Method	1 σ Standard Dev. (mm/s)			Mean Error (mm/s)		
	N	E	D	N	E	D
Uncompensated	1.2	1.0	2.6	-0.2	-0.6	0.3
STANAG	0.7	0.8	1.9	0.0	0.0	0.0

Table 7.5: Leica SR 530 TDD velocity error for static data with tropospheric delay modeled

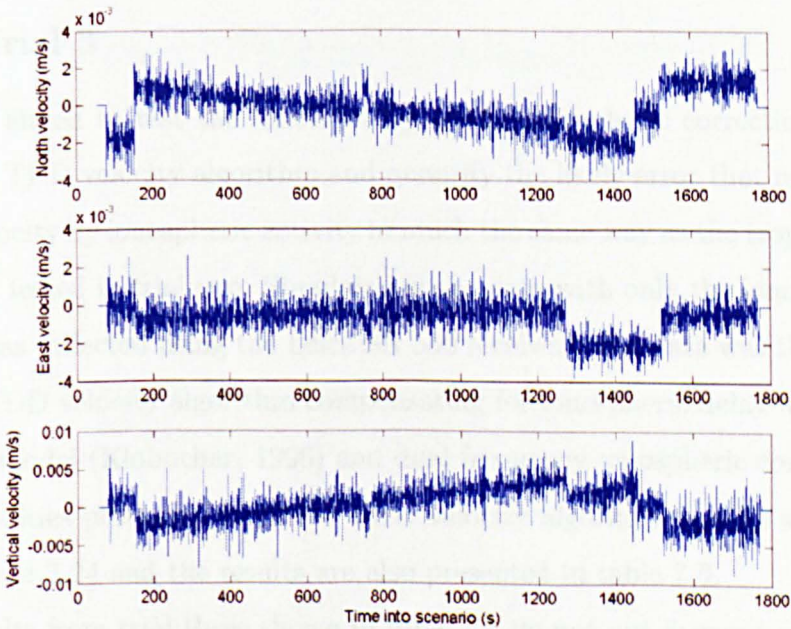


Figure 7.20: Leica SR 530 TDD velocities from simulated static data with tropospheric error modeled and no correction applied

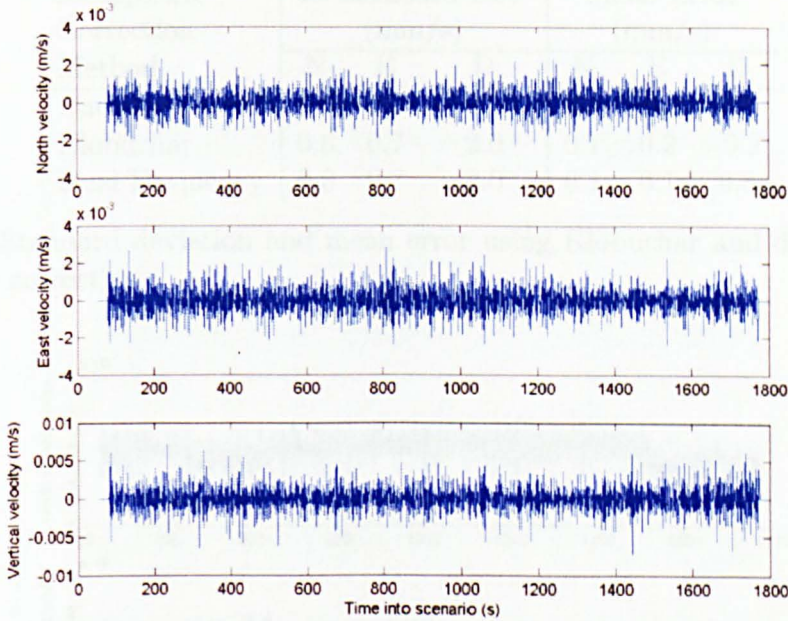


Figure 7.21: Leica SR 530 TDD velocities from simulated static data with tropospheric error modeled and STANAG correction applied

7.4.3 Trial 3

Trial three aimed to test the functionality of the ionospheric correction algorithms used in the TDD velocity algorithm and quantify the likely error that may be caused in TDD velocity by ionospheric activity in much the same way as the tropospheric correction was tested in trial two. Simulated static data with only the ionospheric delay modelled was collected using the Leica SR 530 receiver. The data was then processed using the TDD velocity algorithm compensating for ionospheric delay using both the Klobuchar model (Klobuchar, 1996) and dual frequency ionospheric correction.

The velocities produced using the TDD velocity algorithm can be seen in figures 7.22, 7.23 and 7.24 and the results are also presented in table 7.6.

The results from trial three shown in table 7.6 do not put forward much of a case for the inclusion of an ionospheric delay compensation model in the TDD velocity algorithm. As in trial two, however, the statistics do hide bias errors up to ± 1 mm/s in horizontal velocity and ± 1.5 mm/s in vertical velocity. The inclusion of the ionospheric compensation algorithm is justified therefore and will reduce the errors seen in the TDD velocity estimation. In the context of the use of low cost GPS

Ionospheric Correction Method	1 σ Standard Dev. (mm/s)			Mean Error (mm/s)		
	N	E	D	N	E	D
Uncompensated	0.8	0.7	2.1	0.1	-0.3	0.8
Klobuchar	0.8	0.7	2.0	0.1	0.2	-0.2
Dual Frequency	0.8	0.7	2.0	0.1	0.1	0.8

Table 7.6: Standard deviation and mean error using Klobuchar and dual frequency ionospheric correction

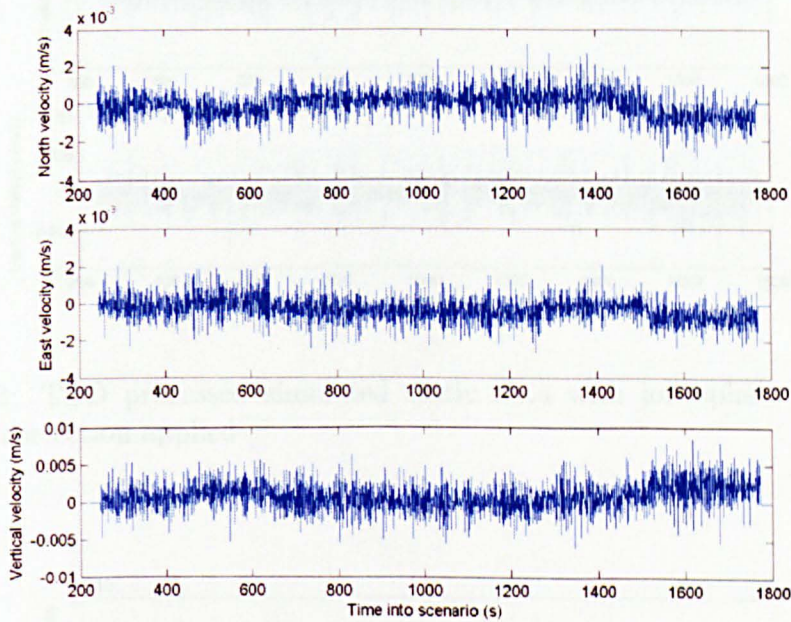


Figure 7.22: TDD processed simulated static data with ionosphere modeled and no correction applied

receivers for the estimation of TDD heave as is used throughout this thesis, the errors associated with single frequency data collection can be expected to be reasonably small and not to give too great a disadvantage.

7.4.4 Trial 4

As a final trial using the simulator data was collected using all three receivers from both the static and marine scenarios with both ionospheric and tropospheric errors modeled. This was thought to be a good final test of the TDD algorithm before the collection and processing of real GPS data. In this trial the TDD velocities seen during the static scenario are presented but, as in trial one, the marine scenario analysis is

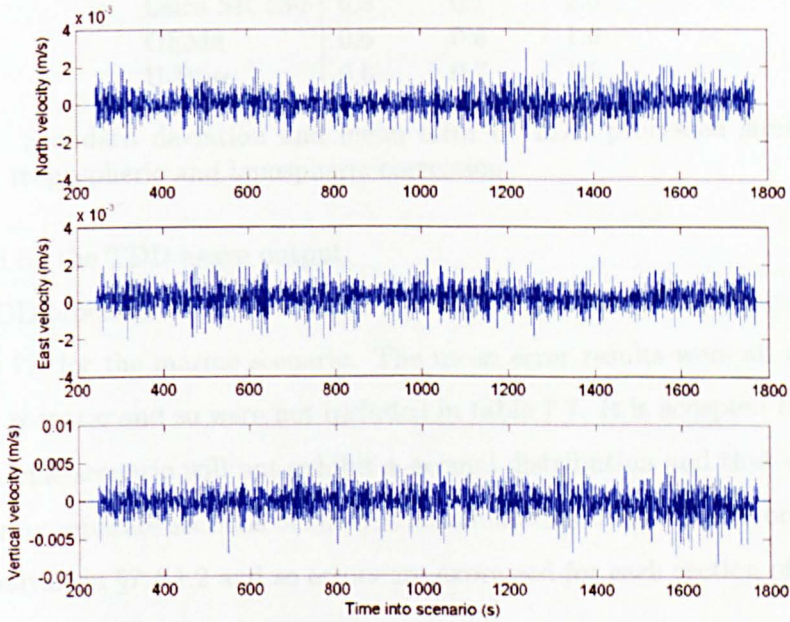


Figure 7.23: TDD processed simulated static data with ionosphere modeled and Klobuchar correction applied

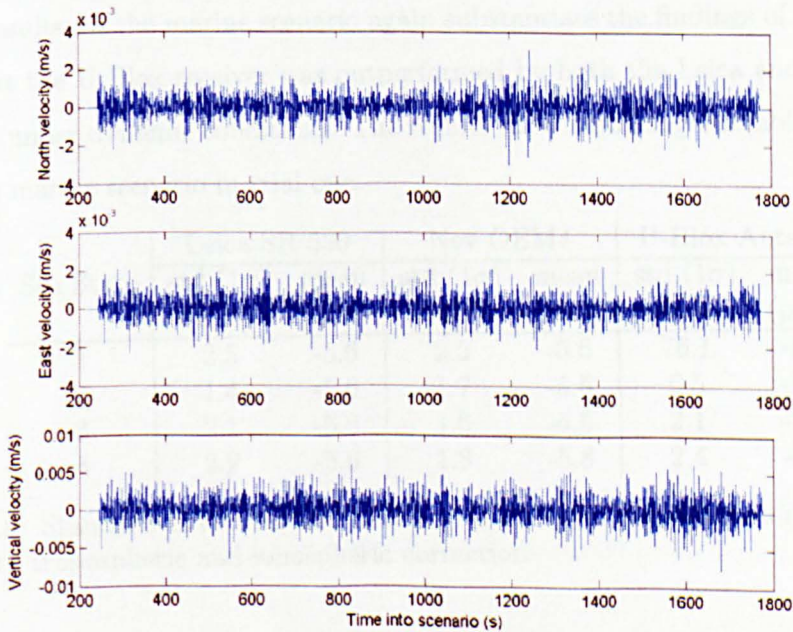


Figure 7.24: TDD processed simulated static data with ionosphere modeled and dual frequency correction applied

Receiver Type	1 σ Standard Dev. (mm/s)		
	N	E	D
Leica SR 530	0.8	0.7	2.0
OEM4	0.6	0.6	1.6
U-Blox	0.6	0.7	1.5

Table 7.7: Standard deviation and mean error of TDD processed simulated static data with tropospheric and ionospheric correction

conducted on the TDD heave output.

The TDD processed velocity errors are presented in table 7.7 for the static scenario and table 7.8 for the marine scenario. The mean error results were all negligible for the static scenario and so were not included in table 7.7. It is accepted that the error for the marine scenario will not exhibit a normal distribution and that errors will be larger during separate sections of the marine simulation due to the errors highlighted by the analysis in §7.4.1.2 and so errors are expressed for each section of the scenario individually.

The results for the static scenario show a strong correlation with the static scenario results seen in trial one. Each receiver had TDD processed velocity errors of a similar magnitude showing that, under static conditions, all receivers had similar performance.

The results for the marine scenario again substantiate the findings of trial one and show that the U-Blox receiver was outperformed by both the Leica and the Novatel receivers under dynamic conditions. The results show a striking resemblance to those from the marine scenario in trial one.

Sea State	Leica SR 530		Nov OEM4		U-Blox Antaris	
	std (1 σ) (mm)	mean (mm)	std (1 σ) (mm)	mean (mm)	std (1 σ) (mm)	mean (mm)
1	2.5	-5.6	2.5	-5.6	76.1	-5.6
2	1.4	-5.6	1.7	-5.5	6.5	-5.4
3	2.1	-5.6	1.6	-5.5	2.1	-5.6
4	2.2	-5.6	1.8	-5.8	2.4	-5.8

Table 7.8: Standard deviation and mean error of TDD processed simulated marine data with tropospheric and ionospheric correction

7.4.5 Trial 5

Trial five has been added to this chapter although it did not involve use of the Spirent simulator. It was designed as an interim trial between data collected on the simulator and data collected during the sea trial, discussed in chapter 8. Static data was recorded using all three receivers from the turret on the IESSG building. Now that the simulator was no longer in use antennas were required for each receiver. It was decided that the antennas used in the sea trial would also be used in this static trial so as to gain an idea of the accuracy of the each receiver/antenna combination.

The results of trial 5 can be seen in table 7.9, and the plots of TDD velocity from each of the three receivers is displayed in figures 7.25, 7.26 and 7.27.

The results shown in table 7.9 agree very strongly with the results shown for trials one and four, conducted with the Spirent simulator. Each antenna appeared able to record raw observations that, when processed through the TDD velocity algorithm, resulted in velocity errors of a similar magnitude. The TDD velocity algorithm was capable of estimating receiver velocity at the mm/s level under static conditions using any of the receivers.

The results of this trial endorse the results of trial three, which suggested that ionospheric effects would have little effect on the TDD velocity algorithm performance. In this trial the U-Blox low cost single frequency receiver has performed as well as the dual frequency Leica and Novatel receivers. Thus, there is little benefit from the use of dual frequency receivers when in use with the TDD velocity algorithm.

Receiver Type	1σ Standard Deviation (mm/s)			Mean Error (mm/s)		
	N	E	D	N	E	D
Leica SR 530	1.9	1.5	3.4	0.0	0.1	-0.2
OEM4	2.0	1.8	3.8	0.0	0.2	-0.1
U-Blox	1.8	1.1	3.6	0.3	0.1	0.6

Table 7.9: Standard deviation and mean error of TDD processed static GPS data

7.5 Spirent Simulator Trial Summary

The simulator trials and the collection of real static GPS data have been a strong aid in the development of the TDD velocity algorithm, the discovery of its limitations and

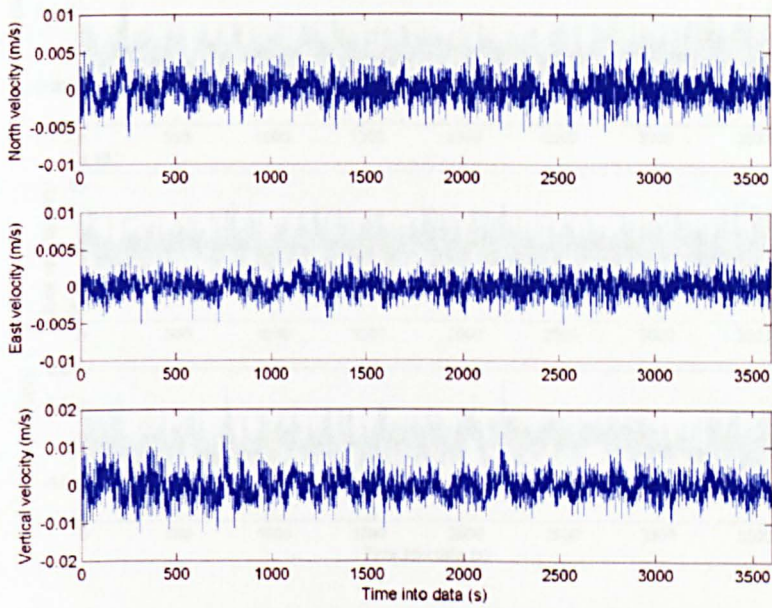


Figure 7.25: TDD processed static GPS collected using Leica SR 530 dual frequency receiver

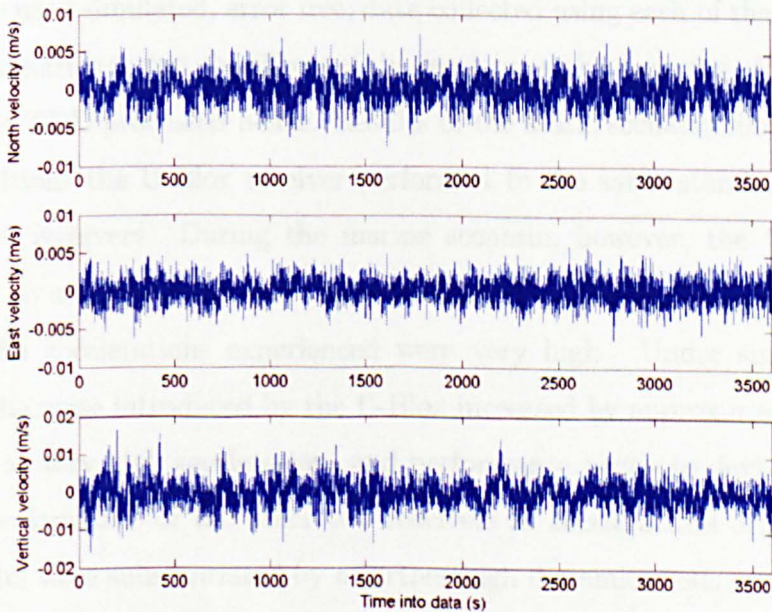


Figure 7.26: TDD processed static GPS data collected using OEM4 dual frequency receiver

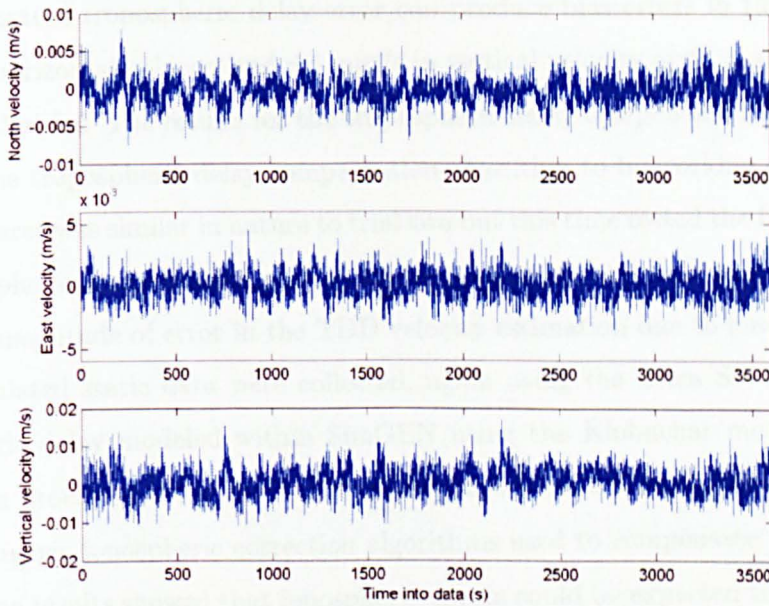


Figure 7.27: TDD processed static GPS data collected using U-Blox Antaris single frequency receiver

for analysis of the effects of the use of low cost receivers compared to dual frequency geodetic receivers.

Trial one used simulated, error free, data collected using each of the three receivers and three scenarios to test the effects of the receiver on the accuracy of TDD processed velocity and TDD processed heave. Results of the static scenario showed that under static conditions the U-Blox receiver performed to the same standard as the Leica and Novatel receivers. During the marine scenario, however, the U-Blox receiver was unable to cope with the same level of dynamic stress as the Leica and Novatel, although the accelerations experienced were very high. Under simulated marine dynamics the noise introduced by the U-Blox increased by approximately an order of magnitude at very high accelerations and performance began to deviate significantly from the performance of the other two receivers at accelerations of around 3 m/s^2 . These results were substantiated by a further high dynamics test.

Trial two collected simulated static data with tropospheric delay only modeled in SimGEN. The data were collected using only the Leica SR 530 receiver and then processed through the TDD velocity algorithm where the STANAG tropospheric

model was used to compensate for tropospheric delay. The results showed that uncompensated tropospheric delay error can produce bias errors in the order of ± 2 mm/s in horizontal velocity and ± 4 mm/s in vertical velocity and, as such, should be compensated for. The results for the tropospheric delay compensated TDD velocities showed the tropospheric delay compensation algorithm to be working effectively.

Trial three was similar in nature to trial two but this time tested the functionality of the ionospheric compensation algorithms for both single and dual frequency receivers and the magnitude of error in the TDD velocity estimation due to ionospheric activity. Simulated static data were collected, again using the Leica SR 530, with only ionospheric delay modeled within SimGEN using the Klobuchar model. The data were then processed using the TDD velocity algorithm and both the Klobuchar and dual frequency ionospheric correction algorithms used to compensate for ionospheric delay. The results showed that ionospheric effects could be expected to have an effect on TDD velocity estimates of up to ± 1 mm/s in horizontal velocity and ± 1.5 mm/s in vertical velocity. This level of error justified the inclusion of compensation models in the TDD velocity algorithm but did suggest that the use of single frequency data from low cost GPS receivers would have little effect on overall velocity accuracy using the TDD velocity algorithm. Trial three also showed both algorithms to be effective in the removal of ionospheric delay. A simulator based anomaly was that the Klobuchar model performed equally as well as the dual frequency algorithm due to the fact that the model applied in SimGEN is Klobuchar. This would not occur with real GPS data.

Trial four used simulated data from both the static and marine scenarios, collected using all three receivers and with both tropospheric and ionospheric delays modeled. These data were processed using the TDD velocity algorithm and the results showed the algorithm to be fully operational and endorsed those results seen in trials one through three.

Trial five has further endorsed the results seen in trials one and four but using real static GPS data. A slightly surprising result was that the single and dual frequency processed data produced TDD velocity errors of a similar magnitude. The simulator trials have demonstrated that receiver based error under static conditions is the same

for all three receivers. The same algorithms are used for all three receivers except when mitigating for the ionosphere. The results of trial five suggest that the Klobuchar model provides rate of change data for ionospheric delay that is of equal accuracy to that provided by the dual frequency algorithm.

Chapter 8

The Plymouth Sea Trial

8.1 Introduction

A sea trial of the developed low cost TDD heave algorithm was conducted in Plymouth on 2 August 2006 with the help of Sonardyne International Ltd., the industrial partner in the PhD project. The trial was intended to test the performance of the TDD heave algorithm as an alternative to inertial based heave algorithms by collecting raw GPS data from the same three receivers used in the simulator trials detailed in chapter 7, processing it through the TDD heave algorithm and comparing the heave results to those obtained from both inertial based sensors and an Applanix POSRS fitted to the vessel.

This was the first time an attempt had been made to assess the performance of a heave algorithm based on TDD velocity and implemented on one of a new generation of commercially available low cost receivers capable of recording the carrier phase pseudo range observable. The use of the Applanix POSRS gave very stable reference data that allowed each of the heave sensors to be assessed in key areas of the trial. The comprehensiveness of the trial that tested TDD heave using a varying array of GPS receivers against both the inertial technologies currently available and a highly accurate GPS-aided INS allowed the first complete assessment of TDD heave using low cost receivers.

This chapter discusses the trial methodology and gives an explicit breakdown of the sensors used in the trial and how they were fitted to the vessel. The results of the trial are also presented for TDD heave from all three receivers compared to reference

data provided by an Applanix POSRS system and heave data recorded with inertial based sensors.

8.2 Trial Methodology

The sea trial was conducted on 2 August 2006. The vessel used for the trial, the Marco, was owned by Sonardyne International Ltd.. Sonardyne have a testing and training facility based at Pier House, Turnchapel, Plymouth where they are able to train industry personnel on Sonardyne equipments and also test their own research and development projects under marine conditions.

Use of the Marco allowed the design and execution of a sea trial for the TDD heave algorithm so that its performance could be measured against reference data and inertial based heave data recorded at the same time. This section outlines the methodology employed when conducting the sea trials and which equipments and sensors were used.

8.2.1 Trial Overview

The sea trial was designed to test the TDD heave algorithm under marine conditions, comparing the heave output produced with both reference data and inertial based heave data. To achieve this the following sensors and equipments were used.

- Applanix POSRS including Novatel OEM4 GPS receiver and a Novatel GPS 600 Pinwheel antenna
- Two Leica SR 530 GPS receivers (numbered 1 and 2) and two Leica 504 choke ring antennas
- U-Blox Antaris AEK-4T GPS receiver and an ANN-MS-0-005 patch antenna
- Honeywell HG1700 tactical grade IMU
- GPS reference station data supplied by Ordnance Survey

A TSS DMS500 MAHRS heave, pitch and roll sensor was also installed on the Marco but the data collected from this sensor were unusable due to time tagging

errors. Once all the required sensors were fitted to Marco a trial was conducted that followed the general procedure of an approximately 20 minute initialization and alignment period followed by a period of simulated survey lines within the Plymouth breakwater.

8.2.2 The Applanix POSRS System

The Applanix POSRS system is a highly accurate GPS-aided INS system purchased by the IESSG to provide reference data for any trials conducted as part of its research threads. The system is similar in nature to the Applanix POSMV system described in §4.4.1. The main difference between the POSMV and the POSRS used in this trial is that a navigation grade IMU (Honeywell CIMU) is used in place of the tactical grade IMU (Litton LN200) in the POSRS. The POSRS system also uses only one Novatel OEM4 dual frequency GPS receiver rather than the two used to provide the GAMS data in the POSMV. The higher grade of IMU provides a degree of accuracy during GPS outages that is greater than that achieved when using the POSMV and once aligned provides a high degree of heading accuracy due to the quality of the gyros. With the POSMV heading stability is provided through GAMS as, with tactical a grade IMU, the use of only one GPS receiver can provide a less stable heading reference during periods when vessel heading experiences little change (Hide, 2003).

The data collected using the POSRS has been processed using POSPac v4.1, the processing software provided with the system, to produce smoothed best estimate of trajectory (SBET) data. The process involved in reaching this output is to process the raw GPS data forwards and backwards to produce interferometric GPS, then to combine this with the IMU data using a loosely coupled Kalman filter algorithm before smoothing forwards and backwards.

The components of the Applanix POSRS can be seen in figure 8.1 and the accuracies of the CIMU are quoted in table 2.1.

8.2.3 The Marco and the Sensor Configuration

The Marco has a length over all of 35', a beam of 12'6" and an approximate cruising speed of nine knots. She is owned and operated by Sonardyne International Ltd. and

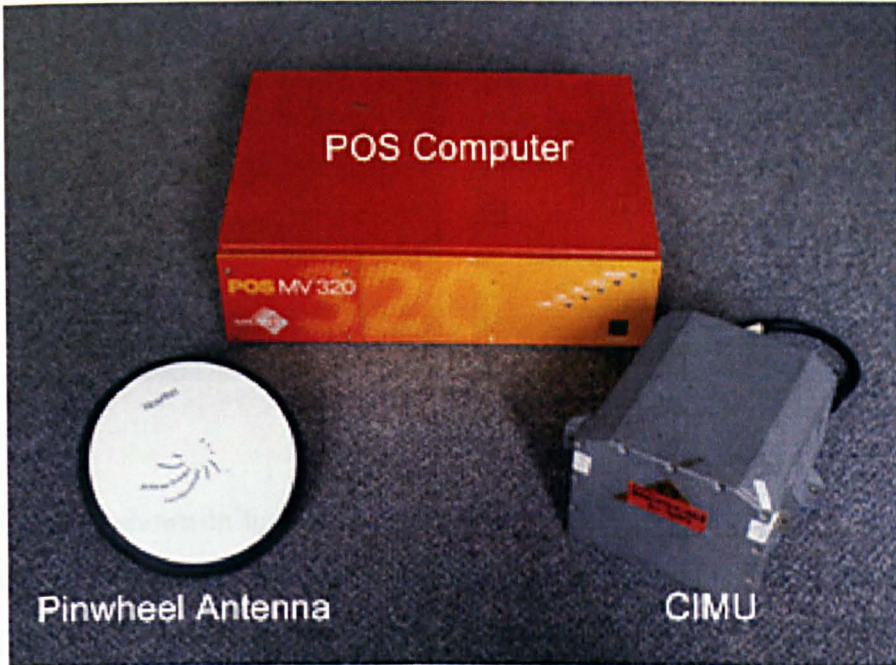


Figure 8.1: The Applanix POSRS

can be seen in figure 8.2. She is used by Sonardyne as a test platform for research and development projects and as a training vessel for industry training courses. The Marco is berthed in Plymouth and was kindly made available by Sonardyne for this sea trial.

All sensors required were fitted to the Marco the day before the trial: the IMUs were fitted below deck as seen in figure 8.3 with the Honeywell CIMU placed on the lubber line and the Honeywell HG1700 just to starboard. GPS antennas were fitted to the vessel in various positions dependent on availability of space. The Novatel Pinwheel antenna which formed part of the POSRS system was fitted to a mast, which was held rigid using two supporting struts, at the bow of the Marco as shown in figure 8.4. The Leica 504 choke ring antennas and the U-Blox ANN-MS-0-005 patch antenna were all fitted on a boom located on the starboard side of the Marco as shown in figure 8.5. The boom was held rigid with respect to the vessel with supporting struts and could be raised and lowered to aid antenna fitting. Figure 8.5a shows the boom in its lowered state with each antenna fitted and 8.5b shows the boom in its elevated state to give a clear view of the sky. When fitted to the boom the Leica 504 antennas were 2 m apart and the U-Blox ANN-MS-0-005 antenna was placed between the two Leica



Figure 8.2: The Marco

504 antennas as shown in figure 8.6.

The setup of the Leica antennas was designed to place them on a fixed baseline which was longitudinally aligned with the vessel to allow data to be collected that could provide vessel heading rate using the TDD velocity algorithm.

8.2.4 Trial Trajectory

The sea trial was conducted on the 2nd August 2006 between the approximate times of 09:30 and 12:30 and the trial SBET trajectory and height profile as computed by POSPac can be seen in figures 8.7 and 8.8 respectively. The trial began by sailing the Marco out into the Plymouth Sound where a period of initialization lasting about 15-20 minutes began, which consisted of repeated figure of eight turns; these dynamics were included in order to align the POSRS. Once the POSRS was aligned then two simulated survey lines were undertaken before the vessel was taken out beyond the breakwater to conduct further survey lines. It can be seen from figure 8.7 that the simulated survey lines do not run parallel to each other at all times. This was due to the Marco only being fitted with a magnetic compass from which to derive current heading. Despite the best efforts of the captain inconsistent survey lines were inevitable.

The approximate timings for each action conducted during the trial are given in table 8.1:

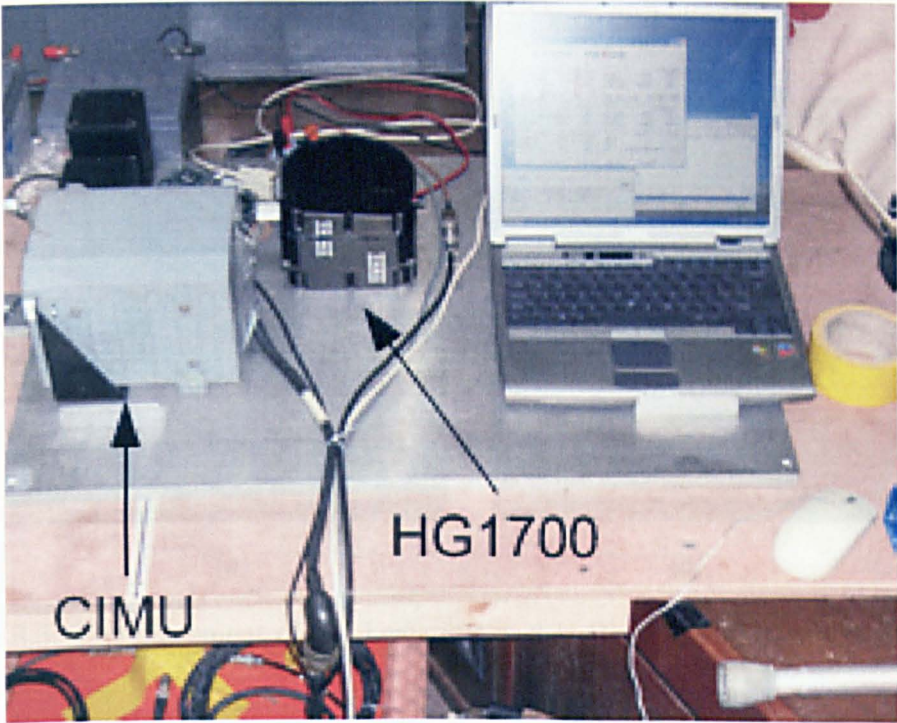


Figure 8.3: IMU configuration below deck on the Marco



Figure 8.4: Placement of Novatel Pinwheel antenna for OEM4 receiver and POSRS system

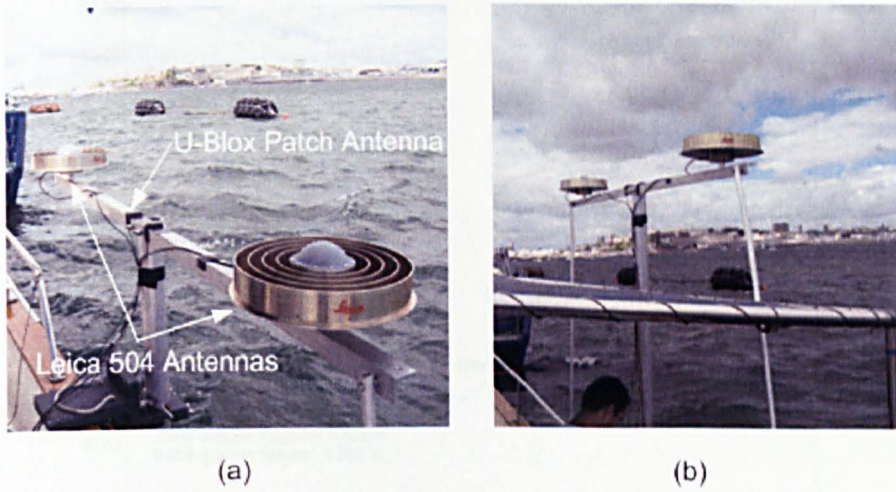


Figure 8.5: The placement of the Leica 504 and U-Blox ANN-MS-0-005 antennas

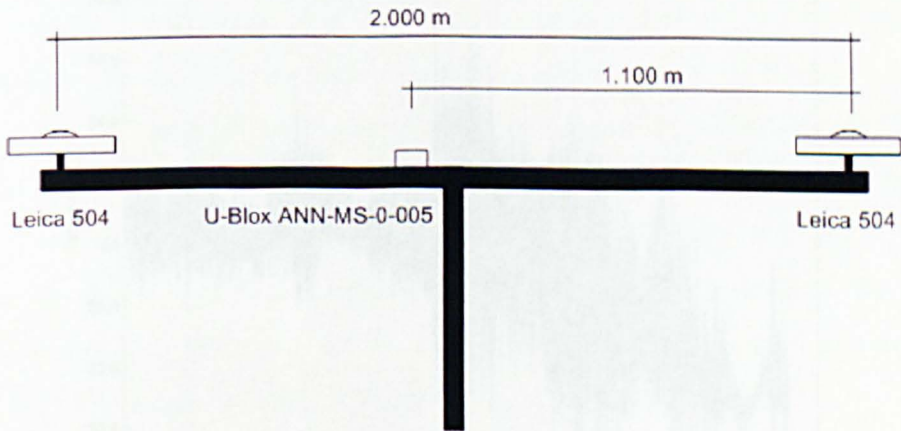


Figure 8.6: Diagram of the boom with the Leica 504 and U-Blox ANN-MS-0-005 antennas fitted

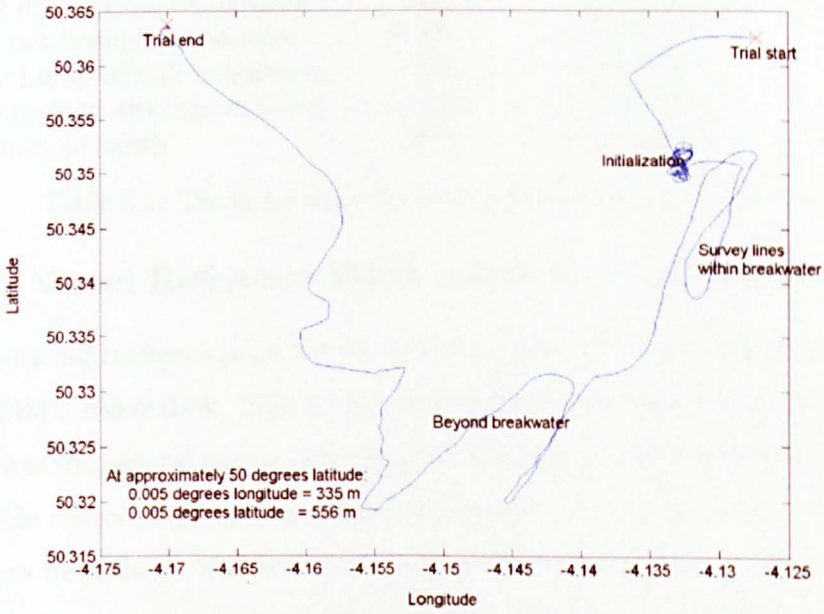


Figure 8.7: Sea trial plan trajectory

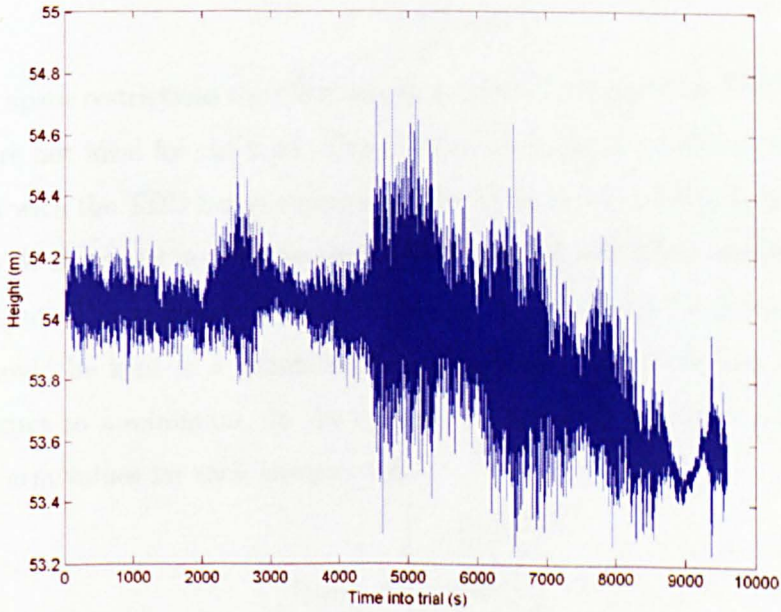


Figure 8.8: Sea trial height profile

Action	Time Taken	Time Into Trial	Key to fig 8.11
Steam into Plymouth Sound	1000 s	0-1000 s	1
Initialization turns	1000 s	1000-2000 s	2
Survey lines within breakwater	1500 s	2000-3500 s	3
Steam out beyond breakwater	1100 s	3500-4600 s	4
Survey Lines beyond breakwater	1500 s	4600-6100 s	5
Steam back to alternative berth	3300 s	6100-9400 s	6
Stationary at berth	200 s	9400-9600 s	7

Table 8.1: Times for each action conducted during the sea trial

8.2.5 Vessel Reference Point and Lever Arm Separations

The positional reference point for the trial was taken to be the computational centre of the CIMU below deck. This is the default option when processing within POSPac and so was the natural choice. This location was also chosen because the POSRS was to provide reference data for the trial and all other sensors were to be compared to it.

As has been shown in figure 8.3 the HG1700 was located very close to the CIMU fitted to the same metal plate. The lever arm between the HG1700 and the CIMU was measured based on their location on the IMU locating plate and knowledge of the computation centres of each IMU (all lever arm dimensions are expressed in metres):

$$l_{HG1700} = \begin{bmatrix} 0.095 \\ 0.240 \\ 0.005 \end{bmatrix}$$

Due to space restrictions the GPS antennas had to be located on the Marco in areas which were not ideal for the trial. The ideal location for the GPS antennas when in operation with the TDD heave algorithm is for them to be collocated with the centre of gravity of the vessel in order to reduce the effects of roll, pitch and heading on the heave output. This is usually impossible but at the very least the X and Y lever arm values should be kept to a minimum, which will also keep lever arm effects on the heave output to a minimum. In the case of the Marco this was not possible and so the lever arm values for each antenna were

$$l_{Leica1} = \begin{bmatrix} -3.250 \\ 2.186 \\ -2.707 \end{bmatrix}$$

$$l_{Leica2} = \begin{bmatrix} -5.250 \\ 2.186 \\ -2.707 \end{bmatrix}$$

$$l_{OEM4} = \begin{bmatrix} 2.336 \\ 0.038 \\ -3.548 \end{bmatrix}$$

$$l_{U-Blox} = \begin{bmatrix} -4.150 \\ 2.186 \\ -2.707 \end{bmatrix}$$

where the x -axis ran from the reference point to the bow, the y -axis ran from the reference point to the starboard side and the z -axis completed the right hand coordinate system and ran from the reference point down through the bottom of the vessel.

The lever arm offsets for the OEM4 and Leica 1 antennas were calculated during the post processing in POSPac; the lever arm offset for the Leica 2 and U-Blox antennas were calculated through knowledge of their fixed baseline with respect to the Leica 1 antenna when all three were placed on the boom. Each lever arm value was used to ‘move’ the data recorded with a particular sensor to the computational centre of the CIMU, the positional reference point for the trial. This was done using the attitude information extracted from the Applanix POSRS.

Lever arm accuracy has an effect on the accuracy of the TDD heave output because inaccuracies in the lever arm estimate result in incorrect lever arm compensation and introduce vertical displacement errors into the TDD velocity algorithm. The effect of lever arm accuracy can be appreciable at the roll and pitch angles experienced on a hydrographic survey vessel if a lever arm estimate of within 10 cm or better cannot be provided. During the Plymouth sea trial the Marco experienced roll and pitch angles

of up to 5 degrees during survey lines, which, using a lever arm estimate with a 10 cm error, would equate to a vertical displacement error of approximately 0.9 cm.

In a marketable TDD heave system used on board a hydrographic survey vessel POSRS attitude would not be available and as a result careful placing of the GPS antenna would be an important factor. As already explained this would involve keeping x and y -axis lever arm to a minimum as they have the greatest effect on the vertical displacement of the antenna due to changes in vessel attitude. When no accurate estimate of vessel attitude is available this will help keep attitude dependent errors to a minimum.

8.3 Trial Results

The results of the sea trial are presented in three distinct sections: POSRS SBET Data, IMU derived heave and TDD heave. The section for SBET heave looks at the reference heave data across the entire trial and describes the vertical motion of the vessel with respect to vessel location and actions. The IMU derived heave section compares IMU derived heave with SBET heave and assesses its performance in key areas of the trial. The TDD heave section compares TDD derived heave from the newly developed algorithm with SBET heave and looks again at the key areas of the trial.

8.3.1 POSRS SBET Data

The Applanix POSRS was used during the trial to provide reference data against which the IMU derived heave and the new method of heave measurement using the low cost U-Blox receiver were compared. This section looks at the quality of the POSRS SBET data and the derivation of the SBET heave before looking at the vertical dynamics of the vessel during the entire trial.

8.3.1.1 SBET Data Quality

The SBET data processed in POSPac represented the best available reference trajectory that can be extracted from the data recorded. The reference station data was provided by the Ordnance Survey and was collected at 1 Hz using a Leica SR 530

dual frequency receiver. The raw GPS data collected on the vessel was recorded at 4 Hz using a Novatel OEM4 dual frequency receiver and the IMU data at 200 Hz using the Honeywell CIMU. All data were time tagged and logged using the Applanix POS computer system. The baseline between the reference GPS receiver and the roving GPS receiver on the vessel ranged between 6 km and 11 km.

The GPS data were processed using the POSGPS software supplied by Applanix. Reference station and rover data were processed both forwards and backwards to provide a post processed interferometric GPS solution for the trial. The satellite availability during the trial can be seen in figure 8.9 and the quality factor for the post processed GPS solution in figure 8.10. There are five possible quality factors for processed GPS data within POSGPS:

1. Fixed integer ambiguity
2. Stable float
3. Converging float
4. DGPS or worse
5. Single point

Figure 8.10 shows that much of the processed GPS for the sea trial had a fixed integer solution with the quality only dropping to a stable float solution for brief periods during the trial. The post processed GPS solution was then processed with the raw CIMU data to attain the SBET solution in POSPac.

The post processed Kalman filtered GPS-aided INS solution that has been forward and backward smoothed within POSPac provides the best estimate of the trajectory of the vessel during the trial. The POSPac derived estimates of position quality for the SBET solution were

- North position error (1σ) 1.0 cm

- East position error (1σ) 1.0 cm

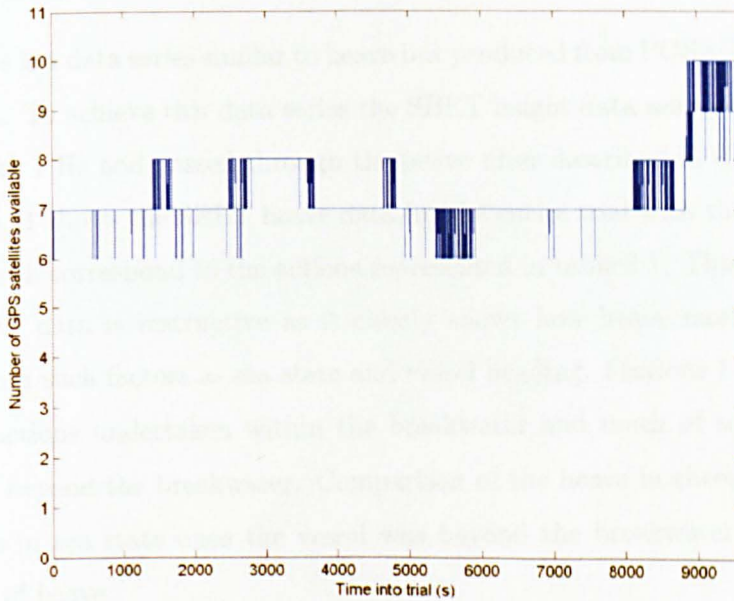


Figure 8.9: The number of GPS satellites available during the sea trial

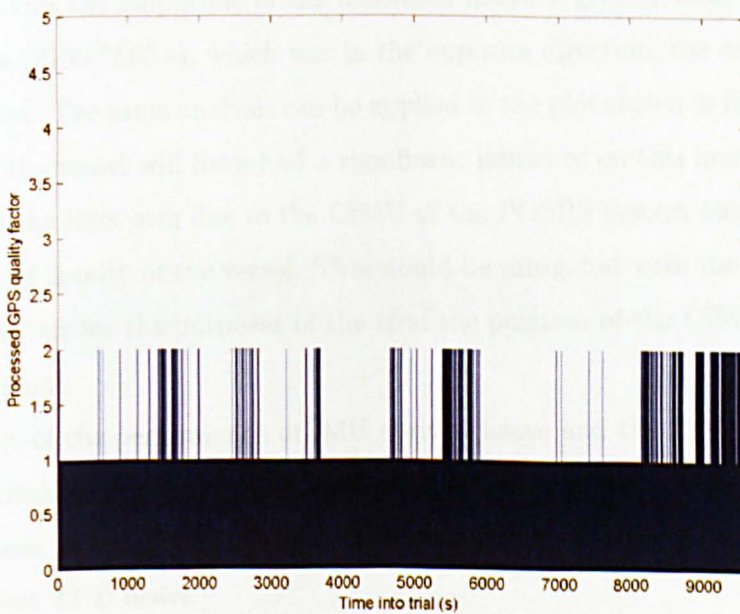


Figure 8.10: The POSGPS quality factor of the processed GPS solution for the sea trial

- Down position error (1σ) 2.3 cm

8.3.1.2 SBET Heave

SBET heave is a data series similar to heave but produced from POSRS post processed height data. To achieve this data series the SBET height data seen in figure 8.8 were resampled to 1 Hz and passed through the heave filter described in §6.3.

Figure 8.11 shows the SBET heave data for the entire trial with the plot split into sections which correspond to the actions represented in table 8.1. This representation of the heave data is instructive as it clearly shows how heave motion can change dependent on such factors as sea state and vessel heading. Sections 1-4 of figure 8.11 represent actions undertaken within the breakwater and much of sections 5 and 6 took place beyond the breakwater. Comparison of the heave in these sections shows the change in sea state once the vessel was beyond the breakwater with a greater amplitude of heave.

Figure 8.12 and 8.13 show an enlarged view of sections 3 and 5 of figure 8.11 respectively. They show a clear difference in the heave motion of the vessel dependent on vessel heading and wave direction. In figure 8.12 the first simulated survey line (2000-2750 s) was in a South-South Westerly direction into the oncoming waves. As a result of this the amplitude of the measured heave is greater than that during the second line (2750-3500 s), which was in the opposite direction, the same direction as wave motion. The same analysis can be applied to the plot shown in figure 8.13. Pitch motion of the vessel will have had a significant influence on this heave measurement because of the lever arm due to the CIMU of the POSRS system not being placed at the centre of gravity of the vessel. This would be mitigated were the data to be used in a survey but for the purposes of the trial the position of the CIMU is used as the reference point.

Analysis of the performance of IMU derived heave and the TDD heave algorithm will be primarily concerned with sections 2, 3 and 5 of the trial as shown in figure 8.11 as these provide dynamics that allow a thorough analysis of inertial based heave and low cost TDD heave.

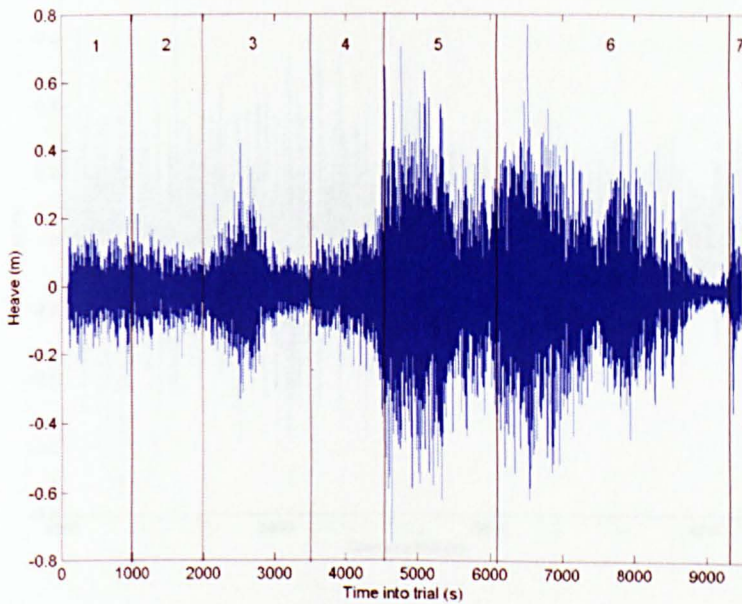


Figure 8.11: SBET heave over the complete trial

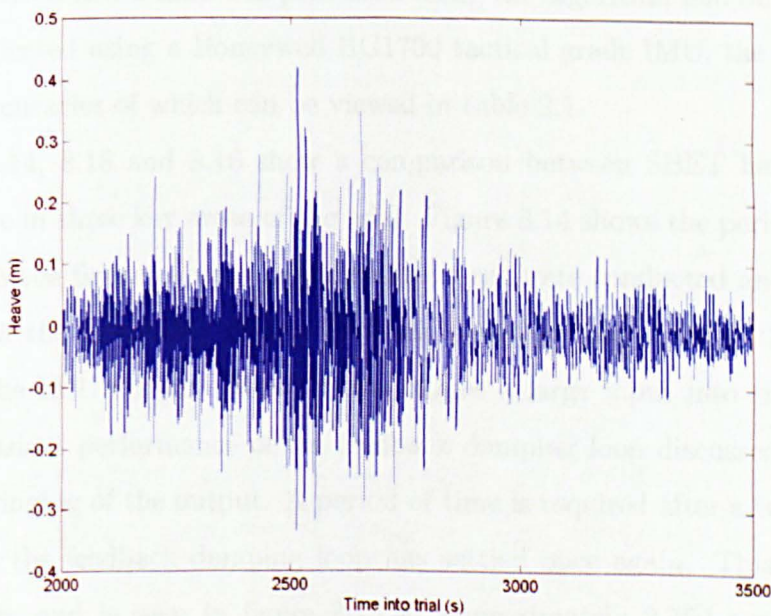


Figure 8.12: SBET heave data for the two survey lines within the breakwater (section 3 of figure 8.11)

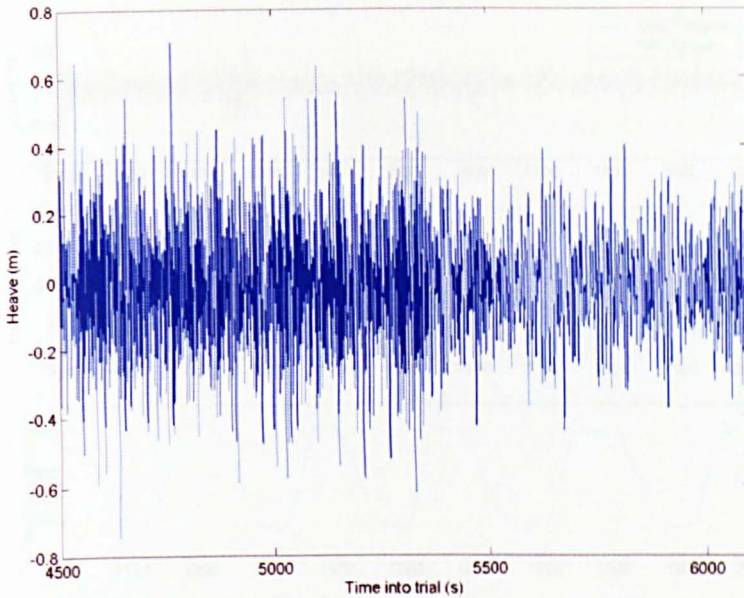


Figure 8.13: SBET heave data for the two survey lines outside the breakwater (section 5 of figure 8.11)

8.3.2 IMU Derived Heave

The IMU derived heave data was processed using the algorithm laid out in chapter 5 and data collected using a Honeywell HG1700 tactical grade IMU, the manufacturer published accuracies of which can be viewed in table 2.1.

Figures 8.14, 8.15 and 8.16 show a comparison between SBET heave and IMU derived heave in three key areas of the trial. Figure 8.14 shows the period of the trial during which the figure of eight initialization turns were conducted and very clearly demonstrates the instability of the feedback damping loop applied to the vertical channel of the IMU output. Vessel turns induce a large input into the heave filter and the transient performance of the feedback damping loop discussed in chapter 5 results in a ringing of the output. A period of time is required after a turn before the output from the feedback damping loop has settled once again. This phenomenon is well known and is seen in figure 8.15 at approximately 2,750 s and in 8.16 at approximately 5,500 s when the vessel put in a turn between the simulated survey lines. Comparison of heave error in figures 8.15 and 8.16 with heading data taken from the SBET solution shows a direct correlation between the IMU derived heave error

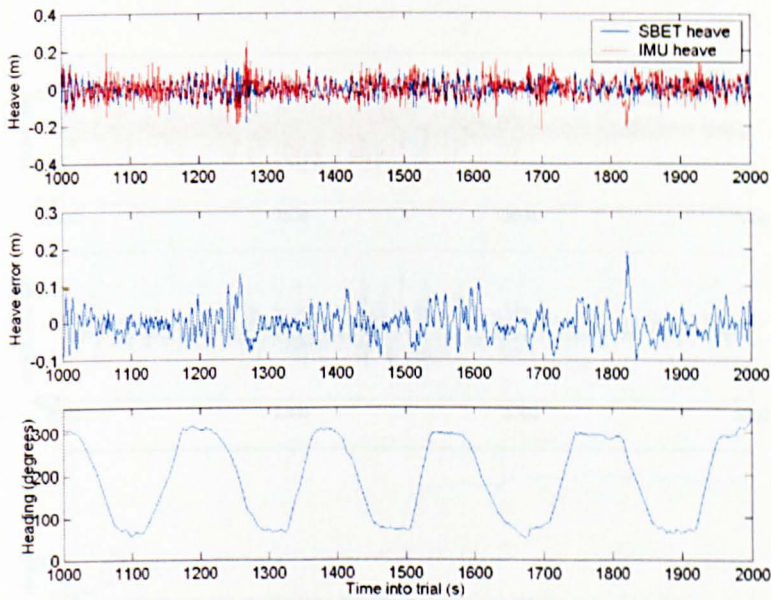


Figure 8.14: Comparison of SBET heave and IMU derived heave during initialization turns

and a subsequent ‘ringing’ of the output with the rapid change in heading caused by the vessel turn.

The results of the IMU derived heave when compared to SBET heave are summarized in table 8.2. The mean error shown in table 8.2 is negligible and likely due to the residual bias left over after high pass filtering the SBET height. As explained in §7.4.1.2, when filtering SBET height, which has a bias component of around 50 m, inevitably some residual height will remain. This hypothesis is borne out by the consistent 3 mm/s mean error results from the three sections of the trial across all heave sensor results.

The standard deviation of the error for the figure of eight initialization turns and the survey lines conducted within the breakwater show a difference in accuracy. As expected, the standard deviation of the error when undergoing initialization was greater than that experienced during survey lines. This was due to the increased amount of turns during initialization, which induced errors in the IMU derived heave algorithm as previously explained.

The results for the survey lines conducted outside the breakwater showed an

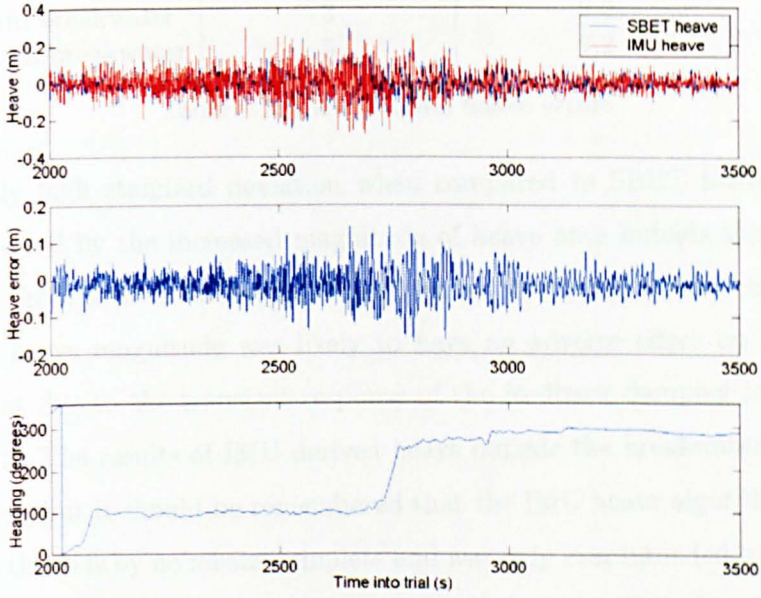


Figure 8.15: Comparison of SBET heave and IMU derived heave during survey lines within the breakwater

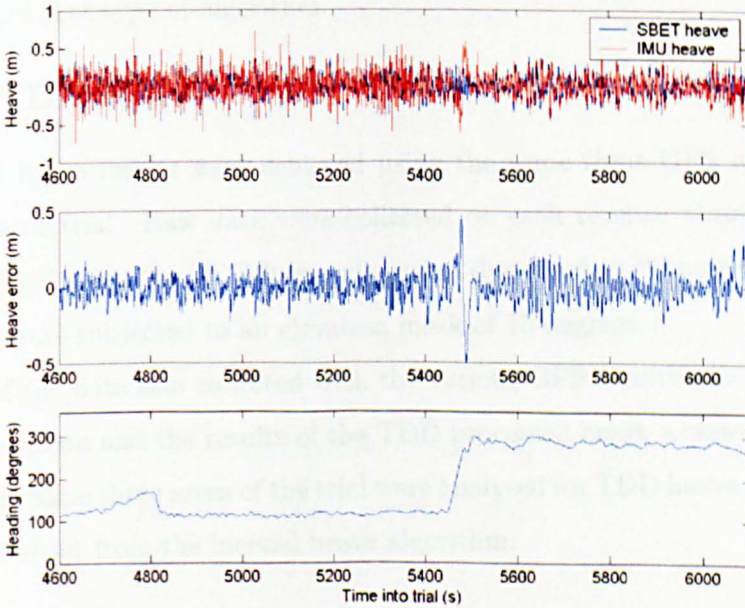


Figure 8.16: Comparison of SBET heave and IMU derived heave during survey lines outside of the breakwater

Action	Key to figure 8.11	Standard Dev. (1σ) (cm)	Mean Error (cm)
Initialization	2	3.8	-0.3
Lines within breakwater	3	2.9	-0.3
Lines beyond breakwater	5	7.2	-0.3

Table 8.2: IMU derived heave errors

unexpectedly high standard deviation when compared to SBET heave. This was probably caused by the increased magnitude of heave once outside the breakwater, which went from a nominal height of ± 0.2 m to a value of around ± 0.5 m. This increase in heave magnitude was likely to have an adverse effect on IMU derived heave output due to the transient response of the feedback damping loop discussed in chapter 5. The results of IMU derived heave outside the breakwater were a little disappointing but it should be remembered that the IMU heave algorithm developed during this thesis is by no means complete and was only ever intended to demonstrate inertial heave characteristics and give an indication of the likely heave errors. It is expected that heave measurement using a commercially available inertial based heave sensor would have greater accuracy.

The IMU derived heave results demonstrated the ability of the inertial based heave algorithm to measure vessel heave motion, but also highlighted the instability inherent in the use of that type of algorithm.

8.3.3 TDD Heave

The TDD heave results were achieved using the same three GPS receivers used in the simulator trial. Raw data were collected on each receiver throughout the trial and processed using the TDD heave algorithm described in chapter 6. All GPS data processed were subjected to an elevation mask of 15 degrees.

Each of the data sets collected with the various GPS receivers is discussed in the following section and the results of the TDD processed heave assessed against SBET heave. The same three areas of the trial were analysed for TDD heave as were analysed with the output from the inertial heave algorithm.

8.3.3.1 Leica SR 530 Receiver

The data collected with the Leica SR 530 receiver were dual frequency data recorded at 1 Hz. The number of satellites available across the duration of the trial can be seen in figure 8.17.

Figures 8.18 and 8.19 and 8.20 show the comparison of TDD heave from the Leica receiver with the SBET derived heave in the three areas analysed in section 8.3.2. The results are summarized in table 8.3. Taking the over arching view of the results shown in table 8.3 the level of noise on the TDD heave produced with the Leica SR 530 receiver can be said to be slightly greater than that found when using the inertial based heave sensor with standard deviations of the error signal over a centimetre greater when conducting survey lines. Looking at each area in more detail does show some interesting results, however.

During the initialization turns undertaken at the start of the trial the error from the TDD Leica heave showed none of the large heading dependent excursions from SBET heave that were seen with the IMU derived heave. Indeed, the amount of error seen in the TDD Leica heave during this period was the same as that seen during the survey lines. This demonstrated the increased stability of the TDD heave algorithm over the inertial based algorithm. This was demonstrated again when the vessel turn between survey lines was undertaken in figure 8.19 (2,750 s). Here no deviation from the SBET heave was seen as a result of the turn. The magnitude of the standard deviation of the error for the Leica TDD heave output was of a similar order to that seen when using IMU derived heave in both of the key areas of the trial, certainly to within the 2.3 cm POSPac quoted vertical position accuracy of the SBET data. The main difference between the two sets of results was that the Leica TDD heave was not adversely affected by vessel turns and instability as was the case in the IMU derived heave.

The results for the Leica, NovAtel and U-Blox TDD heave error during the survey lines conducted beyond the breakwater are discussed later in this chapter at §8.3.4 along with further analysis relating to the quality of the results.

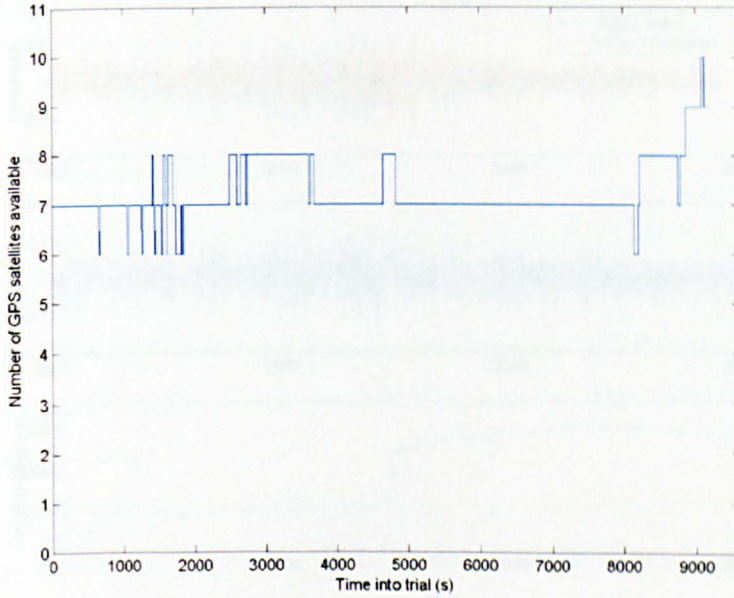


Figure 8.17: Satellite availability for Leica SR 530 receiver during sea trial

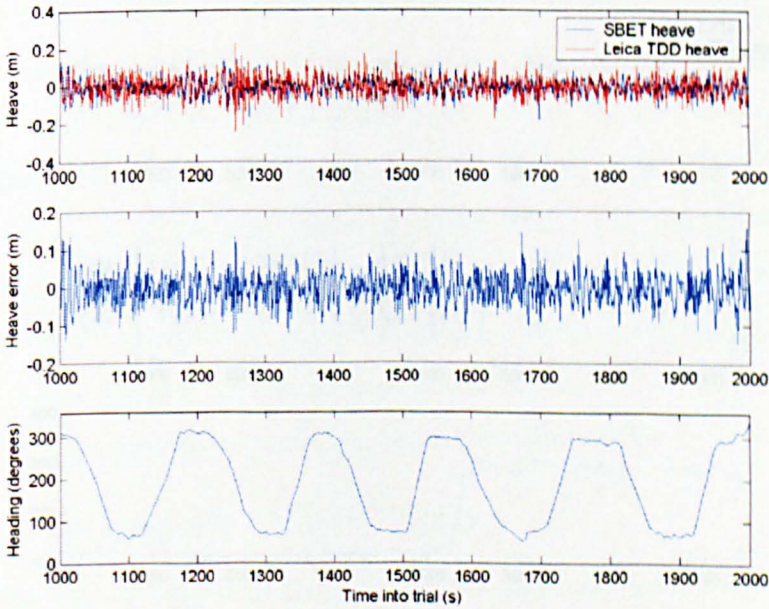


Figure 8.18: Leica SR 530 TDD heave error during initialization turns

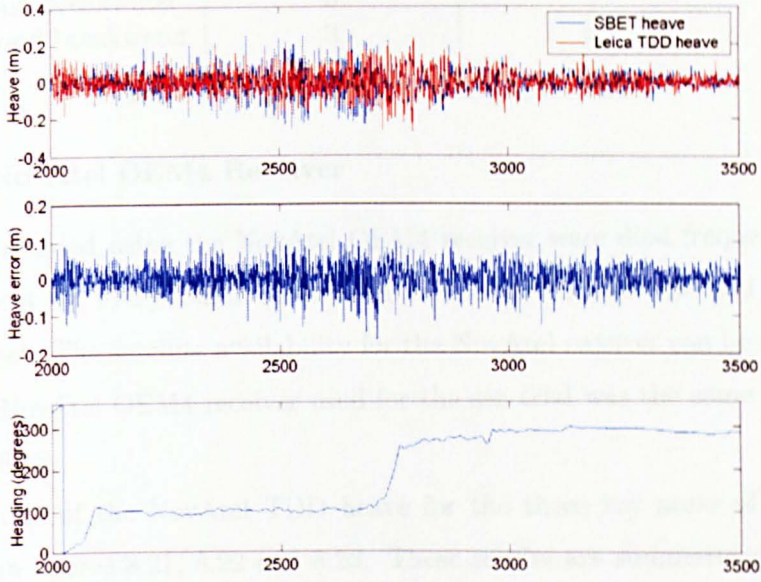


Figure 8.19: Leica SR 530 TDD heave error during survey lines within the breakwater

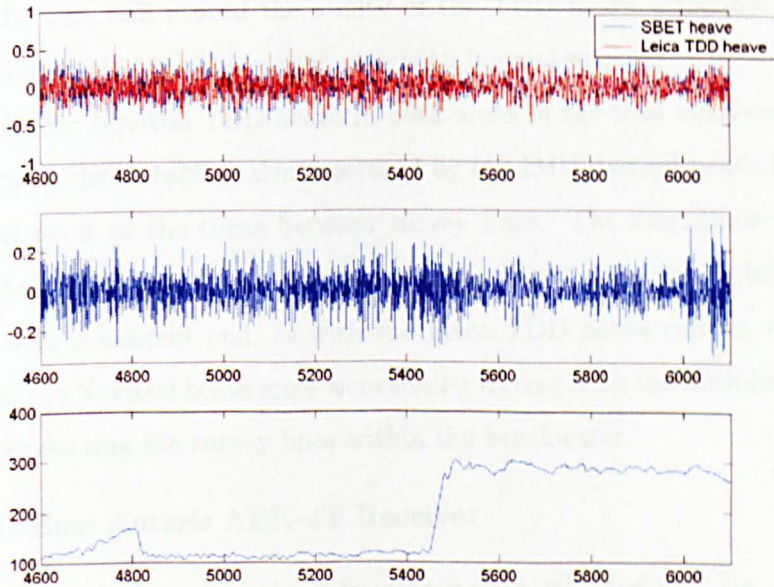


Figure 8.20: TDD Leica SR 530 heave error during survey lines outside the breakwater

Action	Key to figure 8.11	Standard Dev. (1σ) (cm)	Mean Error (cm)
Initialization	2	4.2	-0.3
Lines within breakwater	3	4.1	-0.3
Lines beyond breakwater	3	8.7	-0.3

Table 8.3: Leica SR 530 TDD heave errors

8.3.3.2 NovAtel OEM4 Receiver

The data recorded using the NovAtel OEM4 receiver were dual frequency and at a data rate of 4 Hz; every fourth observation in the RINEX file was used to produce a 1 Hz data set. The satellite availability for the NovAtel receiver can be seen in figure 8.9 as the NovAtel OEM4 receiver used for the sea trial was the same receiver used by the POSRS.

The results of the NovAtel TDD heave for the three key areas of the trial are presented in figures 8.21, 8.22 and 8.23. These results are summarized in table 8.4. The magnitude of the standard deviation of noise on the NovAtel TDD heave was the lowest of all the heave sensors employed during the trial. This was to be expected when it was considered that the same GPS receiver data was used to process the SBET solution in POSPac as was used to process the NovAtel TDD heave solution. This removed some of the independence of the trial for the NovAtel OEM4 TDD heave but, none the less, still proved the ability of the TDD heave algorithm to produce heave of a comparable quality to that seen with inertial sensors.

The results for NovAtel TDD heave in both areas of the trial analysed showed no susceptibility to the instability demonstrated by the IMU derived heave in either the initialization turns or the turns between survey lines. The magnitude of the error of the NovAtel TDD heave was consistent during areas of the trial where the heave conditions were consistent and, as with the Leica TDD heave results, the standard deviations of the NovAtel heave error were similar during both the initialization period and when conducting the survey lines within the breakwater.

8.3.3.3 U-Blox Antaris AEK-4T Receiver

The U-Blox Antaris data were single frequency data collected at 1 Hz. The number of satellites available for the trial using the U-Blox receiver is shown in figure 8.24,

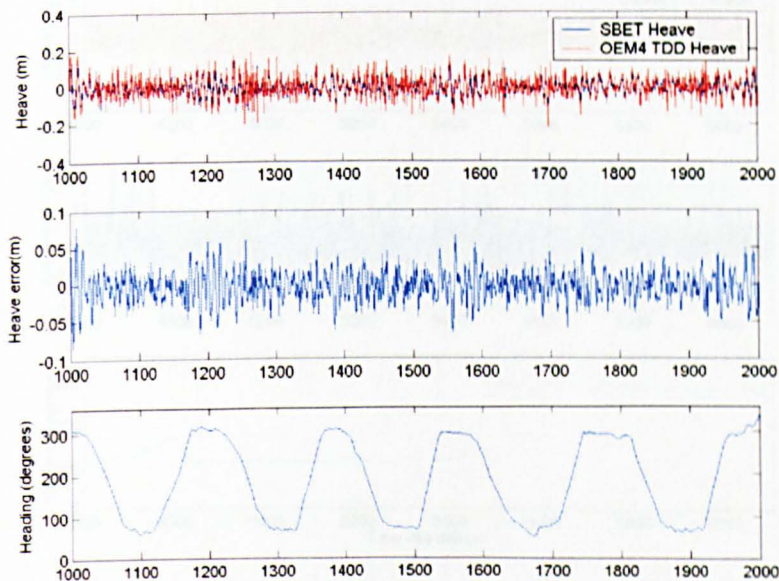


Figure 8.21: NovAtel OEM4 TDD heave error during initialization turns

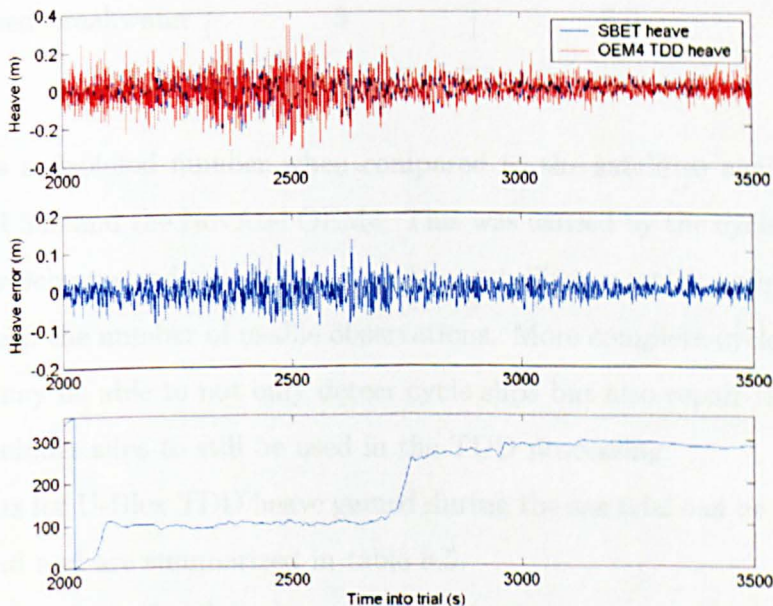


Figure 8.22: NovAtel OEM4 TDD heave error during survey lines within the breakwater

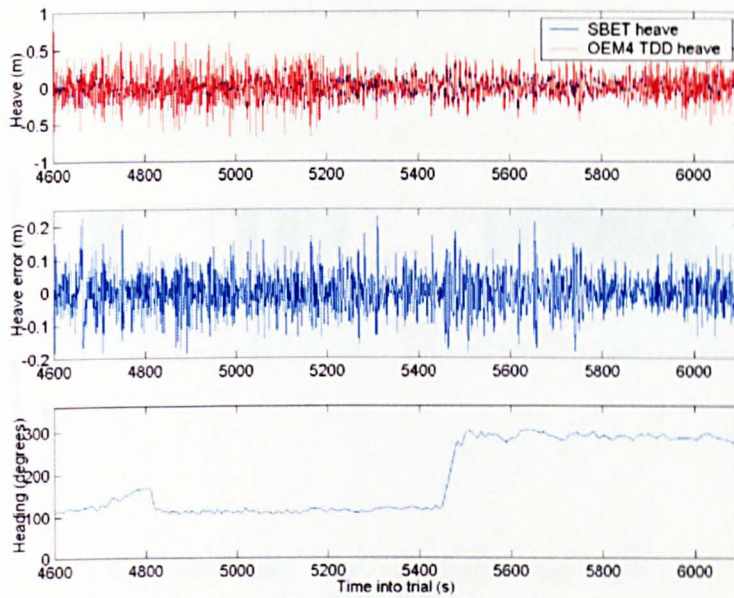


Figure 8.23: NovAtel OEM4 TDD heave error during survey lines outside the breakwater

Action	Key to figure 8.11	Standard Dev. (1σ) (cm)	Mean Error (cm)
Initialization	2	2.5	-0.3
Lines within breakwater	3	2.8	-0.3
Lines beyond breakwater	5	6.0	-0.3

Table 8.4: NovAtel OEM4 TDD heave errors

which shows a depleted number when compared to the satellites available for both the Leica SR 530 and the NovAtel OEM4. This was caused by the cycle slip handling algorithm, which removed the observations from satellites in which a slip had occurred and so reduced the number of usable observations. More complete cycle slip handling algorithms may be able to not only detect cycle slips but also repair them and allow data that includes slips to still be used in the TDD processing.

The results for U-Blox TDD heave gained during the sea trial can be seen in figures 8.25, 8.26 and are summarized in table 8.5.

It can be seen from the plots shown in figure 8.25 that some large excursions of U-Blox TDD heave from SBET heave occurred during the initialization turns conducted during the trial (1,050 s, 1,250 s and 1,430 s). These were caused by cycle slips that

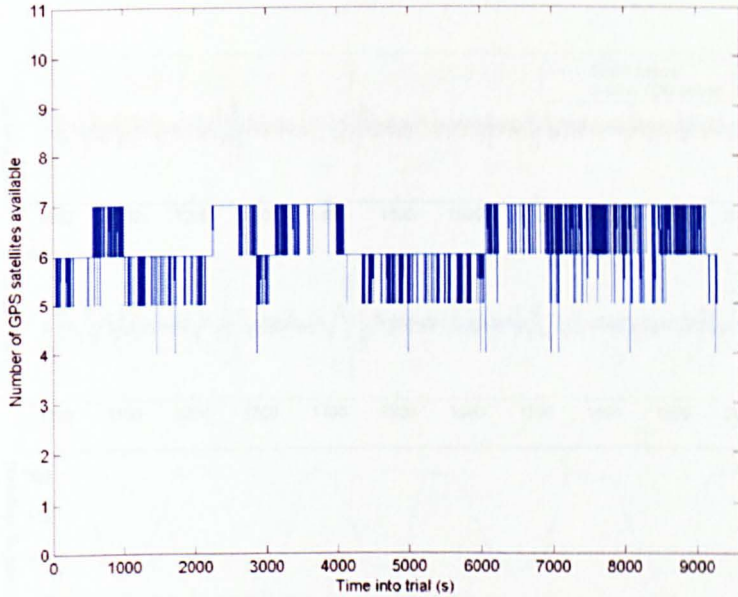


Figure 8.24: Satellite availability for U-Blox Antaris during sea trial

Action	Key to figure 8.11	Standard Dev. (1σ) (cm)	Mean Error (cm)
Initialization	2	5.5	-0.3
Lines within breakwater	3	5.1	-0.3
Lines beyond breakwater	5	10.2	-0.3

Table 8.5: U-Blox Antaris TDD heave errors

were not detected by the cycle slip handling algorithm developed in this research and integrated into the TDD heave algorithm. Despite the removal of the vast majority of the cycle slips in the U-Blox data some still remained and caused spikes in the TDD velocity estimate, which, when integrated and filtered in the TDD heave algorithm, produced long periods of heave estimation with large errors. It is thought that further research into a more suitable cycle slip handling algorithm would remove the remaining cycle slips resulting in better quality data.

The areas of the heave error plots in figures 8.25, 8.26 and 8.27 that were not affected by cycle slip based errors were taken to be representative of the magnitude of errors that would be achievable if all cycle slips were removed from the U-Blox data. As such, the standard deviation of error values quoted in table 8.5 have had the large errors caused by undetected cycle slips removed.

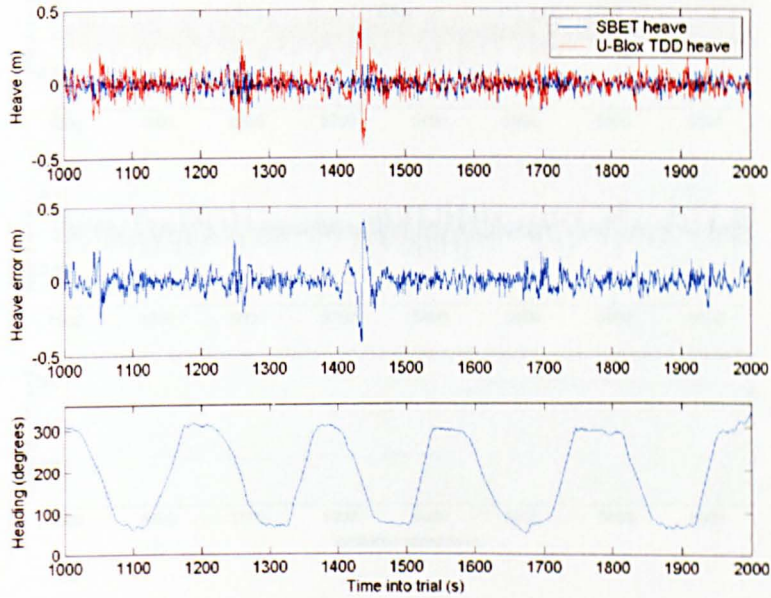


Figure 8.25: U-Blox Antaris TDD heave error during initialization turns

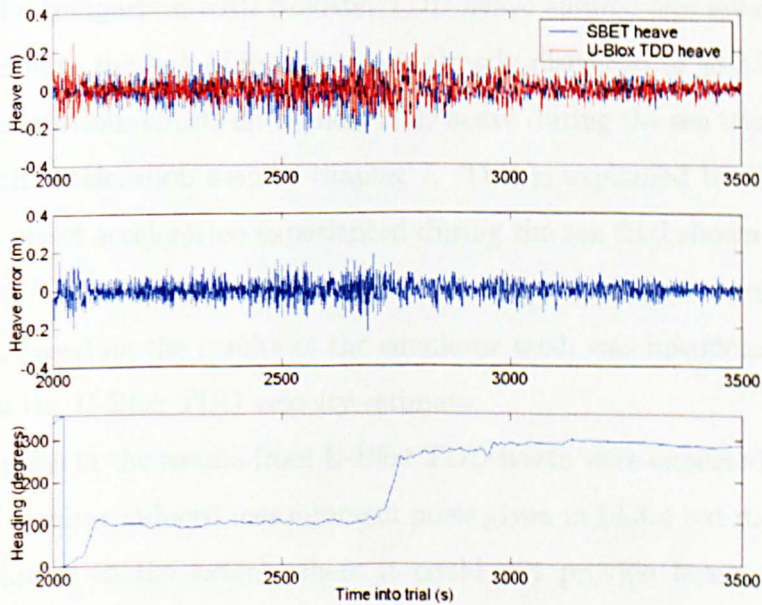


Figure 8.26: U-Blox Antaris TDD heave error during survey lines within the breakwater

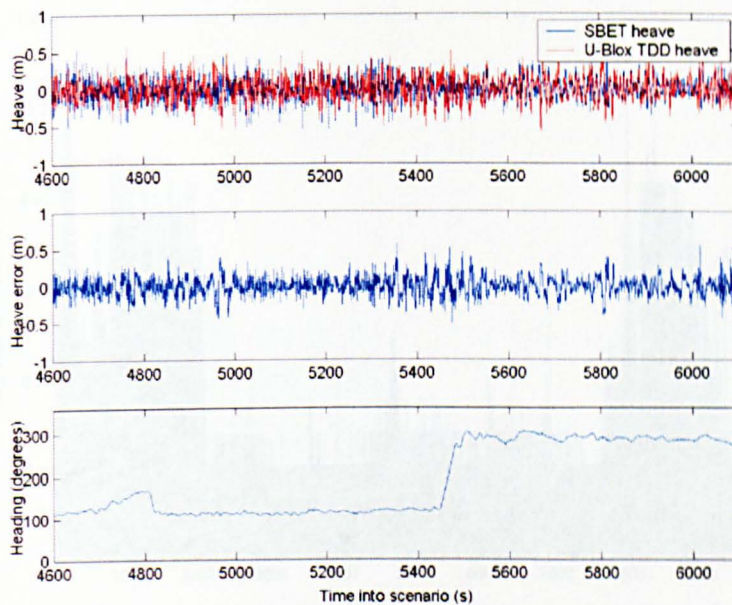


Figure 8.27: U-Blox Antaris TDD heave error during survey lines conducted outside the breakwater

The magnitude of the standard deviation of heave error for U-Blox TDD heave was only slightly greater than that seen for Leica TDD heave and heave from the inertial algorithm. The comparison with NovAtel TDD heave showed less favourable results but this was due to the lack of independence already discussed in §8.3.3.2.

There are no obvious effects on U-Blox TDD heave during the sea trial of the errors correlated with acceleration seen in chapter 7. This is explained by the plot of the magnitude of vessel acceleration experienced during the sea trial shown in figure 8.28 which shows that the accelerations experienced during the sea trial were rarely over 2 cm/s^2 , which, based on the results of the simulator trial, was insufficient to produce large errors in the U-Blox TDD velocity estimate.

The extra noise in the results from U-Blox TDD heave were expected based on the assessment of receiver induced measurement noise given in §3.3.4 but did not degrade the heave solution to the extent where it could not provide heave compensation capable of meeting the IHO survey order one as described in §4.5. Inertial based heave sensors also provide heave data to within IHO survey order one (Parker and Mallace, 2006) meaning that heave measured using the TDD heave algorithm and a

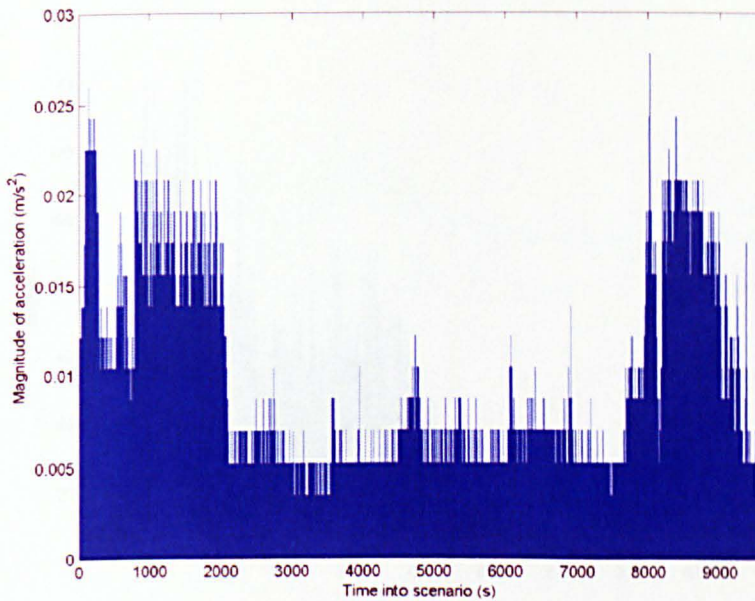


Figure 8.28: Magnitude of acceleration experienced during the plymouth sea trial

U-Blox low cost commercially available receiver is of a comparable standard to inertial based heave technologies.

8.3.4 The Effect of GPS Data Rate on the Sea Trial Results

The TDD heave results presented in the preceding sections of this chapter were all based on GPS data recorded at 1 Hz. When the sea trial was originally conducted it was thought that a 1 Hz data rate would be sufficient to record all the significant heave motion of the vessel. In reality, the results of the TDD heave during the sea trial were disappointing, which prompted an analysis of the effects of the 1 Hz GPS data rate on the resulting TDD heave error.

8.3.4.1 Frequency Range of SBET Heave and 1 Hz TDD Heave Error

Frequency analysis of the SBET heave motion of the vessel during the trial revealed that there was a significant amount of power in vessel heave motion that occurred at or above the Nyquist frequency when using data recorded at 1 Hz. Figure 8.29 shows the vessel heave motion across the entire trial in the frequency domain and a significant proportion of the signal power appears at or above the Nyquist frequency

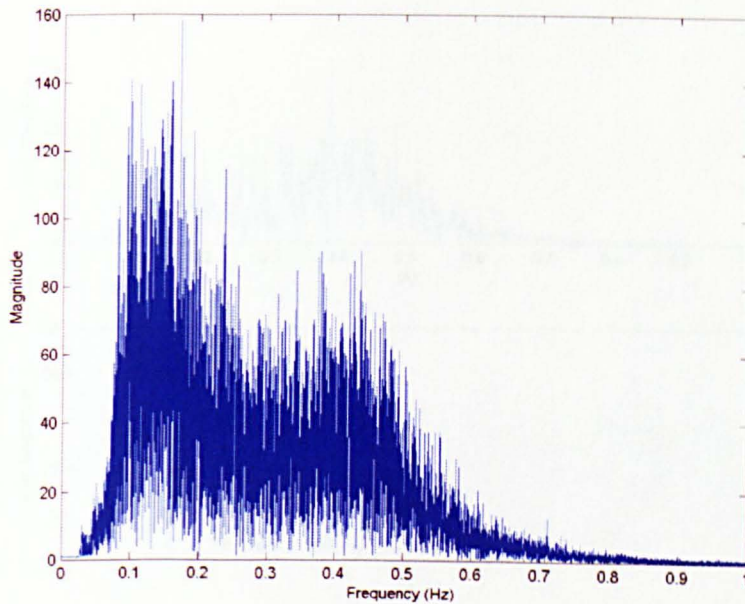


Figure 8.29: Frequency analysis of SBET heave across the entire trial

of 0.5 Hz. Further frequency analysis was conducted on the SBET heave in sections relating to each individual survey line conducted within the breakwater. Figures 8.30 (a) and (b) show the heave motion during survey line one (2,000-2,750 s) and survey line two (2,750-3,500 s) respectively. They show that the heave motion during line two had significantly less power above or near the Nyquist frequency.

Table 8.6 shows the heave error seen on NovAtel OEM4 1 Hz TDD heave during the survey lines within the breakwater split into the individual lines one and two. When the plots shown in figure 8.30 were correlated with the data presented in table 8.6 it was seen that the heave error was greater when the frequencies of the heave motion were at or above the Nyquist frequency. The same analysis could be conducted on each individual survey line conducted beyond the breakwater.

Action	Standard Dev. (1σ) (cm)	Mean Error (cm)
Survey line 1	4.0	-0.3
Survey line 2	1.8	-0.3

Table 8.6: NovAtel OEM4 1 Hz TDD heave error during lines conducted within the breakwater

It was thought that the heave experienced by the vessel that exceeded or was in

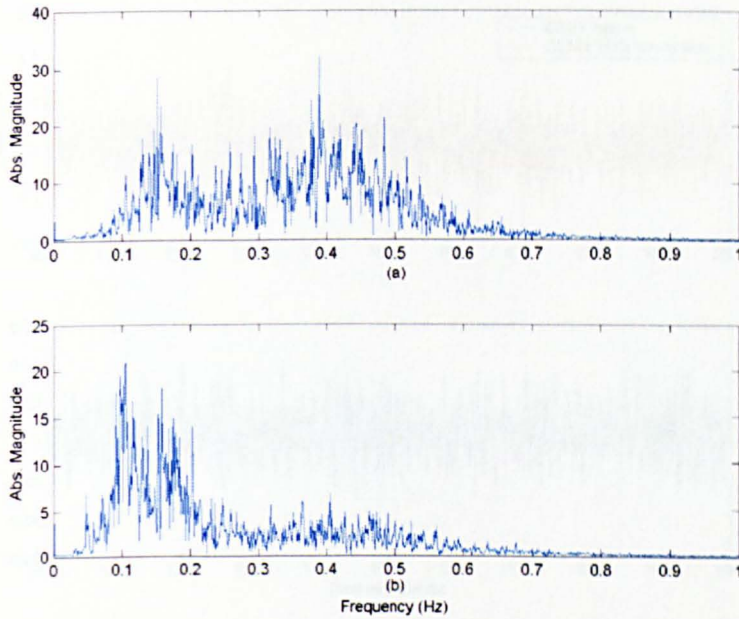


Figure 8.30: Frequency analysis of SBET heave during line 1 (a) and line 2 (b) conducted within the breakwater

the proximity of the Nyquist frequency caused the 1 Hz heave motion to be under sampled. This resulted in signal aliasing in the heave motion when expressed at 1 Hz.

8.3.4.2 NovAtel OEM4 4 Hz TDD Heave

The findings resulting from the heave frequency analysis were endorsed by the results gained from NovAtel TDD heave when processed at 4 Hz shown in figures 8.31, 8.32 and 8.33 for the three key areas of the trial, results which are summarized in table 8.7. The NovAtel OEM4 receiver was the only receiver to record data at a higher rate during the sea trial and so was the only receiver for which higher rate TDD heave could be processed.

Action	Key to figure 8.11	Standard Dev. (1σ) (cm)	Mean Error (cm)
Initialization	2	1.6	-0.3
Lines within breakwater	3	1.7	-0.3
Lines beyond breakwater	5	2.7	-0.3

Table 8.7: NovAtel OEM4 4 Hz TDD heave errors

The results for the 4 Hz NovAtel OEM4 data presented in table 8.7 showed a

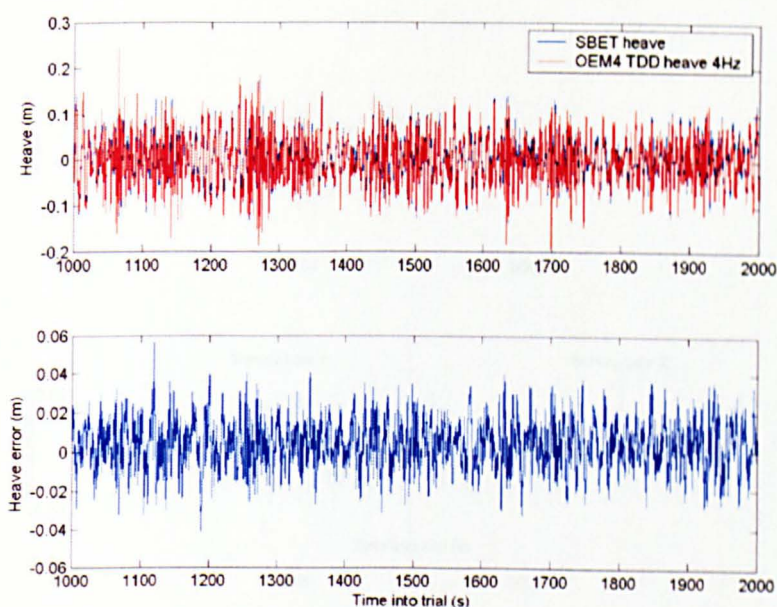


Figure 8.31: NovAtel OEM4 4 Hz TDD heave error during initialization turns

marked improvement over the results for the same receiver recorded at 1 Hz and shown in table 8.4. The increased data rate pushed the Nyquist frequency up to 2 Hz, which was more than adequate to cover all the frequencies of motion seen in figure 8.29 so the 4 Hz heave was not subject to the aliasing which occurred in the 1 Hz data. In addition, the heave error shown in figures 8.32 and 8.33 can be seen to be of a similar magnitude during both individual lines leading to the conclusion that higher frequency heave motion was no longer adversely affecting the heave error.

Doubts were expressed in §8.3.3.2 as to the independence of NovAtel OEM4 TDD heave from the SBET reference data given that the same GPS data being used for both heave solutions. For this reason a new SBET solution was processed using the CIMU data aided by 1 Hz Leica SR 530 GPS data. A heave estimate based on this new SBET solution was compared to the NovAtel 4 Hz TDD heave estimate and the results are presented in table 8.8. These results show similar levels of accuracy to those seen in table 8.7 and demonstrate the high quality of heave estimation possible using the TDD heave algorithm.

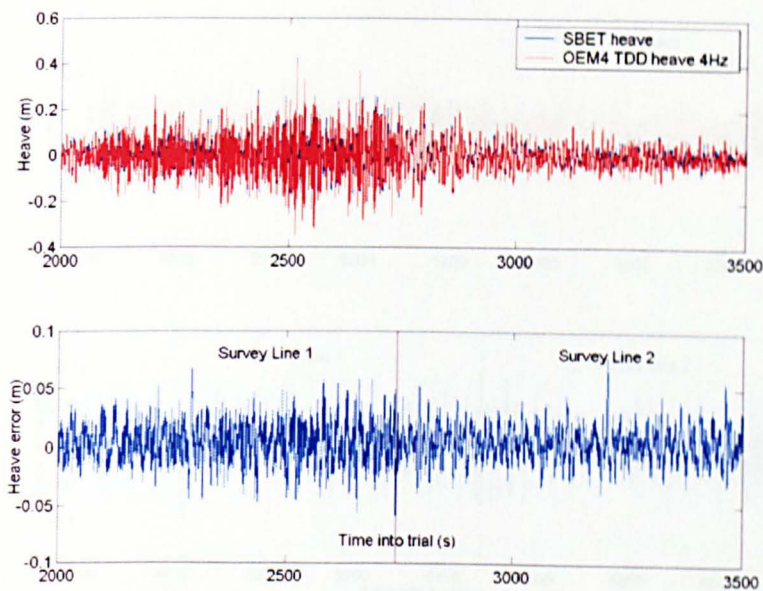


Figure 8.32: NovAtel OEM4 TDD 4 Hz heave error during survey lines conducted within the breakwater

Action	Key to figure 8.11	Standard Dev. (1σ) (cm)	Mean Error (cm)
Initialization	2	1.5	0.4
Lines within breakwater	3	1.8	0.4
Lines beyond breakwater	5	2.7	0.4

Table 8.8: NovAtel OEM4 4 Hz TDD heave errors when compared to SBET data processed using 1 Hz Leica SR 530 GPS data

8.4 Plymouth Sea Trial Summary

The sea trial was conducted on 2 August 2006 between 09:30 and 12:30 in and around the Plymouth Sound. Data was collected using three GPS receivers of various grades to produce TDD heave, an HG1700 IMU to create IMU derived heave using the algorithm developed during this project and a GPS-aided INS Applanix POSRS to provide truth data.

The trial has successfully proved the ability of the TDD heave algorithm to estimate heave to within the tolerances required to achieve the IHO survey order 1, while removing the troubling issues surrounding inertial based heave algorithms such as stability and usability. This section summarizes the main results of the sea trial.

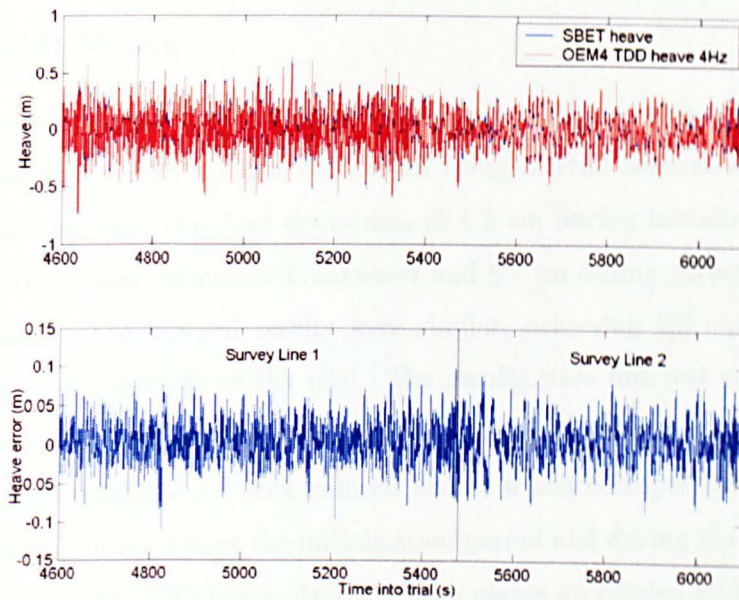


Figure 8.33: NovAtel OEM4 TDD 4 Hz heave error during survey lines conducted beyond the breakwater

8.4.1 IMU Derived Heave

IMU derived heave using the inertial heave algorithm developed during this project was compared to SBET heave recorded using the highly accurate GPS-aided INS Applanix POSRS. The results have shown that the IMU derived heave had an error standard deviation of 3.8 cm during the period of figure of eight initialization turns, 2.9 cm during the simulated survey lines conducted within the breakwater and 7.2 cm during the simulated survey lines conducted outside the breakwater. The magnitude of the errors in IMU derived heave were somewhat disappointing but they should be taken in the context of the IMU heave algorithm quality. The purpose of the IMU heave algorithm is to give an idea of the accuracies possible with inertial technologies but also to highlight their shortcomings in respect to instability and usability.

The instability problems associated with the use of inertial technologies in this application were highlighted with deviations of IMU derived heave from SBET heave during and after turns, a phenomenon known as turn induced heave that resulted in decreased accuracy. Usability is always an issue with inertial based heave measurement as the time constant and damping coefficients for the feedback loop must be

optimally set.

8.4.2 TDD Heave

The TDD heave produced from the two high grade GPS receivers used in the trial was of a similar accuracy to that seen when using inertial sensors with the Leica receiver achieving error standard deviations of 4.2 cm during initialization, 4.1 cm during the survey lines within the breakwater and 8.7 cm during survey lines beyond the breakwater. The Novatel results were similar, achieving 2.5 cm, 2.8 cm and 6.0 cm in the same periods of the trial. The results were not just concerned with heave measurement accuracy, however, and it was important to note that the TDD heave algorithm exhibited no turn induced heave, which corrupted the accuracy of the inertial based heave during the initialization period and during the turn after the first survey line. The TDD heave algorithm also places no burden on the user to set the filter parameters to suit vessel characteristics and current sea state conditions.

The results of the U-Blox TDD heave, although slightly degraded in accuracy from the results seen from the two higher grade receivers and the IMU derived heave, showed that the new TDD heave algorithm designed for use with low cost GPS receivers is likely to be able to compete with inertial based algorithms to provide heave data capable of IHO survey order one. The main problem with data from the U-Blox receiver compared to the data from the higher grade receivers was the existence of a large number of cycle slips, some of which were not detectable using the algorithms employed in this research. Still the standard deviations of the heave error using U-Blox TDD heave were 5.5 cm, 5.1 cm and 10.2 cm in the three key areas of the trial.

A key factor in the accuracy of the TDD heave estimates quoted above has been the data rate of the GPS data. All the results were based on 1 Hz GPS data and analysis has shown that this was insufficient to capture all the heave motion experienced by the vessel and prevent aliasing in the heave estimation. Using Novatel OEM4 data collected at 4 Hz has demonstrated much improved accuracies (1σ) of 1.5 cm, 1.8 cm and 2.7 cm during the three key areas of the trial when compared to an independent SBET solution processed using 1 Hz Leica SR 530 GPS data.

It is strongly expected that U-Blox GPS data recorded at 4 Hz would see accuracy improvements over its 1 Hz counterpart of a similar order to those seen when using the Novatel OEM4.

Chapter 9

Summary, Conclusions and Future Recommendations

This chapter of the thesis summarizes the work undertaken for the project highlighting the main points and the areas of novelty that the work has accomplished. There is also a section that draws conclusions from the results found during the two sets of trials conducted. Finally, there is a section that makes some recommendations for future work based on the experience gained throughout the project and the results of the two trials.

9.1 Thesis Summary

The aim of the project was to develop a heave algorithm for use with off the shelf low cost GPS receivers such as the U-Blox Antaris. This algorithm was to overcome some of the problems and limitations associated with the use of inertial sensors for the measurement of heave in three areas:

- Cost
- Stability
- Usability

This has been achieved through the development of a highly accurate velocity estimation algorithm using stand-alone low cost GPS receivers, termed temporal double difference (TDD). Carrier phase pseudo-range observations from adjacent epochs were differenced to produce user velocity, the vertical channel of which was

then integrated to produce relative vertical position. A high pass filter was also designed that was then used to remove any drift on the relative position output that may exist due to bias errors on the vertical velocity estimation, resulting in highly accurate heave estimation.

The algorithm has been extensively tested in both a simulated and a real world marine environment. The simulator trial, conducted using a Spirent hardware simulator, tested the accuracy of the TDD velocity algorithm under varying dynamic conditions and using receivers of varying grades allowing the errors associated with low cost receivers to be quantified. The sea trial was conducted using a vessel owned by Sonardyne International Ltd. and allowed the testing of the algorithm under marine conditions. The TDD heave algorithm was implemented using data collected from varying grades of GPS receiver and tested against the results from both an inertial heave algorithm developed for the project and highly accurate truth data recorded using an Applanix POSRS GPS-aided INS system.

The recent introduction of off the shelf low cost GPS receivers with the ability to measure and record the raw carrier phase pseudo-range observable has allowed their use in the TDD algorithm developed for this project, and it has been the first work to look at their use for the measurement of hydrographic survey vessel heave motion. The simulator trial conducted using the Spirent simulator purchased by the IESSG has, for the first time, quantified the errors associated with low cost receivers in the measurement of the carrier phase pseudo-range observable through the comparison of the U-Blox Antaris results with those from higher grade dual frequency receivers, and through the collection of data under varying dynamic scenarios. The comprehensive nature of the sea trials conducted in Plymouth have been the first to have produced a full assessment of the TDD heave algorithm implemented on commercially available low cost receivers. It has tested the algorithm against an entire suite of further heave motion sensors including the use of various stand-alone GPS receivers for TDD heave, an inertial based heave sensor and heave data collected using the POSRS; this is something that is not seen in previous works.

9.2 Conclusions

Two separate trials have been conducted for this thesis, which have been used to thoroughly test different aspects of the TDD algorithm developed during the project. Both of these trials have proven the performance of the TDD velocity and heave algorithms and the conclusions that can be drawn from each are presented below.

9.2.1 The Spirent Simulator Trials

The Spirent simulator trial conducted as part of the research contained within this thesis has been the first to explore the quality of the recorded carrier phase pseudo-range observable measured with commercially available low cost GPS receivers when compared to the measurements taken from dual frequency receivers. By using three separate receivers of varying grades to record simulated data from the same scenarios receiver based errors were isolated and quantified. This was extended to cover data from three distinct sets of dynamics that were able to test the performance of the receiver signal tracking loops under dynamic stress. Further tests were able to introduce simulated errors such as tropospheric and ionospheric delay allowing their effects on the TDD velocity estimation to be determined. The conclusions drawn from the Spirent simulator are itemized below.

- Under static conditions the TDD velocity estimation using the U-Blox receiver was of a comparable quality to those seen when using the NovAtel and Leica receivers. This is thought to be caused by the limitation of the bandwidth of the signal tracking loop within the U-Blox receiver based on the knowledge that the receiver is stationary. The use of this extra information enables the U-Blox receiver to level the playing field somewhat, allowing the signal tracking loops within the receiver to record accurate measurements of the carrier phase pseudo-range observable with reduced tracking loop bandwidth whilst acting well within their dynamic stress limitations.
- When under dynamic conditions, of the order of which may be expected in a marine environment, a divergence in the performance of the three receivers was found to exist. The quality of the measurements recorded with the U-Blox

receiver was now significantly reduced when compared to those recorded using either the NovAtel or the Leica. As such the TDD heave estimates produced using the data from the U-Blox receiver were also less accurate than those produced from data recorded using the Leica or NovAtel receivers. Errors in TDD heave from the U-Blox receiver were approximately an order of magnitude greater than those seen from the other receivers at the highest frequencies of motion. These results were emphatically endorsed by those seen when the receivers were subjected to a high dynamic scenario.

- The velocity estimate calculated using the TDD velocity algorithm can be significantly affected by the rate of change of the errors associated with the atmosphere. This was proven during trials two and three when tropospheric and ionospheric errors were modeled within the simulator. The magnitude of potential error in TDD velocity if the simulated tropospheric error source was left unmitigated was ± 2 mm/s in horizontal velocity and ± 4 mm/s in vertical velocity. The magnitude of possible error experienced for unmitigated ionospheric delay was smaller at ± 1 mm/s in horizontal velocity and ± 1.5 mm/s in vertical velocity suggesting that the penalty in TDD velocity accuracy for single frequency data collection may be small.
- The final simulator trial brought together all the aspects of the previous trials by testing the full TDD velocity and heave algorithms in the static and marine environments with atmospheric errors simulated. This provided a natural last step between the simulator trial and the collection of real data and the results were similar to those seen in trial one, which was to be expected given the results that of the previous trials.
- As a final prelude to the collection of data for the sea trial real static GPS data were collected using each of the three receivers used in the simulator trial along with their respective antennas. The results of this trial endorsed the results of the simulator trial inasmuch as the TDD velocity performance of the U-Blox receiver was equal to that of the Leica and NovAtel receivers under static conditions.

9.2.2 The Sea Trial

The sea trial was conducted in order to test the TDD heave algorithm calculated using data recorded with the three receivers previously used in the simulator trial against an IMU derived heave estimate and highly accurate Applanix POSRS reference data.

The magnitude of the IMU derived heave error was considered to be too great, which was likely due to the quality of the algorithm in use. The heave algorithm developed during the project was simply a damped INS vertical channel and employed none of the velocity aiding algorithms that commercial heave sensors use, which are explained in §2.5. The IMU derived heave results did demonstrate the stability and usability issues implicit with the use of inertial heave sensors, however.

The TDD heave for each receiver used in the trial was compared to the SBET heave solution. The results demonstrated clearly the benefits available to the TDD heave user compared to the inertial based heave user. Each receiver's TDD heave output demonstrated increased stability over IMU derived heave and no tuning was required by the user as is required with inertial heave sensors. The magnitude of the errors seen in the TDD heave solution using all three receivers were larger than was expected due to the under sampling of vessel heave motion at 1 Hz. Even with the aliasing that occurred due to that under sampling, the results do show the ability of U-Blox TDD heave to compete with heave produced from other GPS receivers in terms of accuracy.

The TDD heave results for the sea trial were all based on GPS data recorded at 1 Hz. Through analysis this data rate was found to be inadequate for the measurement of the frequency of heave motion experienced by the vessel during the trial. A 4 Hz TDD heave solution was processed using data collected from the NovAtel OEM4 receiver, the only receiver used in the trial to log raw observables at a higher data rate. The NovAtel 4 Hz TDD heave was compared to an SBET solution that was processed in POSPac using the 1 Hz Leica SR 530 collected during the trial; this was done so as to provide independent reference data as the previous SBET solution was processed using the NovAtel OEM4 data. The NovAtel 4 Hz TDD heave showed a vastly increased level of performance over the heave solutions using 1 Hz data and

exhibited no adverse effects due to higher frequency heave motion.

Overall, the results of the sea trial show the ability of TDD heave to measure heave to the accuracy required for at least IHO survey order one and possibly IHO special order when using high grade GPS receivers such as the NovAtel OEM4. It is expected that U-Blox TDD heave would see a marked improvement in accuracy over the figures stated in chapter 8 if data were collected at a higher rate, say 4 Hz. The TDD heave outputs exhibited no errors due to the temporal instability that is experienced in the use of inertial based heave sensors and also required no inputs from the user. These factors show the ability of TDD heave using commercially available low cost GPS receivers to compete with inertial based sensors in terms of accuracy, and generate savings to the survey industry. These savings come in the form of reduced unit cost, reduced lead in time to survey lines and reduced user burden.

9.3 Recommendations for Future Work

The research conducted during this project and presented in this thesis has proven the ability of commercially available low cost GPS receivers to be used in a TDD heave algorithm that can potentially measure heave to meet IHO survey order one. It has also highlighted some of the limitations of these receivers under high accelerations and quantified the level of error introduced by them compared to higher grade receivers. In order to continue the research and make further advancements in this field certain recommendations are made here for future work.

The first, and most obvious, recommendation to be made is that a further sea trial is carried out using the U-Blox GPS receiver or similar recording data at a rate suitable to adequately sample the entire frequency spectrum of vessel heave. The work carried out in this thesis proves the TDD algorithm using a Novatel OEM4 receiver and suggests that similar results could be achievable using a U-Blox receiver but a sea trial is required to fully prove that.

A further recommendation surrounds the issue of vessel attitude. Many applications for heave sensors require the estimation of vessel attitude such as the need for echo-sounder beam steering onboard a hydrographic survey vessel. This is provided as

an output when using inertial based AHRS units but is not available through the use of a single receiver in a TDD heave algorithm. The use of multiple receivers may provide a way to resolve attitude rate through their relative TDD velocities, however, and this should be explored fully so that TDD heave sensors may compete with inertial based technologies in the hydrographic survey industry market. In many instances multiple receivers already exist onboard vessels and the exploitation of raw measurements from these may remove the need the installation of others; a microprocessor based system that can exploit these opportunistic GPS observables to produce heave and attitude rate may be possible.

A severe limitation of the U-Blox receiver used in this trial to produce reliable heave measurement has been the requirement of a robust and accurate cycle slip detection and repair algorithm. The algorithm developed for use in this thesis is based on analysis of the least squares residuals from the TDD velocity algorithm and removing any that appear to differ from the others by a nominal value. This has proved adequate for the purposes of this project and has removed the majority of cycle slips but some still remained. Removal or repair of all cycle slips is a necessary step in the production of a robust low cost TDD heave estimate as the nature of the TDD heave algorithm exacerbates the effects of cycle slips when they are passed through the high pass filter.

A final recommendation offered is the coupling of low cost GPS receivers with low cost MEMS technology IMUs to provide a complete low cost GPS-aided INS for use in the hydrographic survey market. It is thought that the use of inertial based algorithms exploited by AHRSs implemented with MEMS grade IMUs could be aided using the TDD velocities produced from a low cost GPS receiver to produce a Kalman filtered heave solution that will show robustness to momentary GPS signal loss. This notion can be extended further to produce a complete GPS-aided INS based solely on low cost sensors that can provide a low cost alternative to systems currently on the market such as the Applanix POSMV.

References

- Admiralty, 1987. Admiralty Manual of Navigation.
- Alkan, R., 2003. Reduction of heave, pitch and roll effects in hydrographic surveying. *Survey Review* (37), 208–217.
- Ashkenazi, V., Moore, T., Lowe, D., Moore, D., Woodworth, P., Rae, J., 1996. Offshore sea measurement using GPS. *Civil Engineering Surveyor GIS/GPS Supplement* .
- Bingley, R., 1998. GPS observables and algorithms, lecture presented as part of the Royal Navy Long Hydrographic Course.
- Bisnath, S., Wells, D., Howden, S., Dodd, D., Wiesenburg, D., 2004. Development of an operational RTK GPS-equipped buoy for tidal datum determination. *International Hydrographic review* 5 (1), 54–64.
- Blanchard, R. L., November 1971. A new algorithm for computing inertial altitude and vertical velocity. *IEEE Transactions on Aerospace and Electronic Systems* AES-7 (6).
- Canter, P., Corcoran, R., October 2004 2004. New generation of POS a boost for hydrographic surveying. *International Ocean Systems* .
- Chamber of Shipping, 2004. Annual review.
- Chang, C. C., Sun, Y. D., 2004. Application of a GPS-based method to tidal datum transfer. *The Hydrographic Journal* (112), 15–20.
- Collatz, L., 1966. *The Numerical Treatment of Differential Equations*. Springer.

- Collins, J. P., Langley, R. B., March 1999. Possible weighting schemes for GPS carrier phase observations in the presence of multipath. Tech. Rep. DAAH04-96-C-0086/TCN98151, United States Army Corps of Engineers Topographic Engineering Centre.
- Corcoran, R., Pronk, B., 2003. POS/MV model 320 V3 ethernet and SCSI ICD.
- Farrell, J., Barth, M., 1999. The Global Positioning System and Inertial Navigation. McGraw-Hill.
- Gelb, A., 1982. Applied Optimal Estimation, 7th Edition. MIT Press.
- Godhavn, J.-M., September 2000. High quality heave measurements based on GPS RTK and accelerometer technology. In: Oceans 2000 MT S/IEEE Conference and Exhibition. Vol. 1. pp. 309–314.
- GPS JPO, September 1997. Interface Control Document ICD-GPS-200. GPS Joint Programs Office, Revision IRN-200C-002.
- Grubin, C., 1970. Derivation of the quaternion scheme via the euler axis and angle. *Journal of Spacecraft and Rockets* 7, 1261–1263.
- Hare, R., September 1995. Depth and positioning error budgets for multi-beam echosounding. *International Hydrographic Review* .
- Hide, C., 2003. Integration of GPS and low cost INS measurements. Ph.D. thesis, University of Nottingham.
- Hide, C., Blake, S., Meng, X., Roberts, G., Moore, T., Park, D., September 2005. An investigation in the use of GPS and INS sensors for structural health monitoring. In: ION GPS 2005. Long Beach, California.
- Hide, C., Moore, T., Smith, M., August 2004. Performance of gps and low-cost ins integration in marine survey. *International Hydrographic Review* 5 (2).
- Hoffmann-Wellenhoff, B., Lichtenegger, H., Collins, J., 2001. GPS: Theory and Practice, 5th Edition. Springer-Verlag/Wien.

- IEEE, 1979. Programs for Digital Signal Processing. IEEE Press, algorithm 5.1.
- IHO, April 1998. IHO standards for hydrographic surveys: Special publication no. 44.
- Imahori, G., Gibson, W. M., Tronvig, K., 2003. Improvements to water level reducers for hydrographic surveys in hydrodynamically complex tidal regimes. In: US Hydro 2003. Mississippi.
- Ingham, A. E., 1992. Hydrography for the Surveying Engineer. Blackwell.
- Itani, K., Hayashi, N., Ueno, M., 2000. Low-cost wave sensor using time differential carrier phase observations. In: ION GPS 2000. Salt Lake City.
- James, G., 2001. Modern Engineering Mathematics, 3rd Edition. Prentice Hall.
- Jeffrey, A., 1989. Mathematics for Engineers and Scientists, 4th Edition. van Nostrand Reinhold.
- Jekeli, C., 2001. Inertial Navigation Systems with Geodetic Applications. de Gruyter.
- Kalman, R. E., 1960. A new approach to linear filtering and prediction problems. Transactions of the ASME-Journal of Basic Engineering 82, 35-45.
- Kaplan, E. D., 1996. Understanding GPS: Principles and Applications. Artech House.
- Kayton, M., Fried, W. R., 1997. Avionics Navigation Systems, 2nd Edition. John Wiley & Sons.
- Kielland, P., Hagglund, J., 1995. Using DGPS to measure the heave motion of hydrographic survey vessels. In: Institute of Navigation NTM 95.
- Klobuchar, J. A., 1996. Ionospheric Effects on GPS. Vol. 1 of Global positioning System: Theory and Applications. American Institute of Aeronautics and Astronautics, pp. 485-515.
- Kongsberg, January 2005. MRU Z Data Sheet.

- Kreyszig, E., 1988. *Advanced Engineering Mathematics*, sixth Edition. John Wiley & Sons.
- Kunysz, W., January 1998. Effect of antenna performance on the GPS signal accuracy. In: ION National Technical Meeting 1998. Long Beach, California.
- Langley, R. B., June 1997. GPS receiver system noise. *GPS World* 8 (6), 40-45.
- Lidner, D. K., 1999. *Introduction to Signals and Systems*. McGraw-Hill.
- Luscombe, J., 2003. Gyrocompass velocity aiding, internal report for Sonardyne Intl.
- Marine Accidents and Investigations Branch, 2004. Annual report.
- Martin, R. J., Broadbent, G. J., 2004. Chart datum for hydrography. *The Hydrographic Journal* (112), 9-14.
- Maybeck, P. S., 1979. Stochastic models, estimation, and control. Vol. 141 of *Mathematics in Science and Engineering*.
- Milne, P., 1980. *Underwater Engineering Surveys*. E and F N Spon Ltd.
- Misra, P., Enge, P., 2004. *Global Positioning System: Signals, Measurement and Performance*. Ganga-Jamuna Press.
- Mostafa, M., Hutton, J., Reid, B., 2001. GPS/IMU products - the applanix approach. In: 48th Photogrammetry Week. Stuttgart.
- National Geodetic Survey, March 2007. Continually operating reference stations. [Online], available at <<http://www.ngs.noaa.gov/CORS/cors-data.html>>.
- Parker, D., Mallace, D., 2006. Motion sensor performance: Direct comparison using 2005 common dataset. *Hydro International* 10 (1).
- Parkinson, B. W., Spilker, J. J., 1996a. *Global Positioning System: Theory and Application*. Vol. 1. American Institute of Aeronautics and Astronautics.
- Parkinson, B. W., Spilker, J. J., 1996b. *Global Positioning System: Theory and Application*. Vol. 2. American Institute of Aeronautics and Astronautics.

- Port of London Authority, 2004. Port of London Authority annual report. Tech. rep.
- Reefer, 2007. Annual reefer shipping market review and forecast.
- Reinking, J., Harting, A., October 2002. Heave determination by stand-alone GPS and/or inertial sensors. In: Hydro 2002. Kiel, Germany.
- Riley, J. L., Milbert, D. G., Mader, G. L., 2003. Hydrographic surveying on a tidal datum with kinematic GPS: NOS case study in Delaware Bay. In: US Hydro 2003. Mississippi.
- Rogers, R. M., 2000. Applied Mathematics in Integrated Navigation Systems. AIAA.
- Ryan, S., Lachapelle, G., E, C. M., September 1997. DGPS kinematic carrier phase signal simulation analysis in the velocity domain. In: Proceedings of ION GPS '97. Kansas City, Missouri.
- Sanders, P., 2003. RTK tide basics. Hydro International 7 (10), 26-29.
- Scarfe, B., 2002. Measuring water level correction (wlc) using RTK GPS. The Hydrographic Journal (104).
- Serrano, L., Don, K., Langley, R. B., September 2004a. A single GPS receiver as a real time, accurate velocity and acceleration sensor. In: ION GNSS 2004. Long Beach, CA, pp. 2021-2034.
- Serrano, L., Donghyun, K., Langley, R. B., Itani, K., Ueno, M., January 2004b. A GPS velocity sensor: How accurate can it be? - a first look. In: ION NTM 2004. San Diego, CA.
- Siouris, G., 1993. Aerospace Avionic Systems A Modern Synthesis. Academic Press.
- Spirent, September 2006. SimGen Software User Manual. Spirent Communications Ltd., Aspen Way, Paignton, Devon, No. DGP00686AAA, Issue 1-20.
- STANAG, 1990. NATO standardization agreement (STANAG) 4294.

- Steiler, B., Winter, H., September 1982. Flight test instrumentation volume 15 on gyroscopic instruments and their application to flight testing. AGARD AG-160-Vol.15, NATO.
- Terai, K., 2004. Precise vertical position fixing: Kinematic-gps validation in japans inland seas. *Hydro International* 9 (10), 7-9.
- Titterton, D., Weston, J., 2004. *Strapdown Inertial Navigation Technology*, 2nd Edition. IEE.
- USDOD, 1991. NAVSTAR GPS user equipment introduction. Tech. rep., GPS Joint Program Office.
- van Dierendonck, A. J., 1996. GPS Receivers. Vol. 1 of *Global positioning System: Theory and Applications*. American Institute of Aeronautics and Astronautics, Ch. 8, pp. 329-407.
- van Graas, F., Soloviev, A., 2004. Precise velocity estimation using a stand-alone GPS receiver. *Navigation: Journal of the Institute of Navigation* 51 (4).
- VTTSS Ltd, 2005. Meridan Attitude and Heading Reference System Data Sheet.
- Weiss, I., DeVries, T., October 1977. Ship motion measurement filter design. *IEEE Journal of Oceanic Engineering* 2, 325-330.
- Welch, G., Bishop, G., February 2001. An introduction to the kalman filter. Tech. Rep. TR 95-041, University of North Carolina, available at <http://www.cs.unc.edu/~welch/media/pdf/kalman_intro.pdf>, [Accessed March 2007].
- Zhang, J., Zhang, K., Grenfell, R., Deakin, R., 2006. GPS satellite velocity and acceleration determination using the broadcast ephemeris. *Journal of Navigation* 59 (2), 293-305.
- Zhoa, J., Hughes Clarke, J. E., Brucker, S., Duffy, G., 2004. On the fly gps tide measurement along the saint john river. *International Hydrographic Review* 5 (3), 48-58.